The Hong Kong Polytechnic University

Department of Industrial and Systems Engineering

A NEW STEPPING MOTOR SERVO SYSTEM FOR IMPROVED PRECISION PROFILING PERFORMANCE

CHEN WEIDONG

A thesis submitted in partial fulfillment of the requirements for the Degree of Doctor of Philosophy

March 2003

CERTIFICATE OF ORIGINALITY

I hereby declare that this thesis is my own work and that, to the best of my knowledge and belief, it reproduces no material previously published or written nor material which has been accepted for the award of any other degree or diploma, except where due acknowledgement has been made in the text.

____________________________(Signed)

CHEN Weidong (Name of student)

Abstract of dissertation entitled:

A New Stepping Motor Servo System for Improved Precision Profiling Performance

Submitted by CHEN Weidong

For the degree of PhD in Industrial and Systems Engineering

At The Hong Kong Polytechnic University in September 2004

ABSTRACT

The highly nonlinear torque-current-position characteristics make the servo control of hybrid stepping motors very complicated, especially under low operating speed. This thesis focuses on the development of simple and efficient control algorithms for the high-precision tracking control of hybrid stepping motors. The principles of several control schemes have been exploited to minimize the motor's torque ripple, which is periodic and nonlinear in the system states, with specific emphasis on low-speed conditions. The proposed control algorithms are all based on a modular control strategy where the feedback control module is designed to ensure global stability and achieve bounded tracking accuracy, while the feedforward control module is added to compensate for the effect of the torque ripple for improved tracking performance. The interactions between the feedforward and feedback control module have been explored and they have been shown to be complementary to each other. The stability and convergence performance of the control schemes are presented. It has been revealed that all the error signals in the control system are bounded and the motion trajectory converges to the desired value asymptotically. Simulations and experimental results demonstrate the effectiveness and performance of the proposed algorithms. These impressive results pave the way for stepping motors to be used in many applications previously not suitable for open loop steppers such as in low-speed direct-drive systems.

ACKNOWLEDGEMENTS

First of all, I would like to thank The Hong Kong Polytechnic University for providing a superb research environment. I am greatly indebted to my academic supervisor Professor Kai Leung Yung for his continued support, help, advice, encouragement, patience, guidance and instruction throughout the years. Without him, this research work could never have happened. To me, Professor Yung has been more than an advisor but a dear friend. I am proud to be his Ph.D. student and his academic son.

My particular thanks go to Dr Gary Feng, Dr Qing Wang, Dr Hong Yuan Lu, Dr Si Zhu Wu and Mr. S.M. Ko for their inspiration, support and encouragement.

Outside the academic environment, I wish to thank my elder sisters who started to take care of my family after I left for PolyU. Special appreciation goes to my parents. Without their love and care I would never have been what I am. Finally, I wish to thank my wife for everything she has done for our family and me. I truly think she deserves the biggest share of this Ph.D. degree.

TABLE OF CONTENTS

LIST OF FIGURES

CHAPTER 1

INTRODUCTION

1.1 Background and Objective

The driving force behind the flurry of research and development in precision motion systems during the past two decades arose from requirements for much higher product performance, higher reliability, longer life, lower cost, and miniaturization. A significant amount of these efforts have been directed towards motion control research which became a major sub-discipline in the field of precision engineering. The main objective of these efforts was to create a means for driving two or more axes to move in exact coordination with each other for generating a precise profile. Impelled by this, more extensive efforts have been dedicated to developing and exploiting various precision servo systems for the purposes of special motion tracking. These studies along with the development of advanced control strategies and hardware techniques, have contributed to a variety of high-performance drive applications such as industrial robots, ultra precision machine tools, and instrumentation systems.

The motion control industry has been using DC motors widely due to the relative ease in achieving high-performance with linear control. However, DC motors are giving way to AC motors, especially for permanent magnet (PM) synchronous motors, because AC motors are much more reliable and have a much higher torque-to-inertia ratio and greater electrical efficiency. On the other hand, AC motors are nonlinear devices and are thus more difficult to control. Furthermore, current DC or AC servomotors together with their corresponding power amplifiers are expensive and, due to their physical construction, have inherent torque ripples which affect their motion accuracy. It is hence desirable to look for a low-cost alternative to DC or AC servomotors that can effectively tackle the torque ripple issue in order to improve precision motion control.

The hybrid stepping motor appears to be a likely candidate capable of offering such performance and cost advantages because it carries all the advantages of standard PM synchronous motors while its cost is much lower. Its teethed structure that assimilates many pole-pairs (typically 50) to even out the interpole non-linearity can yield a higher torque ripple frequency and hence a lower ripple magnitude. This undoubtedly creates a unique advantage for the hybrid stepping motor over the PM synchronous motor in precision motion at very low speeds (below 60 rpm), and thus it can be employed as an effective actuator in special-purpose applications.

The direct-drive system can be regarded as a typical example of such applications. In this system, no indirect coupling mechanisms, as in the speed-reducing devices, are required. This greatly reduces the effects of contact-type nonlinearities and disturbances such as backlash and friction. At the same time, the advantages of using mechanical transmission are also consequently lost, such as the inherent ability to reduce the effects of model uncertainties and external disturbances. One of the primary considerations of using a hybrid stepping motor in these applications is its considerable torque ripple caused by the detent torque of the permanent magnet and the nonideal motor and drive characteristics which acts as a disturbance torque. This problem is obviated in a high-speed drive system because the torque ripple is filtered out by the inertia of the motor and load. It, however, leads to degradation in the control performance in the direct drive system because the motor is generally operated in a low-speed region. An adequate reduction of this effect, either through a proper physical design or via the control system, is of paramount importance in order to achieve high-precision motion control.

Various techniques have been considered to mitigate this problem. Although the most effective approach to minimize the torque ripple is by optimum motor designs, there are many occasions where they are not sufficient or appropriate to achieve the required level of torque ripple reduction. Moreover, the techniques based on the design concept have the drawbacks of reducing the average torque and increasing the complexity of the motor construction. More importantly, these should be considered in the motor design stage as drive designers may not find them useful. Another category of approaches that has been proposed for neutralizing undesired torque ripple components is to actively control the phase excitation to generate smooth output torque. It will be discussed in Chapter 2 that a number of the techniques using this concept have so far enjoyed various degrees of success, some of which bear direct relevance to the control design of other servomotors. Most of these techniques, however, depend critically on the assumption that sufficient preknowledge is available about the motor. This limits, to a certain extent, the application of such schemes due to imperfect knowledge and variations in the motor parameters. In addition, the control method itself for this purpose faces a significant challenge because the corresponding ripple dynamics is characterized by a time-varying and nonlinear function depending on the rotor position and speed. It is known that the proportional-integral-derivative (PID) control scheme with a widespread acceptance in industrial servo control applications is also proclaimed to be not adequate to reject this ripple, though the simplicity in its structure is appealing.

More complex advanced control approaches, even though they are available for solving this problem, have fared less favourably under practical conditions due to the higher costs associated with their implementation and higher demands in tuning.

Recent developments in advanced and intelligent control strategies have provided a good solution for handling the toque ripple problem. Consequent on the requirement for a low-cost and high-performance control implementation, the new control algorithms must be efficient enough to be executed within the given design domain (time-domain or frequency-domain), yet possess sufficient capacity to provide rapid ripple or disturbance suppression and precision motion tracking. This calls for a good weighted selection of control architectures to address not only the specific dynamics of the servo system involved, but also the control specifications arising from the application. One class of feasible approaches is based on the adaptive robust control concept that can make full use of a prior knowledge of the nonlinear uncertainties in the system dynamics resulting from both torque ripples and external disturbances. This preknowledge arises from the fact that there exists the structured uncertainty associated closely with the dominant ripple effect in the motor. The main benefits of this technique include the efficient estimation of and compensation for undesirable uncertain dynamics achievable with adaptation, and the guaranteed global boundedness of the system with respect to the desired tracking control task. Another class of promising methods is based on the use of the learning control (LC) scheme that can provide the “intelligence” for learning or identifying the torque ripple of the motor and canceling it on-line. The LC scheme is probably the one which is most naturally close to the applications involved owing to the fact that their important features follow from the periodic dynamics of motors. The main advantage of such a scheme is that it is much less model-dependent, and yet has the potential for achieving the desired ripple-free and high-precision motion control by seeking a simple controller structure with high computational efficiency. This is very attractive for real-time applications. Furthermore, such a control algorithm together with the specific phase excitation patterns, allows relatively simplified and practical control hardware configurations of the entire drive system at a low cost.

In short, the development of the aforementioned control concepts has strongly motivated the investigation of high-performance drive applications using hybrid stepping motors, especially in low-speed or direct-drive servo systems. One of the specific applications is to track a pre-specified trajectory, which is the subject of this study. We attempt to exploit the mathematical characteristics of deterministic nonlinear uncertainties relating to the ripple dynamics of a hybrid stepping motor, and then present several efficient and practical control schemes so that high-performance motion control tasks can be accomplished.

The objective of this study is to design an intelligent tracking control system such that through the corresponding control algorithm the hybrid stepping motor drive can generate a precise profile in the sense of low-speed tracking, despite various undesirable uncertainties and disturbances in the motor dynamics.

1.2 Investigation Approach

To understand the control architecture considered in this study, we first scrutinize the dynamical characteristics of a two-phase hybrid stepping motor, which is one of the objectives of this study. The dynamics of a two-phase hybrid stepping motor can be viewed as comprising the electrical dynamics of the stator coils together with the shaft mechanical dynamics, which is inherently nonlinear and highly coupled due to the torque production mechanism in the motor resulting in a number of sinusoidal functions (harmonics) and their multiplication with state variables. It is well known that each harmonic varies with the electrical frequency of the motor that, for a typical 50 pole stepping motor, is integer times of 50 the mechanical frequency. Such large bandwidth differences between the electrical and mechanical dynamics lead to different control configurations at different operating speeds. At low speeds, the nonlinear effects resulting from the nonideal magnetic structure and other physical imperfections in the motor must be considered in the design of the control system if high precision motion control is to be efficiently realized. Among them, the two most prominent nonlinear effects are the ripple and frictional torques.

The two primary components of the torque ripple are the detent torque (including one caused by the flux harmonics) and the reluctance torque. The detent torque arises as a result of the mutual attraction between the rotor's and the stator's poles. This torque exists even in the absence of any phase current and it exhibits a periodic relationship depending on the rotor's position relative to the stator. Detention effect manifests itself by the tendency of the rotor to align in a number of preferred positions regardless of excitation states. The reluctance torque is due to the variation of the self-inductance of the windings with respect to the relative position between the rotor and the stator. Thus, the reluctance torque also has a periodic relationship with the rotor-stator position. Collectively, the detent and reluctance torque constitute the overall torque ripple phenomenon. Even when the motor is not powered, torque ripples are clearly existent when the rotor is moved. At lower speeds, the rippling effects are more fully evident due to the lower momentum available to overcome the magnetic resistance. The torque ripple has a significant effect on the position accuracy achievable and it may also cause oscillations and yield stability problems, particularly at low speeds or with a light load (low momentum). The ripple periodicity has a fixed relationship with respect to the rotor position.

Friction is inevitably present in nearly all moving mechanisms, and it is one major obstacle to achieving precise motion control. Several characteristic properties of friction have been observed, which can be broken down into two categories: static and dynamic. Many empirical friction models have been developed which attempt to capture specific components of observed friction behavior, but generally, it is acknowledged that a precise and accurate friction model is difficult to obtain in an explicit form, especially for the dynamical component. For our present purposes, however, the simple viscous friction model has been proven to be useful and it will be validated adequately.

The special particularities of the physical structure associated with the hybrid stepping motor have motivated us to study some of nonlinear and intelligent control approaches within an appropriate system framework. Before designing and evaluating the control scheme for hybrid stepping motor drives, we follow a common practice of applying the well-known direct-quadrature (DQ) transformation as an initial step towards control design. The DQ transformation can provide such a framework using a sinusoidal commutation pattern together with the desired control input for identifying the nonlinear dynamics and achieving precise tracking control, which will be shown to be useful in the realization of a simple and practical controller for high-performance control purpose. To facilitate the inverse DQ transformation to produce practical control inputs (phase currents) from sinusoidal commutation, the required sinusoidal functions are stored and updated in a look-up table for fast control configuration. By means of this transformation, our study addresses the following key control issues ranging from the control design approach itself to experimental validation of control algorithms.

A. Theoretical aspects of the profiling performance by model-based approaches.

The model-based control approaches rely on the partial knowledge about the motor dynamics in order to project the ripple dynamics with parameter estimation techniques for special control synthesis, which in this study are classified into two different categories: feedback linearizing control and robust adaptive control. Feedback linearizing control is established by using an optimum parameter estimate, traditional linear control, and dynamic feedback control coupled with feedforward compensation. A two-stage control design is suggested to realize the concept. Initially, a traditional control algorithm is employed to give a bounded but coarser control performance. Then, further refinements are introduced into the preliminary design by supplementing some of the compensating terms so as to attenuate ripple components and guarantee precise global trajectory tracking. Robust adaptive control is constructed through the adaptive estimation and compensation of the structured uncertainty arising from the detent ripple and the friction, and meanwhile, the use of the robust control concept to deal with other structured uncertainty caused by nonsinusoidal flux distribution. This control approach provides the advantage of reducing the torque ripple components over a broader ripple frequency band, and guarantees a straightforward tracking control specification. Furthermore, it is anticipated that the second approach will be better than the first one in control performance because of its more reasonable estimate to ripple dynamics with adaptation.

B. Study of profiling performance using learning-based approaches

The learning-based approaches considered here belong to a class of modular control strategy in which the feedback control module is first designed to ensure global stability and achieve uniformly bounded tracking accuracy with an appropriate smoothing scheme, while the learning module is added to further improve the tracking performance whenever the control task repeats or is periodic. It is worth mentioning that most existing repetitive or iterative learning control methods are of the typical feedforward class and thus sensitive to any nonperiodic factors. By incorporating learning into feedback control, the feedback control part will "protect" the learning part to a certain extent by virtue of its excellent robustness property. Generating the desired control profile is the ultimate objective of the learning-based approaches where learning aims at extracting useful control knowledge from past control and tracking error sequences, so as to approximate the desired control for perfect tracking and torque ripple rejection.

Two categories of interest of the learning-based approaches are considered. The first is based on a less model-dependent repetitive learning control. It has a very simple structure consisting of two time-domain components in additive form: a feedback control mechanism using either a pure linear form or some nonlinear form, and a learning mechanism that simply adds up a past tracking error sequence. Under the boundedness and Lipschitz continuity conditions of the system dynamics, the

Lyapunov-based design technique is used to yield a learning-based control estimate to achieve asymptotic tracking in the presence of nonlinear ripple dynamics. The second is based on model-free learning control that is implemented in the frequency domain by means of a Fourier series expansion. Since both the desired trajectory and the actual output can be approximated by a Fourier series with constant harmonic magnitudes under certain conditions, the tracking control problem in the time domain is decentralized into a number of independent regulation problems of the Fourier coefficients. The learning algorithm is designed in such a way that each harmonic magnitude of the actual output converges to that of the desired trajectory within the system bandwidth. Fourier series-based learning can further enhance the robustness property of learning control and improve tracking performance.

C. Experimental verification of dynamic characteristics of the ripple-free drive

The motivation for making an experimental verification is to demonstrate that the aforementioned control approaches can be utilized to compensate for the ripple dynamics in the hybrid stepping motors in order to generate a precise profile. In order to gain more understanding about the control approaches we are interested in, a detailed analysis of the experimental results is necessary, and the performance comparisons between these methods in a variety of shapes are also required. In this stage, it is necessary to design and construct a precision experimental rig and an intelligent profiling algorithm. The control algorithm is implemented on a TMS320C30 DSP chip that can process input signals from the encoder coupled with the motor and supply output control signals to the motor drive in real time. The experimental investigation may shed light on its potential applications in the servo systems.

1.3 Main Contributions

The main contributions of this study are summarized as follows:

(1) A feedback linearizing control approach that employs dynamic feedback control together with feedforward compensation is proposed in order to harness the torque ripple of a hybrid stepping motor at low speeds for precision profile tracking. A novel identification procedure based on the least-squares algorithm using the integral equation model and a power series expansion is first applied to estimate the model parameters for calculation of the ripple dynamics. This produces a more appropriate form of linear regression which avoids the problem of reconstructing important signals such as the rotor speed and the derivatives of driving current, and rejects additional errors created by the quantization of the measurements. A new integration process is then conducted to obtain precise trajectory tracking by combining a reference trajectory, the traditional PID control, and the dynamical feedback linearizing control coupled with feedforward compensation over a certain torque-ripple frequency band.

(2) A robust adaptive control approach is developed to enhance the performance of the above scheme. To facilitate the corresponding control design, the system uncertainties are attributed to two categories of the structured uncertainties. The structured uncertainty arising from the detention effect can be separated and expressed as the product of the known harmonic functions of the rotor position and a set of unknown constants. This uncertainty is estimated with possible adaptations and compensated for. Meanwhile, the robust adaptive method is

applied to deal with other structured uncertainty, resulting from the nonsinusoidal flux distribution, by estimating its bounding constants. The $\mu-$modification scheme is applied to cease parameter adaptation in accordance with the robust adaptive control law. This control scheme guarantees the uniform boundedness of the motor drive system and assures that the tracking error enters an arbitrarily designated zone in a finite period of time.

(3) A class of time-domain learning control approach is proposed which uses a modified standard repetitive update rule. A Lyapunov-based design approach is first utilized to illustrate the generality of the learning-based update law and its ability to force the origin of a general error system with a nonlinear disturbance within a known period to achieve global asymptotic tracking. Through both the Lyapunov-based technique and other stability analysis techniques, the learning-based controller is then designed to compensate for nonlinear ripple dynamics and assure global asymptotic motion tracking for a hybrid stepping motor. The proposed control scheme, as opposed to the use of a multiple step process, is updated continuously with time during the transient response (versus during the steady-state), and hence, an improved transient response is facilitated.

(4) A decentralized learning control scheme is developed and implemented in the frequency domain by means of a Fourier series expansion for tracking control of a hybrid stepping motor. Based on the fact that both the desired trajectory and the actual output can be expressed by a Fourier series with constant harmonic magnitudes, the learning controller is designed to individually control each harmonic component of the actual output to converge to that of the desired

trajectory within the system bandwidth. Since this decentralized learning controller is designed in Fourier space instead of time domain, the system's time-delay can be easily compensated for. Moreover, this learning controller is only based on the local input and output information so that no prior system modeling is required. The control scheme can significantly improve the tracking control performance by identifying and simultaneously compensating for deterministic uncertainties caused by the ripple and frictional torque.

(5) The behavior of the proposed control schemes in precision profile generation are evaluated via the experiments conducted on a typical hybrid stepping motor to illustrate their effectiveness. Experimental results also give the performance comparison between them, and offer guidance for the selection of a practical control algorithm for tuning computer-controlled drives.

1.4 Thesis Organization

The remainder of the dissertation is organized as follows: Chapter 2 provides first a detailed literature review on the closed-loop control of the hybrid stepping motor. The anticipated control schemes are then introduced in an appropriate framework. Chapter 3 gives the design procedures of the model-based tracking control schemes and the performance analysis, simulations and experimental results. The development of two classes of learning control approaches for precision tracking control and related experimental results are presented in detail in Chapter 4 and Chapter 5 respectively. Finally conclusions are drawn in Chapter 6.

CHAPTER 2

LITERATURE SURVEY

2.1 Introduction

Attempts have been made in the past decade to use closed-loop control for enhancing open-loop performance of stepping motors by providing another degree of freedom in the design of the stepping motor. However, this was often complicated due to the nonlinear dynamical characteristics of the motor, especially at low speeds, which makes the control difficult to design and implement. Amongst the work reported in the literature are several methods for the closed-loop control of hybrid stepping motors; the methods range from lead angle control, feedback linearizing control to torque ripple minimization. In this chapter, we conduct an extensive review of these methods and justify our control strategies for low-speed tracking control applications.

2.2 A Review of Lead-Angle Based Control

The lead angle is one of the most important parameters for the closed-loop control of stepping motors. The lead angle reflects the relationship between the rotor's present position and phase(s) to be excited. Alternatively it can be defined as the distance between the switching point and the equilibrium position of a given phase (Acarnley. 1982 and Kenjo. 1984). The physical implication of lead-angle based control is that each change in phase excitation must occur earlier relative to the rotor position so that the phase current has sufficient time to be established before the rotor reaches the position of maximum phase torque. Hence, variation of the lead angle has an important effect on the torque ripple and even the power output of the stepping motor.

For systems in which there is little variation of both load torque and distance of travel, it may be appropriate to operate with a fixed lead angle, so as to minimize the controller costs. However more sophisticated systems require the lead angle to vary with speed. In a closed-loop control scheme with a continuously-variable lead angle the motor is able to develop its maximum (pull-out) torque at all speeds and therefore the system performance is maximized. To perform this function, the controller requires information about the instantaneous speed of the motor and must then generate the lead angle appropriate to that speed.

The most important consideration in this scheme is that a small lead angle should be chosen at low speeds such that a high torque is available. This argument is reversed when a high operating speed is required. This constitutes the core meaning of “optimum switching angle” concluded by Acarnley and Gibbons (1982). They made first use of this concept in the position control of stepping motors, in which the position command to the motor was modified based on the positional response and the optimum lead angle. Although this technique offered some advantages over purely open-loop control, it can lead to unpredictable results because the dynamics of the motor were not included (Clarkson and Acarnley. 1988). Considerable torque ripple and thus speed ripple are often unavoidable especially at low speeds.

Brown *et al.* (1989) developed a “near time optimal control” based on the maximum-average-torque lead angle function, which was determined instantaneously from the rotor speed response and the parameters of the motor, to improve the efficiency of the position control system and suppress to some extent the effect of torque ripple. Bodson *et al.* (1993) verified and extended this concept by taking into account field-weakening for fast and precise positioning problems where it was essential to avoid saturation of phase voltages at high rotor speeds.

The closed-loop commutation method proposed by Yung and Liu (1994) focused on carefully adjusting the lead angle to reduce the torque ripple. Experiments and simulations have been carried out to determine the relationship between speeds, lead angle, driving waveform and torque ripple. The results showed a good match between them. This provided a means of minimizing speed ripple by using the model-based simulation scheme to improve the accuracy of motion control systems. Furthermore, Yung *et al*. (1997) took advantage of this control strategy to further explore the profile tracking capability. The results showed a smaller ripple at high speeds, but required further improvement at low speeds.

Subsequently, Mak and Yung (1998) derived and implemented a dual control strategy. The experimental result has shown that the magnitude of the driving voltage waveform and the corresponding lead angle has given an additional dimension to the control of the closed-loop commuted stepping motor where its torque ripple and tracking characteristics may be further improved. It has also shown in its performance in position control and in its capability of positioning that it can achieve an accuracy of one count out of a 4,000 counts per revolution encoder, a resolution much higher than one step of the stepping motor.

One of the appealing features of the lead-angle based scheme for the closed-loop control of stepping motors is that the phase excitations are in the form of a sinusoidal commutation. As a result, it may simplify the hardware implementation of this scheme by using familiar circuit techniques such as lookup tables to store the phase excitation waveshape data.

2.3 A Review of Torque Ripple Minimization Scheme

One of the important issues associated with low-speed high-performance motion control applications using hybrid stepping motors is to minimize the torque ripple which is due mainly to inter-pole movements. The two primary components of the torque ripple are the detent torque and that caused by the flux harmonics. These ripple components, arising as a result of the mutual attraction between the rotor's and the stator's poles, all exhibit a periodic relationship with respect to the rotor position relative to the stator. But the detent torque exists even in the absence of any phase current. For example, the desirable detent torque from the permanent magnet, which provides passive braking when the motor is de-energized, has contributed to the non-uniformity of the developed torque during low-speed tracking operation. The effects of torque ripple directly lead to speed oscillations that cause deterioration in the system performance. Consequently, the use of the hybrid stepping motor in servo systems, requiring smooth rotation at low speeds and the capability to apply torque when nearly static, has been limited.

One of the most popular approaches for torque ripple minimization is a harmonic cancellation technique using the programmed or injected current. However, since this was only implemented in an off-line manner using fixed parameters, a desired performance can not be achieved under various operating conditions. Chen and Paden (1990) considered a high-precision low speed control of the hybrid stepping motor by the cancellation of torque ripple components using an adaptive current control. This was the first systematic approach to torque ripple minimization through adaptive control. Experimental results demonstrated a dramatic reduction of torque ripple at the rotor pole frequency. However, the presented adaptation process was complex and converged slowly which resulted in an unpredictable coupling between certain ripple harmonics.

Another approach of interest for this purpose is instantaneous torque control, which utilizes the torque-control loop instead of the current-control loop. It is natural that this is effective for reducing the torque ripple because instantaneous torque can be directly controlled. This technique, however, has the significant problem of obtaining the information on the instantaneous torque. Since the torque measuring mechanism is very expensive and bulky, it is not available for most industrial applications. Therefore, the estimation technique is generally used. Low *et al.* (1990, 1992) employed a least-square method (LSM) to estimate the instantaneous torque. However, since this required the differentiation of the measured current having the switching noise, it was difficult to expect good estimating performance. Moreover, this was very complex and thus required intensive computing ability for the practical implementation.

The control method for the instantaneous torque is also a significant problem because the instantaneous torque pulsates sinusoidally depending on the rotor position. It is known that the PI control is not adequate to reject this pulsation. A robust control such as the variable structure control (VSC) was thus used in the previous approaches (Low *et al.*, 1990, 1992). Theoretically, the VSC provides an excellent control to suppress the torque ripple. However, this still has some practical problems such as the chattering and steady-state error caused by a non-ideal sliding motion (Chung *et al.*, 1995).

In order to reduce the above disadvantages, Chung *et al.* (1998) developed a new instantaneous torque control controller where the linkage flux of a motor was estimated by the model reference adaptive system (MRAS) technique and the torque was calculated by using the estimated flux and measured current. Since the proposed estimation method using the MRAS technique did not require the differentiation of the motor current, the estimating performance was less sensitive to the measurement noise than that of the conventional approach employing the LSM. Furthermore, the proposed control using the Integral VSC provided the advantages of improving the steady state performance and switching characteristics.

Subsequently, Lam *et al.* (1999) took advantage of this scheme to develop a learning-based dynamic torque controller along with a conventional current controller for torque ripple minimization. This torque controller compared the desired motor torque with the instantaneous motor torque, and generated the reference current iteratively from cycle to cycle so as to reduce the torque error.

It should be pointed out that the above instantaneous torque control schemes belong to an estimator-based approach which relies on the preknowledge of the motor parameters. The parameter variations such as phase resistances and inductances are the significant factors degrading the control performance. A good knowledge of these parameters is necessary for realizing high-performance control. In addition, on-line torque estimation works only for a specific speed range. Thus, the effectiveness of such control schemes is limited.

Apart from the techniques described above, an alternative technique counts on a surrounding closed-loop speed regulator to attenuate torque ripple. Matsui *et al.* (1993)

considered a speed-loop compensation using the load torque observer. This is quite useful for rejecting slow-varying disturbance such as the load torque variation. It is, however, questionable that this has the capability of reducing the torque ripple caused by the detent torque and flux harmonics, which vary much faster than the speed-loop dynamics.

Lam *et al.* (2000) proposed an outer loop speed control that was performed by a PI controller in conjunction with an iterative learning controller (ILC). The PI speed controller provided the main reference current. In the steady-state, the speed error signal was learnt by ILC in order to produce the reference compensation current that supplemented the main reference current to minimize the speed ripple. In deed, the added compensation acts so as to attenuate the speed ripple that is closely associated with the torque ripple for their coordinated reduction. Although this resulted in some success, this approach remains open to further improvement because of its very principle. In any event, the effectiveness of this approach actually increases for low-speed applications where torque smoothness is most critical.

2.4 A Review of Feedback Linearizing Control

Feedback linearizing control is one of the most popular control approaches for stepping motor servo drives. Its point is to find a (nonlinear) state-space transformation such that, in the new coordinates, the nonlinearities may be canceled out by state feedback. With the hybrid stepping motor, the appropriate nonlinear coordinate transformation is known as the direct-quadrature (DQ) transformation (Liu *et al.* 1989).

Zribi and Chiasson (1991) considered the position control of hybrid stepping motors by exact feedback linearization and showed how it naturally reduced to the well-known direct-quadrature (DQ) transformation of electric machine theory. This is a very promising global feedback linearizing approach. Subsequently, Aiello *et al*. (1991) presented some preliminary experimental results of implementing this nonlinear feedback controller along with a least-squares parameter identification process.

Bodson *et al.* (1993) reported on an impressive experimental investigation implementing the control algorithm in an industrial test-bed. This model-based feedback linearizing controller was shown to be able to guarantee global trajectory tracking for high-speed point-to-point tracking by using field-weakening, a speed observer and reference trajectory.

Schweid *et al*. (1995) investigated low speed regulation of hybrid stepping motors amidst torque disturbances by exploiting the nonlinear dynamics to create an analog positional controller in conjunction with a traditional linear control law that exercises current control and linearizes the controlled response. Experimental results showed that this controller attained high positioning accuracy at extremely low speeds.

Chu *et al.* (1994) presented a mathematically strict feedback linearizing controller that consists of a current controller and a torque controller. An explicit characteristic of this control method is that the designed torque controller can make the generated torque of a hybrid stepping motor exactly linear with respect to the torque command. Moreover, this torque controller contains a function, which can be chosen arbitrarily under some constraints, and through an optimal choice it can give minimal power loss due to phase windings. Unfortunately, this approach assumes that sufficient information is available a priori about the motor characteristics to construct the desired controller. The resulting sensitivity of this approach to imperfect knowledge and variations in the motor parameters is one of the factors which must be considered when adopting this scheme.

It is worth noting that most of the previous approaches rely on the use of the PID design philosophy with a special emphasis on integral action, regardless of the dependence of each compensation term on either voltage or current, to form the key prerequisite for effective implementation of feedback linearizing techniques in hybrid stepping motor control systems.

It should also be pointed out that these controllers depend heavily on the identification of the system model, including its structure selection, parameter estimation and validation. In this respect, Blauch *et al.* (1993) applied a batch least-squares algorithm to determine the stepping motor parameters for the implementation of a nonlinear control algorithm (Aiello *et al*., 1991 and Bodson *et al.*, 1993). Some of the significant parameters that affect control performance were reliably estimated. A primary drawback of the identification procedure is that it is necessary to obtain the derivatives of those states that are not directly measurable and then to reconstruct them using the difference equation, which may increase high-frequency noise. Moreover, the selection of the order of the model is affected by different operating conditions. The complete fourth order model needed for high-speed operations may be unnecessary at low speeds because current amplifiers can effectively control the phase winding current. Hence, it is quite reasonable to make use of current choppers and the second order model for low-speed direct-drive applications.

2.5 Applications of Advanced Control Approaches

A. Robust Adaptive Control

In many applications, dynamics of the system are partially or incompletely known with estimation and robustness being the key in designing a successful control. Adaptive control, robust control and their combinations represent means of achieving online estimation and robustness. Roughly speaking, a control system is adaptive if the unknown parameters of either the system or its corresponding controller are estimated online and the estimates are used to synthesize a stabilizing control. A control system is considered robust if its stability and performance under a fixed controller is guaranteed for a specific class of uncertainties which could be unknown functions, parameter variations, unmodeled dynamics and disturbances.

Robust control of nonlinear uncertain systems has been a focus of research in the recent years. Conceptually, a control system is made to be robust if a specific class of uncertainties has been taken into consideration in control design and stability analysis. Typically, robust control design requires that the uncertainties be bounded in some norm and have a certain structural property in terms of their functional dependence and locations in system dynamics. Classes of stabilizable uncertain systems have been found, and several robust control design procedures have been proposed (Coreless *et al.* 1983, Krstic *et al.* 1995, Khalil 1996, Qu 1993, 1998 and Isidori 1999). On the other hand, adaptive control is the technique of choice if the uncertainties can be expressed linearly in terms of unknown constants. Its popularity is due to the fact that standard adaptive control results (Krstic *et al.* 1995) are concerned about how to estimate the unknowns and to use the estimates in control design. In addition, adaptive and robust controls are often combined as uncertainties are unknown by nature and, in a system, several types of them structured or unstructured may be presented. It is straightforward to design a control containing both components to handle different kinds of unknowns. For example, one part of the control is adaptive to estimate unknown but constant parameters while the rest of the control is robust to compensate for bounded uncertainties.

One of the approaches to maintain robustness while reducing conservatism is to blend an adaptive control scheme into the robust control design called *adaptive robust control*. This is an adaptive version of robust control and the first of such results was proposed by Coreless *et al.* (1983), in which uncertainties of the system is bounded by a function linearly parameterized in terms of unknown constant parameters while robust control is made adaptive to estimate these parameters.

So far numerous adaptive robust control algorithms for systems containing uncertainties have been developed (Peterson and Narendra 1982, Ioannou and Kokotivic 1983, Narendra and Annaswamy 1989, Sastry and Isidori 1989, Taylor *et al.* 1989, Liao *et al.* 1990, Kokotovic 1991, Brogliato and Neto 1995, Ioannou and Sun 1996, Xu *et al.* 1997, 1999). Liao *et al.* (1990) developed a VSC with an adaptive law for an uncertain input-output linearizable nonlinear system, where the linearity-in-parameter condition for uncertainties is assumed. The unknown gain of the upper bounding function is estimated and updated by the adaptation law so that the sliding condition can be met and the error state reaches the sliding surface and stays on it.

To deal with a class of nonlinear systems with partially known uncertainties, Brogliato and Neto (1995) proposed an adaptive law using a dead-zone and a hysteresis function to guarantee both the uniform boundedness of all the closed-loop signals and the uniform ultimate boundedness of the system states. In both control schemes, it is assumed that the system uncertainties are bounded by a bounding function which is the product of a set of known functions and unknown positive constants. The objective of adaptation is to estimate these unknown constants.

Cai *et al.* (1997) proposed a model-free adaptive robust decentralized control for robot manipulators by using the Taylor series to estimate the system's uncertainties and phase plane to design the adaptive robust controller. Xu *et al.* (1997) developed an adaptive robust control scheme for a class of nonlinear uncertain systems with both parameter uncertainties and exogenous disturbances. Including the categories of system uncertainties used by Liao *et al.* (1990) and Brogliato and Neto (1995) as its subsets, it is assumed that the disturbances are bounded by a known upper bounding function. Furthermore, the input distribution matrix is assumed to be constant but unknown. Xu *et al.* (1999) extended this scheme to the more general classes of nonlinear uncertain dynamical systems. The unknown input distribution matrix of the system input can be state dependent. To reduce the robust control gain and to widen the application scope of adaptive techniques, the system uncertainties are supposed to be composed of two different categories: the first can be separated and expressed as the product of a known function of states and a set of unknown constants, and the other category is not separable but has partially known bounding functions. The first category of uncertainties is dealt with by means of the well-used adaptive control method. Meanwhile an adaptive robust method is applied to deal with the second category of uncertainties, where the unknown parameters in the upper bounding function are estimated with adaptation. It is shown that the control scheme that has been developed can guarantee the uniform boundedness of the system and assure that the tracking error enters the arbitrarily designated zone in a finite time.

It is worth pointing out that the performance of pure adaptive control hinges on how efficiently accurate information of the system can be inferred from the system signals and also whether it can be robust enough to modeling uncertainties difficult to consider in control design. In response to this demand, *robust adaptive control* is required. This combined scheme is a modified adaptive control in order to gain certain robustness property. For example, robust adaptive controls have been proposed for slowly time varying systems (Zhang 1996), fast time varying systems (Marino *et al.* 2000, Qu 2000), and systems with internal dynamics (Freeman *et al*. 1996, Isidori 1999). Typically, adaptive control may be augmented to nonlinear control input to achieve robust control with an uncertain model inheriting some inherent nonlinear uncertainties, possibly inseparable or coupled with system variables. It is very desirable to look for a robust adaptive control that not only can provide the adaptation of the model parameters to the actual system parameters so as to enable the suppression of a part of undesirable uncertainties, but also can effectively account and compensate for residual nonlinear uncertainties, structured or unstructured. One of the most typical configurations for such a controller is the use of standard adaptive control plus a robustified adaptive compensating component (Xu *et al.* 1997, Tan *et al.* 2001).

In short, robust adaptive control has established its theoretical significance followed by its potential applications. As far as the motion control using hybrid stepping motors is concerned, robust adaptive control will be very competitive due to the good knowledge of the nonlinear uncertainties relative to the motors. The reason is that the system's structured uncertainties can easily be extracted from the torque production mechanism in the motor and incorporated into the design of the controller that focus on both parameter uncertainties and bounding functions. Since these uncertainties in the motor exactly reflect overall torque ripple contents to be cancelled, robust adaptive control can be used to compensate for their adverse effects and to achieve the control task within specified bounds. Therefore, this control approach has been considered for tracking control in our study.

B. Learning Control Scheme

It is known that an adaptive control scheme does not require a precise model of the systems, but it requires that the estimated parameters can be represented in at least quasi-linear form. Hence, it can only be used to handle structured uncertain systems. When the nonlinear effects, such as friction and disturbance, cannot be expressed in the quasi-linear form, the efficiency of this scheme would be reduced. In addition, adaptive control strategies may not guarantee that the estimated parameters converge to their true values, and they certainly do not ensure that the controlled system would follow the desired trajectory perfectly. It is worth pointing out that tracking errors may be considered to be repeatable when the control task is defined over a finite time interval and the controller repeats its operation for tracking. Learning control is another strategy for addressing such uncertain problems. It attempts to eliminate tracking errors in repeated trials of an operation by learning from previous experience in executing the same command. This method can guarantee the convergence of error through the entire period since the information of the previous trial on the system dynamics and the tracking error at each time step is reflected in the next trial. As the learning controller requires very little or no model information of the controlled system, it has been widely used in many industrial applications.

Given the myriad of industrial applications that require the systems to operate in a repetitive manner, researchers have been motivated to investigate control methods that exploit the periodic nature of the system dynamics, and hence, increase tracking control performance. As a result of this work, many types of learning controllers have been developed to compensate for periodic disturbances. Some advantages of these controllers over other approaches include the ability to compensate for disturbances without high frequency or high gain feedback terms, and the ability to compensate for time-varying disturbances that can include time-varying parametric effects.

Some of the initial learning control research targeted the development of betterment learning controllers. Unfortunately, one of the drawbacks of the betterment learning controllers is that the system is required to return to the same initial configuration after each learning trial. Moreover, Heinzinger *et al.* (1989) provided several examples that illustrated the lack of robustness of the betterment learning controllers to variations in the initial conditions of the system. To address these robustness issues, Arimoto (1990) incorporated a forgetting factor in the betterment learning algorithms given by Arimoto *et al.* (1984) and (1988). Motivated by the results from the betterment learning research, several researchers investigated the use of repetitive learning controllers. One of the advantages of the repetitive learning scheme is that the requirement that the system returns to the exact same initial condition after each learning trial is replaced by the less restrictive requirement that the desired trajectory of the system be periodic. Some of the initial repetitive learning control research was performed by Hara *et al.* (1988), Tomizuka *et al.* (1989), and Tsai *et al.* (1988); however, the asymptotic convergence of these basic repetitive control schemes can only be guaranteed under restrictive conditions on the plant dynamics that might not be satisfied. To enhance the robustness of these repetitive control schemes, these researchers modified the repetitive update rule to include the so-called Q-filter. Unfortunately, the use of the Q-filter eliminates the ability of the tracking errors to converge to zero.

In the search for new learning control algorithms, Horowitz (1993) and Messner *et al.* (1991) proposed an entirely new scheme that exploited the use of kernal and influence functions in the repetitive update rule; however, this class of controllers tends to be fairly complicated in comparison to the control schemes that utilize a standard repetitive update rule.

Sun and Wang (2001), and Wang (2000) developed iterative learning controllers (ILCs) that do not require differentiation of the update rule, so that the algorithm can be applied to sampled data without introducing differentiation noise. Cheah *et al.* (1994), (1996) and Wang *et al.* (1995) developed ILCs to address the motion and force control problem for constrained robot manipulators. Cheah and Wang (1997) developed a model-reference learning control scheme for a class of nonlinear systems in which the performance of the learning system is specified by a reference model.

Xu and Qu (1998) utilized a Lyapunov-based approach to illustrate how an ILC can be combined with a variable structure controller to handle a broad class of nonlinear systems. Ham *et al.* (2000) utilized Lyapunov-based techniques to develop an ILC that is combined with a robust control design to achieve global uniformly ultimately bounded link position tracking for robot manipulators. The applicability of this design was extended to a broader class of nonlinear systems by Ham *et al.* (2001).

Recently, Kim *et al.* (1999), (2000) have utilized a class of multiple-step “functional” iterative learning controllers to damp out steady-state oscillations. The fundamental difference between the previous learning controllers and the controllers proposed by these authors, is that the ILC is not updated continuously with time, rather, it is switched at iterations triggered by steady-state oscillations. Han *et al.* (1998) utilized this iterative update procedure to damp out steady-state oscillations in the velocity set-point problem for servomotors. This work was extended to compensate for friction effects (Cho and Ha 2000) and applied to VCR servomotors (Kim and Ha 1999).

Upon examination of some of the aforementioned work, it seems that many of the recent ILC and repetitive control results exploit a standard repetitive update rule as the core part of the controller; however, to ensure that the stability analysis validates the proposed results, the authors utilize many types of additional rules in conjunction with the standard repetitive update rule. Unfortunately, these additional rules and additional complexity injected into the stability analysis are not necessary for the development of learning controllers that utilize the standard repetitive update rule. It is also conjectured that a statement concerning the boundedness of learning controllers made by Messner *et al.* (1991) may have caused some researchers to attempt a modification of the standard repetitive update rule with additional rules or abandon the use of the standard repetitive update rule entirely; hence how to realize a simple and effective modification of this repetitive update rule remains a challenging problem.

To address important practical considerations, several researchers investigated the implementation of learning controllers in the frequency domain to achieve better tracking performance. Mita and Kato (1985) designed a learning controller in the

Laplace frequency-domain. Lee *et al.* (1993) employed a Fourier series to approximate the input/output (I/O) characteristics of a dynamic system and proposed an iterative learning control algorithm based on identified I/O mapping matrix. Some related papers (Tomizuka 1987, Chew and Tomizuka 1990, Kavli 1992, Padiew and Su 1990) proposed more sophisticated algorithms. Gorinevsky *et al.* (1997) proposed a learning controller for robot manipulator tracking. Their scheme uses B-spline to approximate an input shaping function of feedforward. They claimed that their method could cope with strong nonlinearities and the convergent rate of their algorithm (five to six cycles) is faster than those of many other algorithms.

Recently, Huang (1999) designed a model-free learning controller in Fourier space with orthogonal bases by which the nonlinear tracking control problem in the time domain may be simplified to a number of independent regulation problems in the frequency domain. Xu (2002) implemented a learning variable structure controller (LVSC) by means of a Fourier series expansion to enhance the robust property of the proposed learning mechanism. Frequency domain learning improves tracking accuracy since the integration process nullifies the majority of high frequency components caused by quantization error due to limited sampling frequency, and obtains fast convergence. Moreover, the requirement that the system must return to exactly the same initial state after each learning trial can be relaxed.

On the subject of tracking control associated with the use of hybrid stepping motors, it is now very natural to choose the learning-based control scheme because of the periodicity property concerning the motor dynamics. In this study, Lyapunov-based design techniques have been used to develop a learning-based control estimate to achieve asymptotic tracking in the presence of nonlinear ripple dynamics. In addition, frequency-domain design approaches have been also considered to construct and design a model-free learning controller for high-performance tracking control.

2.6 Summary

Servo control of the hybrid stepping motor is complicated due to its highly nonlinear torque-current-position characteristics, especially under low operating speeds. The effect of torque ripple inherent in the hybrid stepping motor is a major obstacle in achieving high-performance tracking control at low speeds. Closed-loop control using the rotor position feedback for commutation is a common practice that is found to give an additional control dimension in the form of lead angle in addition to the voltage control for a low cost servo system. Although experimentations have shown that the torque ripple with careful adjustment of the lead angle is comparable to that of other servo motors, it is felt that there is room for further improvement on precision profile tracking where the requirement is for good control of not only the rotor position and speed, but higher orders of the dynamics. A number of other techniques using closed-loop control concept have also enjoyed various degrees of success. Most of those techniques, however, depend critically on the assumption that sufficient preknowledge is available about the motor. This limits, to a certain extent, their application in the low-speed tracking control due to imperfect knowledge and variations in the motor parameters. In addition, the control method itself for this purpose faces a significant challenge because the corresponding ripple dynamics is characterized by a time-varying and nonlinear function depending on the rotor position and speed. As a result, it is very desirable that further study should be switched to develop and exploit a set of simple and efficient control algorithms to compensate for this dynamic characteristic so as to realize high-precision tracking control of the hybrid stepping motor.

The special particularities of the physical structure associated with the hybrid stepping motor have motivated us to study some of nonlinear and intelligent control approaches within an appropriate system framework, which can be divided into two parts. The first deals with the use of modular control concept in which the feedback control module is first designed to ensure global stability and achieve bounded tracking accuracy, while the feedforward control module is added to further improve the tracking performance. By incorporating feedforward into feedback control, the feedback control part will "protect" the feedforward part to a certain extent by virtue of its good robustness property. The second rests on the utilization of the well-known direct-quadrature (DQ) transformation as a platform for control design. This transformation will easily be used to form a sinusoidal commutation pattern together with the desired control input for fast control implementation. Based on such a system framework, the principles of several control schemes will be exploited and examined in the subsequent chapters, which range from feedback linearizing control, robust adaptive control to learning control.

CHAPTER 3

MODEL–BASED CONTROL SCHEMES

3.1 Introduction

In this chapter, the model-based control approaches for both torque ripple reduction and improved tracking accuracy are considered for the closed-loop control of hybrid stepping motors. According to the mathematical nature of the motor dynamics as described in Section 3.2, the corresponding ripple dynamics can be converted into some deterministic nonlinear uncertainties, each of which is associated with either structured or parameter uncertainty. Two concrete control schemes are developed to handle such problem in order to achieve high-performance tracking control of the motor.

Section 3.3 considers a feedback linearizing control approach that employs dynamic feedback control together with feedforward compensation. This approach uses a model-based control design that targets the control of the phase current based on the DQ transformation of second-order nonlinear dynamics. A novel identification scheme based on the least-squares algorithm is first applied to estimate the model parameters for calculation of the ripple dynamics. This produces a more appropriate form of linear regression which avoids the problem of reconstructing important signals such as the rotor speed and the derivatives of driving current, and rejects additional errors created by the quantisation of the measurements. This paves the way for an integrative process for achieving precise trajectory tracking by combining a reference trajectory, the traditional PID control, and the dynamical feedback linearizing control coupled with feedforward compensation over a certain torque-ripple frequency band.

In Section 3.4, a robust adaptive control approach is considered for the purpose of improving the performance of the above scheme. In order to construct a completely integrated control design philosophy to reduce torque ripple and at the same time to enhance tracking performance, we first uncover the properties of nonlinear uncertainties in the system dynamics, and then incorporate them into the design of the controller. The system uncertainties concerned with ripple dynamics and other external disturbances are considered to be composed of two categories: The first with the form of parameter uncertainties arising from the detention effect can be separated and expressed as the product of known harmonic functions of the rotor position and a set of unknown constants. The other coupled with the control input, resulting from the nonsinusoidal flux distribution, is estimated by its bounding function. The first category of uncertainties is dealt with by means of the well-known adaptive control method. A robust adaptive method is applied to deal with the second category of uncertainties so that the torque pulsation problem of a hybrid stepping motor in a low-speed region can be solved. The $\mu-$modification scheme is applied to cease parameter adaptation in accordance with the robust adaptive control law, which initially ensures that the filtered tracking error enters a designated zone in a finite period of time, and in turn ensures that the trajectory (position) tracking error asymptotically converges to a pre-specified boundary.

In Section 3.5 the behavior of the proposed control schemes and their performance under an ideal environment are evaluated via computer simulations and experiments respectively. Different experiments are conducted and the advantages of each are discussed. A detailed analysis and discussion of the experimental results are also presented.

3.2 Modeling of Hybrid Stepping Motors

A full model of a two-phase hybrid stepping motor consists of the electrical dynamics of the stator coils together with the rotor mechanical dynamics. However, the electrical response is much faster than the mechanical response, allowing us to consider the mechanical dynamics only. The use of current amplifiers to effectively control the phase winding current at low speeds is a further justification. Additional assumptions used here are that of linear magnetic materials and symmetry between the two phases.

With these assumptions, the dynamic equation of the rotor angle is given by

$$J\ddot{\theta} = \frac{1}{2} i^T \frac{\partial L}{\partial \theta} i - T_l \tag{3.2.1}$$

where J is the equivalent inertia seen by the rotor shaft; θ is the rotor position; T_l is the load torque and frictional torque; $L \in \Re^{3\times3}$ is the $\theta-$dependent inductance matrix; $i^T = (i_a, i_b, i_r) \in \Re^{1\times3}$ in which i_a and i_b are the currents in phase a and phase b respectively, and i_r is a fictitious equivalent rotor current due to the permanent magnet used in the field generation.

Before evaluating the electric torque, we first follow a common practice of applying the so-called DQ transformation as an initial step towards linearization. This transformation transforms from the natural stator frame to a decoupled quadrature frame fixed to the rotor. The transformed decoupled and quadrature currents i_d and i_q are defined by

$$\begin{bmatrix} i_a \\ i_b \\ i_r \end{bmatrix} = \begin{bmatrix} \cos(N_r\theta) & -\sin(N_r\theta) & 0 \\ \sin(N_r\theta) & \cos(N_r\theta) & 0 \\ 0 & 0 & 1 \end{bmatrix} \begin{bmatrix} i_d \\ i_q \\ i_r \end{bmatrix}$$

where N_r is the number of pole pairs. The decoupled current i_d is so named since it does not contribute to torque production in the ideal motor. Setting $i_d = 0$, the above transformation reduces to

$$\begin{cases} i_a = -\sin(N_r\theta)\, i_q \\ i_b = \cos(N_r\theta)\, i_q \end{cases}$$

This way of determining the phase currents from the quadrature current i_q is termed *sinusoidal commutation*. This commutation, in the ideal motor, generates an electric torque proportional to the quadrature current as stated later.

For an ideal motor, each entry of the inductance matrix is a constant offset plus a pure sinusoidal function of θ whose frequency is determined by the symmetries of the motor. However, due to the nonsinusoidal gap saliency in real motors, these inductances contain phase shift and higher order harmonics. This geometric imperfection is the source of torque ripple.

Expanding the inductance in a Fourier series and setting $i_d = 0$ together with the adoption of viscous friction model, (3.2.1) is equivalent to

$$\ddot{\theta} = \frac{K_m i_q + i_q \sum_{l=1}^{\infty} [K_{qsl} \sin(lN_r\theta) + K_{qcl} \cos(lN_r\theta)]}{J}$$

$$+ \frac{\sum_{l=1}^{\infty} [K_{dsl} \sin(lN_r\theta) + K_{dcl} \cos(lN_r\theta)] - B\dot{\theta}}{J} \qquad (3.2.2)$$

where, all the K's are constant parameters that relate to torque production including the main or ideal torque term together with a number of ripple components; B is the coefficient of viscous friction.

Here we have ignored the non-ideal terms in the self and mutual phase inductances L_{aa}, L_{bb} and L_{ab} for simplification. These terms contribute to the variable reluctance torque which is usually made small in hybrid stepping motors by winding the phase coils properly. This simplification eliminates terms quadratic in i_q (also periodic in θ) in the above equation.

Suppose we want to cancel the first n harmonics. Then (3.2.1) can be further simplified to the following form:

$$\ddot{\theta} = k_m i_q + i_q \sum_{l=1}^{n} [k_{sl} \sin(lN_r\theta) + k_{cl} \cos(lN_r\theta)] + \sum_{l=1}^{n} [k_{dsl} \sin(lN_r\theta) + k_{dcl} \cos(lN_r\theta)] - b\dot{\theta} \tag{3.2.3}$$

where, $k_m = K_m / J$ is the nominal main torque constant, and all other k's (K's/J) are the normalized torque-ripple constants; $b=B/J$ is the normalized coefficient of viscous friction. All sinusoidal terms in (3.2.3) are due to geometric or physical imperfections. In other words, the second and third parts of the right hand side in (3.2.3) correspond to the ripple components caused by the harmonics in the induced EMF due to the rotor magnet, and the detent effect (Kenjo. 1994 and Chen. 1990), respectively. Neglecting these and the friction yields the ideal motor model. It is obvious from (3.2.3) that the dynamic model of the motor is characterized by a nonlinear dynamics resulting from the ripple dynamics. At low speeds, the rippling effects, especially for the detent torque, are more fully evident due to the lower momentum available to overcome the magnetic resistance, and must be considered in the design of the control system if high precision motion control is to be efficiently realized. In the light of the mathematical nature of the ripple dynamics, it is periodic with respect to the rotor position and a linear estimation model regarding all the torque-ripple constants can be easily constructed. On the other hand, the ripple component arising from the detent torque dominates the overall torque ripple spectrum which can be expressed as the product of known harmonic functions of the rotor position and a set of unknown ripple constants $[k_{dsl},\ k_{dcl}],\ l = 1,2,\cdots,n$. This has a typical form of the structured uncertainties with linear parameterization, and according to torque production mechanism, is usually bounded to about 10% of the rated torque. Furthermore, there also exists an important feature that nominal main torque constant k_m dominates the torque constant variation, i.e.,

$$\left|\sum_{l=1}^{n} k_{sl}\sin(N_r\theta) + k_{cl}\cos(N_r\theta)\right| << k_m . \tag{3.2.4}$$

The left-hand summation in (3.2.4) exactly reflects the ripple component caused by the nonsinusoidal flux distribution, and can be estimated by its bounding function in terms of its coupling with the control input (current). In conclusion, the entire ripple dynamics is associated with deterministic structures or parametric uncertainties.

In this chapter, Equation (3.2.3) will serve to establish our model-based controller for a hybrid stepping motor. The term n of the ripple components to be canceled can be determined by analyzing the torque ripple spectrum in an open-loop measurement, and this will determine the size of the controller structure. However, this problem does not need to be considered in designing the model-less-dependent or model-free controller because the controller has the inherent capability of nonlinear functional identification to compensate for ripple dynamics as explained in the subsequent chapters.

3.3 Feedback Linearizing Control Design

3.3.1 Parameter Identification Method

As a primary step towards the control design we are interested in, a parameter estimate for the motor dynamics is required to facilitate further parametrization of the feedback linearizing controller. Using the DQ model given in (3.2.3), an output equation can be formed which is linear with respect to parameters corresponding to all k's, provided that the state variables $\dot{\theta}$ (rotor speed) and θ (rotor position) are measurable. Accordingly, the least-squares algorithm can be directly applied to achieve their estimations. The number of parameters that need to be identified depends on the expected frequency components of the torque-ripple to be canceled, and this determines the scale of the least-squares solution. If the rotor speed $\dot{\theta}$ is not easily obtained, a modification has to be performed on the original output equation to eliminate the need for its reconstruction and to make the output equation rely simply on the position measurement, except for the normal phase excitation i_q.

Consider the integral equation corresponding to the model in (3.2.3):

$$\frac{d\theta}{dt} = k_m \int_0^t i_q dt + \sum_{l=1}^{n} k_{sl} \int_0^t i_q \sin(lN_r\theta)dt + k_{cl} \int_0^t i_q \cos(lN_r\theta)dt \tag{3.3.1}$$

$$+ \sum_{l=1}^{n} k_{dsl} \int_0^t \sin(lN_r\theta)dt + k_{dcl} \int_0^t \cos(lN_r\theta)dt - b\theta \, .$$

By introducing the modulating functions $\{p_j(t)\}_{j=1}^{M}$, multiplication of all terms of the integral equation model (3.3.1) to be identified and subsequently integrating both sides of the equation gives the relationship:

$$\int_0^T p_j \frac{d\theta}{dt}dt = k_m \int_0^T p_j (\int_0^t i_q d\tau)dt + \int_0^T p_j [\sum_{l=1}^n k_{sl} \int_0^t i_q \sin(lN_r\theta)d\tau]dt$$

$$+ \int_0^T p_j [\sum_{l=1}^n k_{cl} \int_0^t i_q \cos(lN_r\theta)d\tau]dt - b\int_0^T p_j \theta\, dt$$

$$+ \int_0^T p_j [\sum_{l=1}^n k_{dsl} \int_0^t \sin(lN_r\theta)d\tau]dt + \int_0^T p_j [\sum_{l=1}^n k_{dcl} \int_0^t \cos(lN_r\theta)d\tau]dt \qquad (3.3.2)$$

for each function $p_j(t)$. The modulating functions can be chosen from any set of differentiable functions over an interval [0,*T*]. In this example, the trigonometric functions $p_j(t) = \sin(j\Omega t)$ are used, however other orthogonal functions are also suitable.

The problem raised in this equation is how to find the value of the left-hand integral in equation (3.3.2) since $\dot{\theta}$ might be unmeasurable (unobservable). This problem is resolved if the { $p_j(t)$ } are selected so that their time derivatives { $\dot{p}_j(t)$ } exist. Integrating the left hand equation by parts we have:

$$\int_0^T p_j \frac{d\theta}{dt}dt = [p_j\theta]_0^T - \int_0^T \dot{p}_j \theta dt\,. \qquad (3.3.3)$$

A similar method is applied to the right-hand integral terms in (3.3.2) and gives:

$$k_m \int_0^T p_j (\int_0^t i_q d\tau)dt = k_m[(\int_0^T p_j dt)(\int_0^T i_q dt) - \int_0^T (\int_0^t p_j d\tau) i_q dt] \qquad (3.3.4)$$

$$\int_0^T p_j [\sum_{l=1}^n k_{sl} \int_0^t i_q \sin(lN_r\theta)d\tau]dt =$$
$$\sum_{l=1}^n k_{sl}[(\int_0^T p_j dt)(\int_0^T i_q \sin(lN_r\theta)dt) - \int_0^T (\int_0^t p_j d\tau) i_q \sin(lN_r\theta)dt] \qquad (3.3.5)$$

$$\int_0^T p_j [\sum_{l=1}^n k_{cl} \int_0^t i_q \cos(lN_r\theta)d\tau]dt =$$
$$\sum_{l=1}^n k_{cl}[(\int_0^T p_j dt)(\int_0^T i_q \cos(lN_r\theta)dt) - \int_0^T (\int_0^t p_j d\tau) i_q \cos(lN_r\theta)dt] \qquad (3.3.6)$$

$$\int_0^T p_j[\sum_{l=1}^{n} k_{dsl}\int_0^t \sin(lN_r\theta)d\tau]dt = \\ \sum_{l=1}^{n} k_{dsl}[(\int_0^T p_j dt)(\int_0^T \sin(lN_r\theta)dt) - \int_0^T (\int_0^t p_j d\tau)\sin(lN_r\theta)dt] \tag{3.3.7}$$

$$\int_0^T p_j[\sum_{l=1}^{n} k_{dcl}\int_0^t \cos(lN_r\theta)d\tau]dt = \\ \sum_{l=1}^{n} k_{dcl}[(\int_0^T p_j dt)(\int_0^T \cos(lN_r\theta)dt) - \int_0^T (\int_0^t p_j d\tau)\cos(lN_r\theta)dt] \tag{3.3.8}$$

To facilitate the introduction of a moderate framework in the context of the nonlinear system identification encountered here, we need to select a finite number of terms in each of the above summations relating to parameters ($k_{sl}, k_{cl}, k_{dsl}, k_{dcl}$), $l = 1, 2$ which are used to determine the predominant ripple components. Computation of the integral of (3.3.2) for M different modulating functions $\{p_j(t)\}_{j=1}^{M}$ yields:

$$\begin{pmatrix} \gamma_1 \\ \vdots \\ \gamma_M \end{pmatrix} = \begin{pmatrix} \varphi_{11} & \varphi_{12} & \varphi_{13} & \varphi_{14} & \varphi_{15} & \varphi_{16} & \varphi_{17} & \varphi_{18} & \varphi_{19} & \varphi_{110} \\ \vdots & \vdots & \vdots & \vdots & \vdots & \vdots & \vdots & \vdots & \vdots & \vdots \\ \varphi_{M1} & \varphi_{M2} & \varphi_{M3} & \varphi_{M4} & \varphi_{M5} & \varphi_{M6} & \varphi_{M7} & \varphi_{M8} & \varphi_{M9} & \varphi_{M10} \end{pmatrix} \begin{pmatrix} k_m \\ b \\ k_{s1} \\ k_{c1} \\ k_{s2} \\ k_{c2} \\ k_{ds1} \\ k_{dc1} \\ k_{ds2} \\ k_{dc2} \end{pmatrix} \tag{3.3.9}$$

where: $\gamma_j = [p_j\theta]_0^T - \int_0^T \dot{p}_j\theta dt$

$$\varphi_{j1} = (\int_0^T p_j dt)(\int_0^T i_q dt) - \int_0^T (\int_0^t p_j d\tau) i_q dt, \qquad \varphi_{j2} = -\int_0^T p_j\theta dt$$

$$\varphi_{j3} = (\int_0^T p_j dt)(\int_0^T i_q \sin(N_r\theta)dt) - \int_0^T (\int_0^t p_j d\tau) i_q \sin(N_r\theta)dt$$

$$\varphi_{j4} = (\int_0^T p_j dt)(\int_0^T i_q \sin(2N_r\theta)dt) - \int_0^T (\int_0^t p_j d\tau) i_q \sin(2N_r\theta)dt$$

$$\varphi_{j5} = (\int_0^T p_j dt)(\int_0^T i_q \cos(N_r\theta)dt) - \int_0^T (\int_0^t p_j d\tau) i_q \cos(N_r\theta)dt$$

$$\varphi_{j6} = (\int_0^T p_j dt)(\int_0^T i_q \cos(2N_r\theta)dt) - \int_0^T (\int_0^t p_j d\tau) i_q \cos(2N_r\theta)dt \quad j=1,2, ..., M$$

$$\varphi_{j7} = (\int_0^T p_j dt)(\int_0^T \sin(N_r\theta)dt) - \int_0^T (\int_0^t p_j d\tau) \sin(N_r\theta)dt$$

$$\varphi_{j8} = (\int_0^T p_j dt)(\int_0^T \cos(N_r\theta)dt) - \int_0^T (\int_0^t p_j d\tau) \cos(N_r\theta)dt$$

$$\varphi_{j9} = (\int_0^T p_j dt)(\int_0^T \sin(2N_r\theta)dt) - \int_0^T (\int_0^t p_j d\tau) \sin(2N_r\theta)dt$$

$$\varphi_{j10} = (\int_0^T p_j dt)(\int_0^T \cos(2N_r\theta)dt) - \int_0^T (\int_0^t p_j d\tau) \cos(2N_r\theta)dt .$$

By rearranging equation (3.3.9) in the form of $\gamma = \boldsymbol{\Phi} \boldsymbol{q}$ the equation is reduced to a straightforward linear estimation problem.

It is obvious from the above procedures that the updated linear regression model (3.3.9) is suitable for identification purposes. Based on the integral equation model and a power series expansion, it can successfully alleviate the problem of reconstructing the rotor speed which is the most significant source of quantization errors. In addition, the resulting integral action along with a modulating function offers the possibility of averaging and smoothing the observed variables (θ and i_q) for rejecting other noise. It is very clear that the proposed identification method overcomes the drawback of the algorithm Blauch *et al.* (1993) applied to determine the stepping motor parameters. The estimation method also does not require special re-configuration of the motor, and can be performed quickly with response data from its normal operation. An important point in the implementation is to check the numerical properties of the least-squares estimation as well as the least-squares residual sum. The computation of the $\boldsymbol{q}$ through QR factorization has been found preferable for solving our problem.

3.3.2 Dynamic Feedback Linearizing Controller

The control for smooth tracking here makes use of the assumption that at low speeds a high bandwidth current control circuit is effective in forcing the desired current through the phase windings for accurate quadrature current i_q control. A two-stage controller design will be performed in order to realize the concept. Initially, a traditional PID algorithm is employed to give a bounded but coarser control performance. Then, further refinements are introduced into the preliminary design by supplementing some of the compensating terms so as to attenuate ripple components and guarantee precise global trajectory tracking.

The tuning is achieved by first choosing $[\theta_d, \dot{\theta}_d, \ddot{\theta}_d]^T$ as a desired (reference) trajectory. Let $[\theta_d, \dot{\theta}_d]^T$ be the corresponding state trajectory and define the error state variables to be $e_1 = \dot{\theta} - \dot{\theta}_d$ and $e_2 = \theta - \theta_d$ with the addition of $e_3 = \int(\theta - \theta_d)dt$ to the error vector, i.e., $\boldsymbol{e} = [e_1, e_2, e_3]^T$, via a PID controller

$$i_q = (-g_d e_1 - g_p e_2 - g_i e_3 + \ddot{\theta}_d + b\dot{\theta}_d)/k_m$$

with g_d, g_p and g_i being constant control gains, the tracking error system equation for the system in (3.2.3) may be compactly written as:

$$\dot{\boldsymbol{e}} = \boldsymbol{A_c e} + \boldsymbol{f_1} d_{t1} + \boldsymbol{f_2} d_{t2} \tag{3.3.10}$$

where $$\boldsymbol{A_c} = \begin{bmatrix} -b-g_d & -g_p & -g_i \\ 1 & 0 & 0 \\ 0 & 1 & 0 \end{bmatrix}, \quad \boldsymbol{f_1} = \begin{bmatrix} 1 \\ 0 \\ 0 \end{bmatrix}, \quad \boldsymbol{f_2} = \begin{bmatrix} 1 \\ 0 \\ 0 \end{bmatrix}$$

$$d_{t1} = i_q \sum_{l=1}^{n} k_{sl} \sin(lN_r\theta) + k_{cl}\cos(lN_r\theta)$$

$$d_{t2} = \sum_{l=1}^{n} k_{dsl} \sin(lN_r\theta) + k_{dcl} \cos(lN_r\theta).$$

It is apparent from (3.3.10) that the tracking error dynamics produces a completely linear portion that couples with a number of state-dependent disturbances associated with the torque ripples. As the linear portion is controllable and those disturbances can reasonably be considered to be bounded, the PID feedback gain (g_p, g_i, g_d) can transform the underdamped open-loop system into a highly damped system, making the trajectory tracking algorithm quickly enter the steady-state. On the other hand, adding integral feedback adds an additional degree of freedom in the controller design, in not only drastically reducing the position error but also prompting the PID dynamical feedback control and inducing global linear behavior. By focusing on the first four terms in the summation of d_{t1} and d_{t2} that will be validated experimentally, it is suggested that a reasonable indication of this property to be true in the typical case of $N_r = 50$ is the position error $|e_2| \le 0.0025$ rad. With integral action, this position error will be satisfied easily, and thus the modified PID controller can be designed in a form easier for implementation:

$$i_q = \frac{-g_d e_1 - g_p e_2 - g_i e_3 + \ddot{\theta}_d + b\dot{\theta}_d}{k_m + \sum_{l=1}^{4}[k_{sl} \sin(lN_r\theta_d) + k_{cl} \cos(lN_r\theta_d)]}. \tag{3.3.11}$$

This is in the form of a typical dynamic feedback control law (together with part of the feedforward quantity) to linearise overall tracking dynamics as in (3.3.10) with the ripple spectrum from d_{t1} compensated for. Furthermore, the dynamic feedback gains can be computed easily provided that the position reference trajectory θ_d is given in advance.

At this stage, the global linearising effect of the dynamic feedback controller used here for low-speed operation still can not guarantee global trajectory tracking due to the persistent excitation stemming from the detent torque d_{t2}. This may now be seen as equivalent to an uncontrollable input to the tracking error system, and generally, speed ripple is still dominant at this stage. Therefore, it is desirable to add another compensator to attenuate this ripple. Fortunately, the results obtained using the feedback linearising control provide the route to develop a compound controller that can be used to achieve the final objective. The method is to add a feedforward compensator, that operates on the tracking system which has been modified by the feedback linearising scheme, to the above feedback controller that allows it to be designed and implemented in a linear control framework. Accordingly, an updated version of the controller (3.3.11) can be expressed as follows:

$$i_q = \frac{-g_d e_1 - g_p e_2 - g_i e_3 + \ddot{\theta}_d + b\dot{\theta}_d + \tau_{ff}}{k_m + \sum_{l=1}^{4}[k_{sl}\sin(lN_r\theta_d) + k_{cl}\cos(lN_r\theta_d)]} \tag{3.3.12}$$

where $\tau_{ff} = \sum_{l=1}^{4} w_{sl}\sin(lN_r\theta_d) + w_{cl}\cos(lN_r\theta_d)$ in which w_{sl} and w_{cl} are the feedforward compensating coefficients to be determined subsequently.

The method chosen to determine these coefficients is based on a time-averaged gradient (TAG) descent algorithm that relies on the speed regulation to evaluate the torque smoothness and accomplish the ripple attenuation. In fact, the compensator acts so as to attenuate speed ripple that is closely associated with the torque ripple for their coordinated reduction. By taking the detention effect coefficients estimated in the previous subsection as an initial choice, A TAG algorithm can be employed to quickly optimize the coefficients of the feedforward compensator for achieving the final control goal. A number of methods of implementing the TAG algorithm exist and may be found in the literature. The method selected in this study was based upon the Newton method (Clarkson. 1993). However, the method varied slightly where each element of the feedforward compensator was independently updated to compute the effect on the gradient.

Assuming the availability of a high-quality rotor speed signal, the speed error output for the TAG algorithm can be modeled in the discrete form as follows:

$$\begin{aligned} e_1(k) &= \sum_{n=0}^{\infty} H_d(n) d_{t2}(k-n) + \sum_{n=0}^{\infty} H(n) \tau_{ff}(k-n) \\ &= \sum_{n=0}^{\infty} H_d(n) d_{t2}(k-n) + \sum_{n=0}^{\infty} H(n) \sum_{i=1}^{N_w} w_{si} \sin(iN_r \theta_d(k-n)) + w_{ci} \cos(iN_r \theta_d(k-n)) \end{aligned}$$

(3.3.13)

where k is the time step number, H_d is the impulse response function used to model the system between d_{t2} and e_1, H is the impulse response function used to model the system between the feedforward control input τ_{ff} and e_1, (w_{si}, w_{ci}) is the ith pair of coefficients of the feedforward controller, N_w is the pair number of the feedforward compensating coefficients implemented.

The cost function is chosen as the expected value of the mean square error defined as follows:

$$J = E[e_1^2] \tag{3.3.14}$$

where E is the expectation operator. The tracking error system to be controlled is linear as explained earlier, resulting in a quadratic performance surface with a single optimal solution with respect to the feedforward coefficients (w_{si}, w_{ci}). The TAG algorithm proposed in this study employs central difference equations to estimate the first and second derivative of the cost function. Perturbation is introduced into each feedforward coefficient, which is a variable in the cost function, to find the optimal value of the cost function. The mean square error is computed over several cycles; For example, if 10 samples per period are obtained, then the averaging must occur over 10 samples. Defining $w_i \in (w_{si}, w_{ci})$, after averaging at each perturbation, the derivatives are expressed as follows:

$$\frac{\partial J}{\partial w_i} = \frac{E\{[e_1(w_i + \Delta w)]^2\} - E\{[e_1(w_i - \Delta w)]^2\}}{2\Delta w} \tag{3.3.15}$$

and

$$\frac{\partial^2 J}{\partial {w_i}^2} = \frac{E\{[e_1(w_i + \Delta w)]^2\} - 2E\{[e_1(w_i)]^2\} + E\{[e_1(w_i - \Delta w)]^2\}}{(\Delta w)^2} \tag{3.3.16}$$

where Δw is the perturbation weighted vector coefficient. Implementing a coefficient by coefficient Newton method based on the derivative estimations in Equations (3.3.15) and (3.3.16), each coefficient is updated as follows:

$$w_i(k+1) = w_i(k) - \beta(k)\Delta w \tag{3.3.17}$$

where

$$\beta(k) = \frac{E\{[e_1(w_i(k) + \Delta w)]^2\} - E\{[e_1(w_i(k) - \Delta w)]^2\}}{2(E\{[e_1(w_i(k) + \Delta w)]^2\} - 2E\{[e_1(w_i(k))]^2\} + E\{[e_1(w_i(k) - \Delta w)]^2\})}.$$

Since the feedforward coefficients are continuously updated in the TAG algorithm, the solution never rests at the optimal value for each coefficient. The system is continuously introducing an "error" in the feedforward compensator to "monitor" the performance. Theoretically, if a sufficiently small Δw is chosen, the perturbation can be used to control the residual error introduced by the compensation algorithm, which is relatively straightforward to quantify. However, we must beware that upon implementing the algorithm on the above linearized system or real systems in the presence of noise and limited dynamic range, a lower bound would be placed on the perturbation quantity Δw to maintain the prespecified speed error tolerance, which is often a measure of the speed ripple.

Remark 1: The main reason to use the TAG algorithm for the refined feedforward design is because the detent torque is a major obstacle to achieving excellent trajectory tracking performance at low speeds. An important consideration in implementing this algorithm is that by taking the estimated ripple coefficients as an initial choice, it can be employed to speed up optimization of the coefficients of the feedforward compensator.

Remark 2: In terms of discrete implementation of the TAG algorithm, two key factors must be considered. The first deals with the proper choice of the sampling rate, which will be determined by the synthesis of the frequency information of ripple harmonics, and is now chosen at 1 kHz, fast enough for our low-speed applications. The second focus is on the reasonable selection of the perturbation weighted coefficients. On the basis of the initially estimated ripple components, it is suggested that they are up to 5–10 percent of the initial values, and are diversified with specific attention being given to the dominant ripple component. It is also necessary to observe each update carefully in order to validate our design criterion.

3.4 Robust Adaptive Control Design

3.4.1 Control Formulation

To achieve tracking control, consider the error dynamics corresponding to (3.2.3) by defining a sliding surface as follows:

$$z = \dot{e} + \alpha e \tag{3.4.1}$$

where $e(t) = \theta(t) - \theta_d(t)$ and $\dot{e}(t) = \dot{\theta}(t) - \dot{\theta}_d(t)$ denotes the position and speed tracking error respectively, and α is a positive constant control gain which will be used soon. After taking the time derivative of (3.4.1), utilizing (3.2.3), and then performing simple algebraic manipulation, we obtain the following expression:

$$\dot{z} = \alpha \dot{e} - \ddot{\theta}_d + k_m \left\{ \left[1 + E_k(\theta) \right] i_q - d_t(\dot{\theta}, \theta) \right\} \tag{3.4.2}$$

where

$$E_k = \frac{1}{k_m} \sum_{l=1}^{n} k_{sl} \sin(lN_r\theta) + k_{cl} \cos(lN_r\theta) \tag{3.4.3a}$$

$$d_t = \frac{1}{k_m} [b\dot{\theta} + \sum_{l=1}^{n} k_{dsl} \sin(lN_r\theta) + k_{dcl} \cos(lN_r\theta)] . \tag{3.4.3b}$$

The following properties hold for the function E_k and d_t that will be used in the controller development and analysis.

Property 1: The parameter k_m is unknown but $k_m > 0$, and for $E_k \in \Re$, there exists a constant r such that

$$1 > E_k \geq r > -1, \qquad \forall \theta \in \Re . \tag{3.4.4}$$

Property 2: The structured uncertainty $d_t \in \Re^1$ is a typical nonlinear function which can be expressed as

$$d_t = \Theta^T \xi(\dot{\theta}, \theta) \tag{3.4.5}$$

where $\Theta^T = [b/k_m, k_{ds1}/k_m, k_{dc1}/k_m, \ldots, k_{dsn}/k_m, k_{dcn}/k_m]$ is an unknown parameter vector and $\xi^T = [\dot{\theta}, \sin(N_r\theta), \cos(N_r\theta), \cdots, \sin(nN_r\theta), \cos(nN_r\theta)]$ is a known function vector.

Property 1 follows from the fact that the main torque constant dominates the overall torque constant variation as specified by (3.2.4).

Thus, the control problem is to design a suitable control law i_q which ensures that the tracking error $z(t)$ lies in the predetermined boundary ε_0 in a finite time.

3.4.2 Robust Adaptive Control With μ-Modification

The robust adaptive control concept is used in this subsection to develop a controller which guarantees the global boundedness of the system. The design procedures are presented in detail as follows:

A. The robust adaptive control law

Define the parameter error as

$$\tilde{\Theta} = \hat{\Theta} - \Theta \,, \tag{3.4.6}$$

$$\tilde{\phi} = \hat{\phi} - \phi \tag{3.4.7}$$

where $\hat{\Theta}$ and $\hat{\phi}$ are the estimates of Θ and ϕ respectively, and

$$\phi = k_m^{-1} . \tag{3.4.8}$$

The control law i_q and the corresponding adaptive law are chosen to be

$$i_q = i_{q1} + i_{q2} \tag{3.4.9}$$

where $$i_{q1} = -k_P z + \hat{\Theta}^T \xi - \hat{\phi}(\alpha \dot{e} - \ddot{\theta}_d),$$

$$i_{q2} = -\frac{i_{q1}^2 z}{(1+r)(|z i_{q1}| + \varepsilon)},$$

with $$\dot{\hat{\Theta}} = \Gamma_1(-z\xi - \mu_1 \hat{\Theta}), \tag{3.4.10a}$$

$$\dot{\hat{\phi}} = \Gamma_2[z(\alpha \dot{e} - \ddot{\theta}_d) - \mu_2 \hat{\phi}], \tag{3.4.10b}$$

where ε is a positive constant; k_P is a positive constant control gain; Γ_i , i =1, 2 are positive constants; μ_i, i =1, 2, which constitute the μ–modification scheme, are defined as

$$\mu_i = \begin{cases} g_i(\varepsilon_0 - |z|), & z \in Z_0 \\ 0, & \text{elsewhere,} \end{cases} \tag{3.4.11}$$

where g_1 and g_2 are positive constants;

$$Z_0 = \{ z : |z| < \varepsilon_0 \} \tag{3.4.12}$$

where ε_0 is a positive constant specifying the desired tracking error bound. It is clear that i_q in (3.4.9) is a robustified adaptive control (Qu 2003 and Xu *et al*. 1997) in which i_{q1} is designed to ensure global stability and achieve adaptive estimation and cancellation of the dominant detent torque and the friction, while i_{q2} is added to further compensate for the ripple effect arising from nonsinusoidal flux distribution.

B. Convergence analysis

For the above robust adaptive controller, we have the following theorem.

Theorem 1: By choosing the control gain k_P such that $k_P \geq (\varepsilon + c)/\varepsilon_0^2$ with $c > 0$, the proposed adaptive robust control law (3.4.9)–(3.4.11) ensures that the filtered tracking error z enters the set Z_0 in a finite period of time. Moreover the tracking errors as well as the parameter estimation errors are bounded by the set

$$D = \{ z, \tilde{\Theta}, \tilde{\phi} : \ z^2 + \tilde{\Theta}^T \tilde{\Theta} + \tilde{\phi}^2 < g'[\tfrac{1}{2} g_1 \varepsilon_0 \Theta^T \Theta + \tfrac{1}{2} g_2 \varepsilon_0 \phi^2 + \varepsilon]\} \qquad (3.4.13)$$

where g' is defined to be

$$g' = \frac{1}{g'' \min\{ k_m^{-1}, \Gamma_1^{-1}, \Gamma_2^{-1}\}},$$

$$g'' = \frac{2\min\left\{ k_P, \ g_1\delta, \ g_2\delta \right\}}{\max\{ k_m^{-1}, \ \Gamma_1^{-1}, \ \Gamma_2^{-1}\}},$$

and δ is a positive value to be defined later.

Proof: To prove Theorem 1, we define a Lyapunov function $V(t) \in \Re^1$ as follows:

$$V = \tfrac{1}{2} k_m^{-1} z^2 + \tfrac{1}{2} \Gamma_1^{-1} \tilde{\Theta}^T \tilde{\Theta} + \tfrac{1}{2} \Gamma_2^{-1} \tilde{\phi}^2 . \qquad (3.4.14)$$

Taking the derivative of *V* along the trajectory of the dynamics (3.4.2) with the control (3.4.9) and (3.4.10), we have

$$\begin{aligned}
\dot{V} &= k_m^{-1} z \dot{z} + \Gamma_1^{-1} \tilde{\Theta}^T \dot{\hat{\Theta}} + \Gamma_2^{-1} \tilde{\phi} \dot{\hat{\phi}} \\
&= k_m^{-1} z \left\{ \alpha \dot{e} - \ddot{\theta}_d + k_m [(1+E_k) i_q - \Theta^T \xi] \right\} + \Gamma_1^{-1} \tilde{\Theta}^T \dot{\hat{\Theta}} + \Gamma_2^{-1} \tilde{\phi} \dot{\hat{\phi}} \\
&= z \left\{ -\Theta^T \xi + \phi(\alpha \dot{e} - \ddot{\theta}_d) + (1+E_k)(i_{q1} + i_{q2}) \right\} \\
&\qquad + \tilde{\Theta}^T (-z\xi - \mu_1 \hat{\Theta}) + \tilde{\phi}[z(\alpha \dot{e} - \ddot{\theta}_d) - \mu_2 \hat{\phi}] \\
&= z[-\Theta^T \xi + \phi(\alpha \dot{e} - \ddot{\theta}_d) + (1+E_k) i_{q2} + E_k i_{q1} \\
&\qquad - k_P z + \hat{\Theta}^T \xi - \hat{\phi}(\alpha \dot{e} - \ddot{\theta}_d)] - z\tilde{\Theta}^T \xi + z\tilde{\phi}(\alpha \dot{e} - \ddot{\theta}_d) \\
&\qquad - \mu_1 \tilde{\Theta}^T \hat{\Theta} - \mu_2 \tilde{\phi} \hat{\phi} \\
&= z[\tilde{\Theta}^T \xi - \tilde{\phi}(\alpha \dot{e} - \ddot{\theta}_d) + (1+E_k) i_{q2} + E_k i_{q1} - k_P z] \\
&\qquad - z\tilde{\Theta}^T \xi + z\tilde{\phi}(\alpha \dot{e} - \ddot{\theta}_d) - \mu_1 \tilde{\Theta}^T \hat{\Theta} - \mu_2 \tilde{\phi} \hat{\phi}
\end{aligned}$$

$$\leq -k_P z^2 - \frac{(1+E_k)\, i_{q1}^2 z^2}{(1+r)(\left|z i_{q1}\right| + \varepsilon)} + \left|z i_{q1}\right| - \mu_1 \tilde{\Theta}^T \hat{\Theta} - \mu_2 \tilde{\phi} \hat{\phi}\,. \tag{3.4.15}$$

Using the fact that

$$\frac{1+E_k}{1+r} \geq 1,$$

it follows that

$$\begin{aligned}
\dot{V} &\leq -k_P z^2 - \mu_1 \tilde{\Theta}^T \hat{\Theta} - \mu_2 \tilde{\phi} \hat{\phi} + \varepsilon \\
&\leq -k_P z^2 - \mu_1 \tilde{\Theta}^T (\tilde{\Theta} + \Theta) - \mu_2 \tilde{\phi} (\tilde{\phi} + \phi) + \varepsilon \\
&\leq -k_P z^2 - \mu_1 \tilde{\Theta}^T \tilde{\Theta} - \mu_1 \tilde{\Theta}^T \Theta - \mu_2 \tilde{\phi}^2 - \mu_2 \tilde{\phi} \phi + \varepsilon \\
&\leq -k_P z^2 - \tfrac{1}{2} \mu_1 \tilde{\Theta}^T \tilde{\Theta} - \tfrac{1}{2} \mu_2 \tilde{\phi}^2 + \tfrac{1}{2} \mu_1 \Theta^T \Theta + \tfrac{1}{2} \mu_2 \phi^2 + \varepsilon\,.
\end{aligned} \tag{3.4.16}$$

By choosing k_P such that

$$k_P \geq (\varepsilon + c) \big/ \varepsilon_0^2\,, \tag{3.4.17}$$

where c is an arbitrary positive constant, then from (3.4.11) we have

$$\dot{V} \leq -k_P z^2 + \varepsilon \leq -c, \quad \forall z \in \Re - Z_0\,. \tag{3.4.18}$$

Note that, in terms of the robust adaptive control law (3.4.9)-(3.4.11), $\dot{V}$ is a continuous function. We can show that there exists a constant $0 < \varepsilon_0' < \varepsilon_0$ such that (see Appendix A)

$$\dot{V} < 0, \quad \forall z \in \Re - Z_0'\,, \tag{3.4.19}$$

where $Z_0' = \{ z : |z| < \varepsilon_0' \}$ is a subset of Z_0. Noting the relation $Z_0' \subset Z_0$, (3.4.19) implies that the system will enter the set Z_0 in a finite time.

When $z \in Z_0'$, it is obvious that

$$g_i(\varepsilon_0 - \varepsilon_0') \le \mu_i \le g_i \varepsilon_0, \quad i = 1, 2. \tag{3.4.20}$$

Define $\delta = \varepsilon_0 - \varepsilon_0' > 0$, then from (3.4.11), (3.4.16) and (3.4.20) we obtain

$$\begin{aligned}\dot{V} &\le -k_P z^2 - \tfrac{1}{2}\mu_1 \tilde{\Theta}^T \tilde{\Theta} - \tfrac{1}{2}\mu_2 \tilde{\phi}^2 + \tfrac{1}{2}\mu_1 \Theta^T \Theta + \tfrac{1}{2}\mu_2 \phi^2 + \varepsilon \\ &\le -k_P z^2 - \tfrac{1}{2} g_1 \delta \tilde{\Theta}^T \tilde{\Theta} - \tfrac{1}{2} g_2 \delta \tilde{\phi}^2 + \tfrac{1}{2} g_1 \varepsilon_0 \Theta^T \Theta + \tfrac{1}{2} g_2 \varepsilon_0 \phi^2 + \varepsilon \\ &\le -g'' V + \tfrac{1}{2} g_1 \varepsilon_0 \Theta^T \Theta + \tfrac{1}{2} g_2 \varepsilon_0 \phi^2 + \varepsilon \end{aligned} \tag{3.4.21}$$

where

$$g'' = \frac{2\min\{\, k_P,\, g_1\delta,\, g_2\delta \,\}}{\max\{\, k_m^{-1},\, \Gamma_1^{-1},\, \Gamma_2^{-1}\}}.$$

By solving (3.4.21) we can establish that

$$V(t) \le -e^{-g'' t} V(0) + \frac{1}{g''}[\tfrac{1}{2} g_1 \varepsilon_0 \Theta^T \Theta + \tfrac{1}{2} g_2 \varepsilon_0 \phi^2 + \varepsilon]$$

which implies that $z, \tilde{\Theta},$ and $\tilde{\phi}$ converge exponentially to the residual set

$$D = \{\, z, \tilde{\Theta}, \tilde{\phi} :\ z^2 + \tilde{\Theta}^T \tilde{\Theta} + \tilde{\phi}^2 < g'[\tfrac{1}{2} g_1 \varepsilon_0 \Theta^T \Theta + \tfrac{1}{2} g_2 \varepsilon_0 \phi^2 + \varepsilon]\} \tag{3.4.22}$$

where

$$g' = \frac{1}{g'' \min\{\, k_m^{-1},\, \Gamma_1^{-1},\, \Gamma_2^{-1}\}}$$

which completes the proof.

Remark 3: From the previous convergence analysis, it is observed that by means of Lyapunov-based technique the control law given by (3.4.9) with (3.4.10)–(3.4.11) can ensure that the parameters are uniformly bounded and that the filtered tracking error $|z(t)| < \varepsilon_0$ in a finite time. In addition, $z(t) = \dot{e}(t) + \alpha\, e(t)$ corresponds to a stable sliding surface because α is a positive constant, which in turn implies that $|\dot{e}(t)+\alpha\, e(t)|<\varepsilon_0$ leads to $\dot{e}(t)\to 0$, $|e(t)|<\varepsilon_0/\alpha$ as $t\to\infty$ according to the comparison principle; Hence the position tracking error asymptotically converges to a designated boundary ε_0/α .

Remark 4: Notice that $k_P z$ in the control law is actually standard PI control. In principle, any existing PI tuning method can be employed to tune and determine k_P, α subject to (3.4.17). In light of the entire control law, this initial tuning is just a rough one, since the system performance must be improved by the adaptive feedforward components included in the control law.

Remark 5: The control input is greatly dependent on the choice of the design parameters ε_0 and ε. The greater the parameter ε, the smoother is the control input. Note that, if ε is set to zero, the control scheme is discontinuous. From (3.4.17), we can also see that ε_0 has great influence on the control gain k_P, and a smaller ε_0 results in a larger gain. Therefore, there should be a trade-off between the desired tracking error and the discontinuity of the input which is tolerable.

3.5 Simulation and Experimental Results

In this section, the proposed control schemes were simulated and experimentally verified using a stepping motor servo, with a typical hybrid stepping motor for tracking at low speed. The feedback linearizing control approach was first examined. The model parameters were identified using the above mentioned least-squares technique. A computer simulation was used to evaluate the behavior of this control scheme, and its performance under an ideal environment. The results were compared with the conventional control algorithm in terms of the active suppression of speed ripple in tracking a constant reference speed. Then, practical experiments were performed with the typical hybrid stepping motor to demonstrate the feasibility of the two control schemes. By the same token, their capabilities in profile tracking were tested and compared with each other.

The desired reference position θ_d, speed $\dot{\theta}_d$, and acceleration $\ddot{\theta}_d$ were chosen so as to make the motor system operate at a rotor speed of around 3.14 rad/s (30 rpm). The steady-state behaviour of the closed-loop system was first investigated. Traditional PID feedback control was used at $t = 0$. The controlled speed and position error of the motor are presented in Fig. 3.1(a) and Fig. 3.2(a), respectively. It is found from these figures that the PID control adds significant damping to the motor system which makes the closed-loop system settle quickly to the steady-state condition. The integral feedback action has reduced the position error to within 0.0025 rad, which further indicates that the PID dynamic feedback control as given in (3.3.11) is effective. The modified feedback controller has worked well in the simulation, and has been able to improve the ripple structure as depicted in Fig. 3.1(b).

The point to be noted in Fig. 3.1 is that whilst the feedback controller maintains the high speed tracking capability and the ripple compensation to a certain extent, there is still dominant speed oscillation coming from the undesired continuous disturbance associated with the detent effect. The frequency of this speed oscillation is equal to that of the disturbance. When the feedforward compensation is added to the feedback control scheme, as evident in Fig. 3.1(c), the combined controller is capable of minimising the speed tracking error by 28 dB, with the remaining speed ripple staying within 1% of the reference value. Another benefit from this controller is the significant improvement in positioning accuracy where the position error has been decreased to below 0.0005 *rad* as illustrated in Fig. 3.2(b). Obviously, the two control parts used in the feedback linearizing controller are complementary in their performances as predicted in the preceding analysis. With this control, the actual tracking accuracy will be restricted only by the resolution of the position measurement or estimation rather than the step resolution of the motor.

With the improved performance in tracking the constant reference speed, the capacity of the feedback linearizing controller to generate different kinds of profiles is demonstrated through further simulation. Two typical profile tracking problems were attempted that cover the trapezoidal and sinusoidal contours. The results, as shown in Fig. 3.3, have a reasonably small ripple component.

Next, experiments were performed with a typical two-phase bifilar-wound hybrid stepping motor with 50 rotor teeth (1.8° per step). The rotor position and speed were obtained by using the well-known MT method along with an optical encoder of 4000 pulses per revolution.

The proposed control algorithms were implemented on a TMS320C30 DSP chip. The corresponding trigonometric functions as in (3.3.12) along with the reference control input (phase currents) from sinusoidal commutation were stored and updated in a look-up table in the RAM for fast control configuration. The reference phase currents were delivered to the high bandwidth current control circuit. The block diagram for the experimental setup is shown in Fig. 3.4.

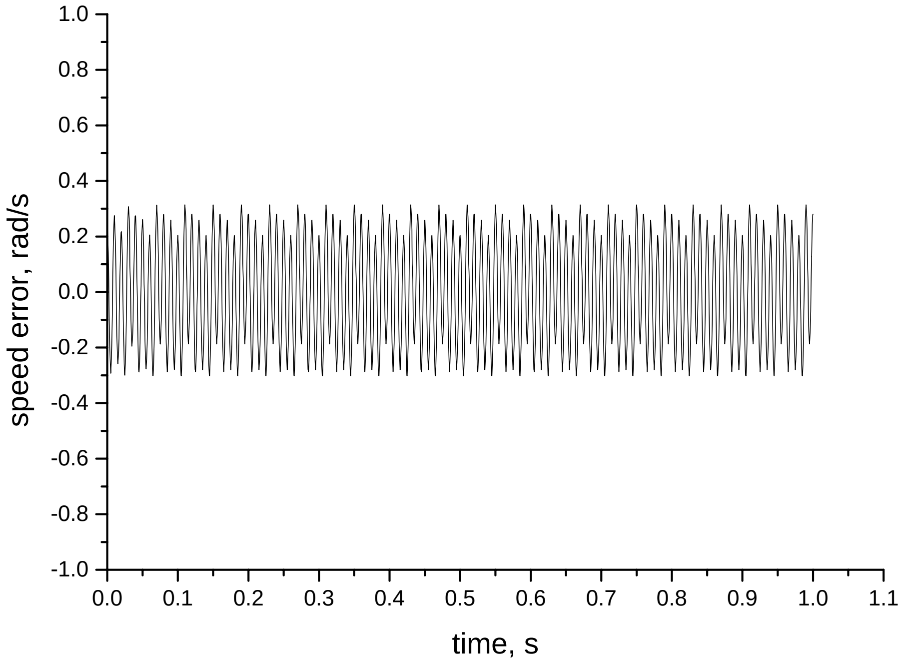
1.0
0.8
0.6
0.4
0.2
0.0
-0.2
-0.4
-0.6
-0.8
-1.0
speed error, rad/s
0.0
0.1
0.2
0.3
0.4
0.5
0.6
0.7
0.8
0.9
1.0
1.1
time, s

a

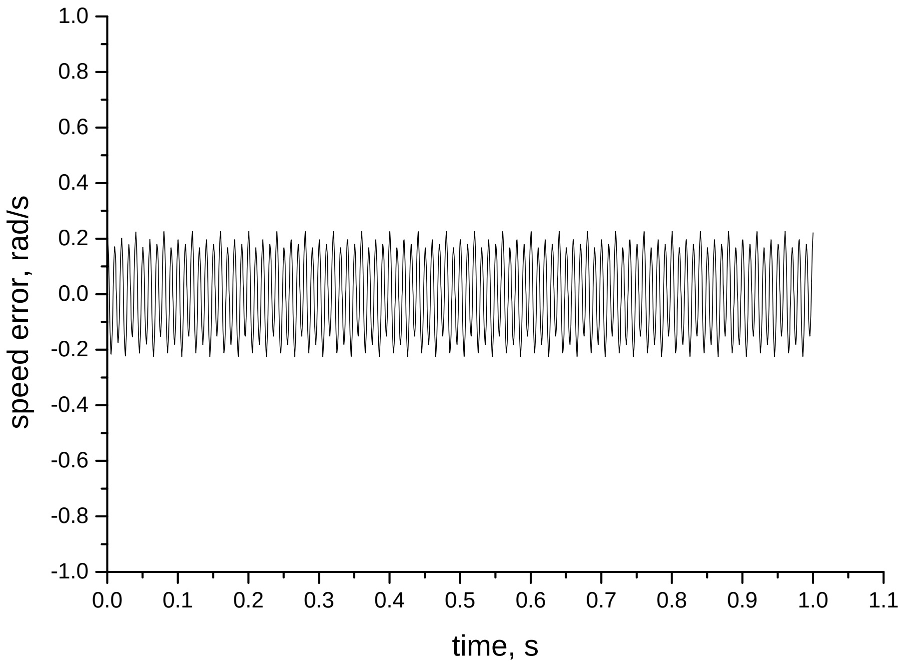
1.0
0.8
0.6
0.4
0.2
0.0
-0.2
-0.4
-0.6
-0.8
-1.0
speed error, rad/s
0.0
0.1
0.2
0.3
0.4
0.5
0.6
0.7
0.8
0.9
1.0
1.1
time, s

b

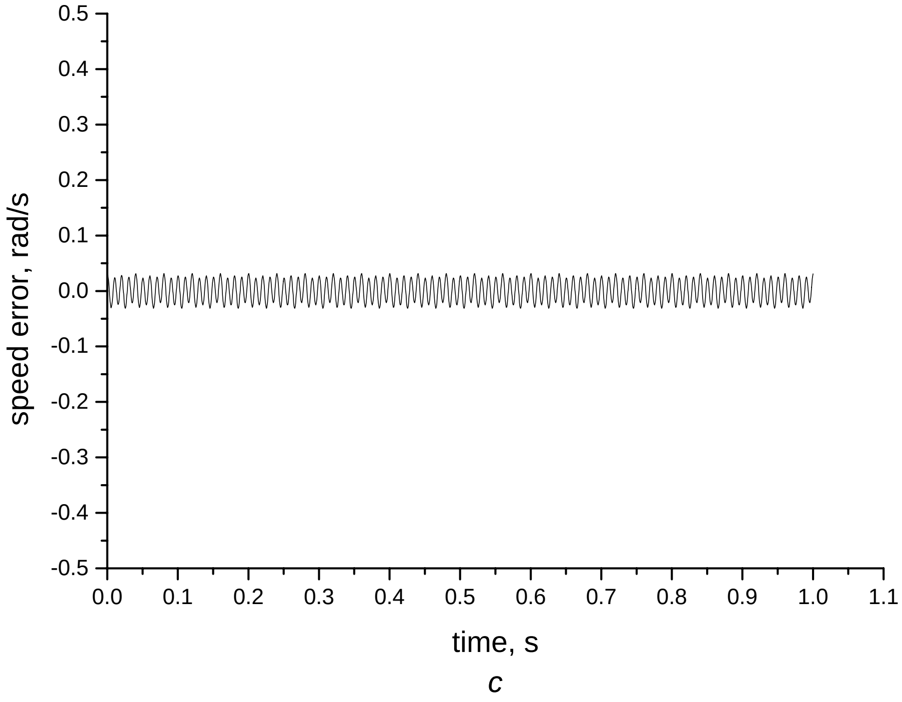

Fig. 3.1 Simulation results of PID control and proposed control scheme
(a) Speed error of PID control
(b) Speed error of modified PID control
(c) Speed error of feedback linearizing control

To show the effectiveness of the proposed control schemes, the experimental performance based on the feedback linearizing control is first compared with that of the conventional sinusoidal current control system, and then with the robust adaptive control. The experimental results of the three schemes are summarized in Fig. 3.5–3.8. Fig. 3.5 shows the speed tracking error, where the reference speed is given as 30 rpm (same as in the simulation) and the PI controller is employed as a speed regulator in the outer loop of these schemes. It is observed in Fig. 3.5(a) that the torque ripple causes the speed fluctuation in the pure sinusoidal control. However, this can be effectively reduced by using the proposed feedback linearizing control as shown in Fig. 3.5(b). The speed ripple factor defined as $\mathrm{SRF} \cong (\dot{\theta}_{peak} - \dot{\theta}_d)/\dot{\theta}_d$ is adopted to evaluate the control

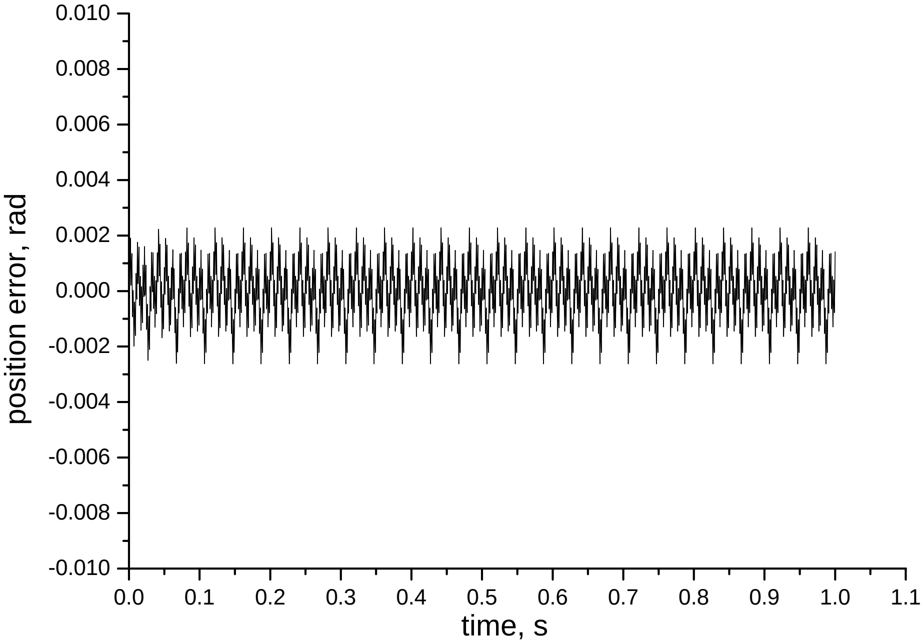

a

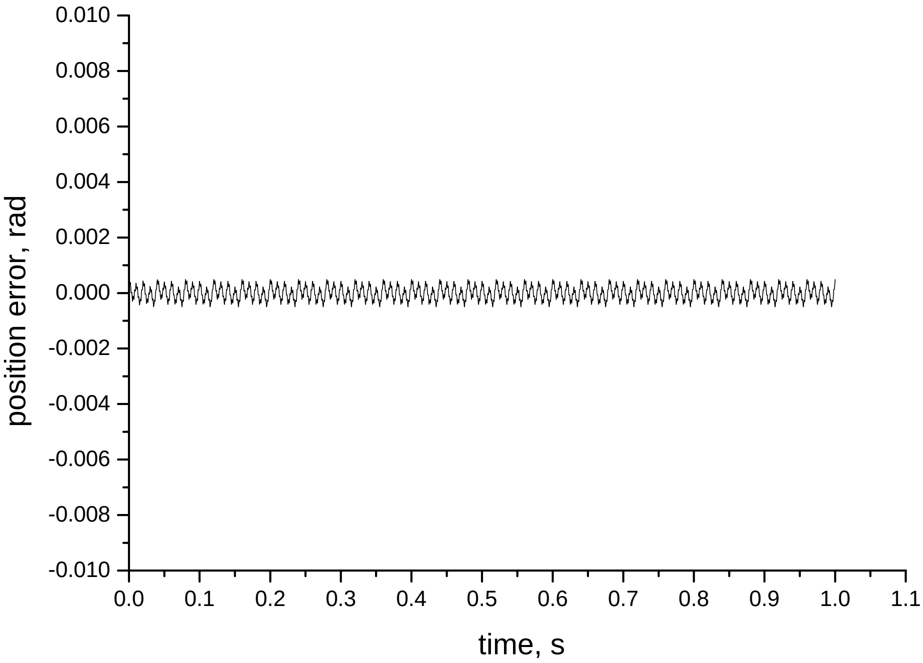

b

Fig. 3.2 Steady-state time histories of controlled position errors
(a) Position error of PID control
(b) Position error of feedback linearizing control

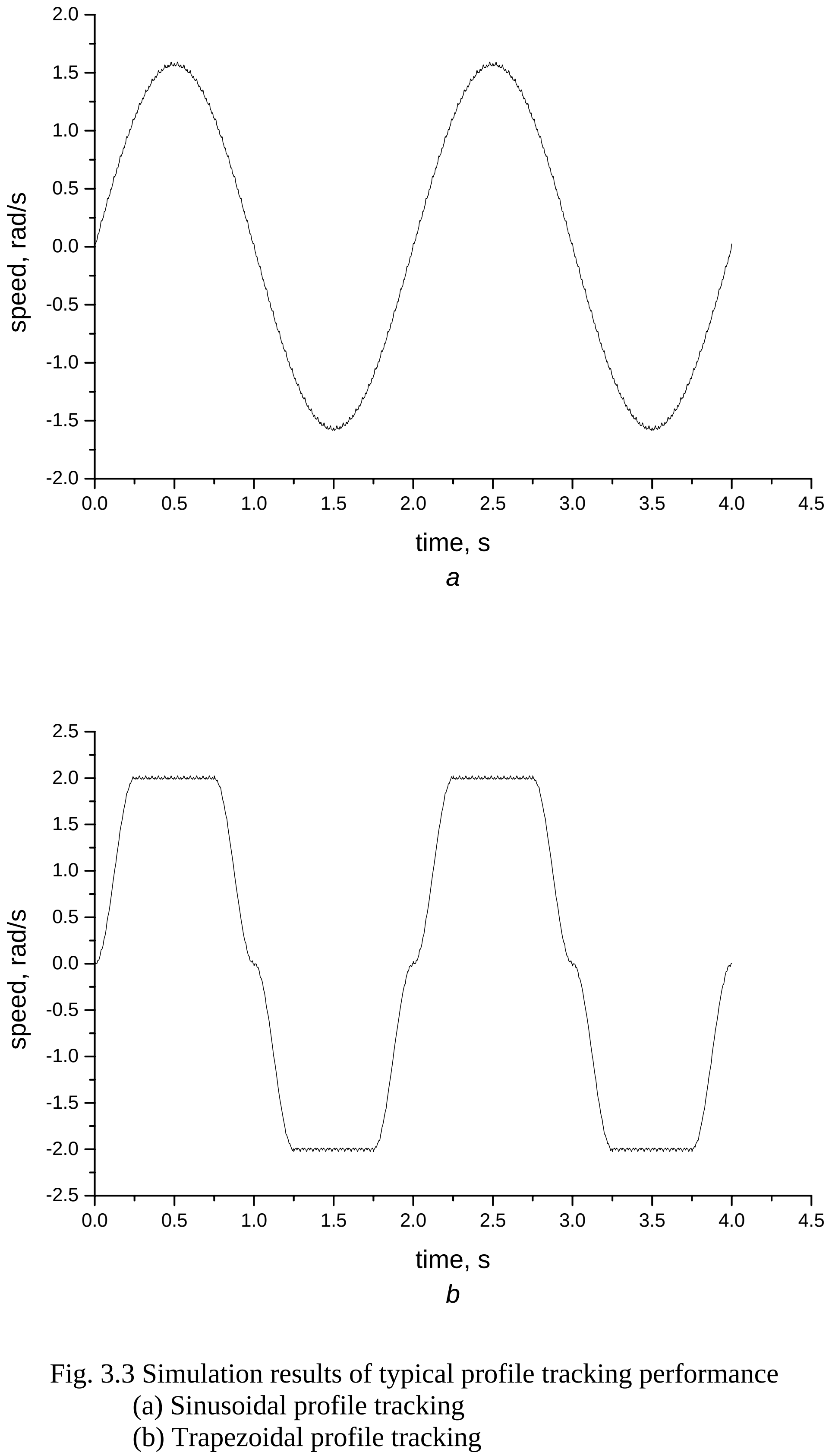

Fig. 3.3 Simulation results of typical profile tracking performance
(a) Sinusoidal profile tracking
(b) Trapezoidal profile tracking

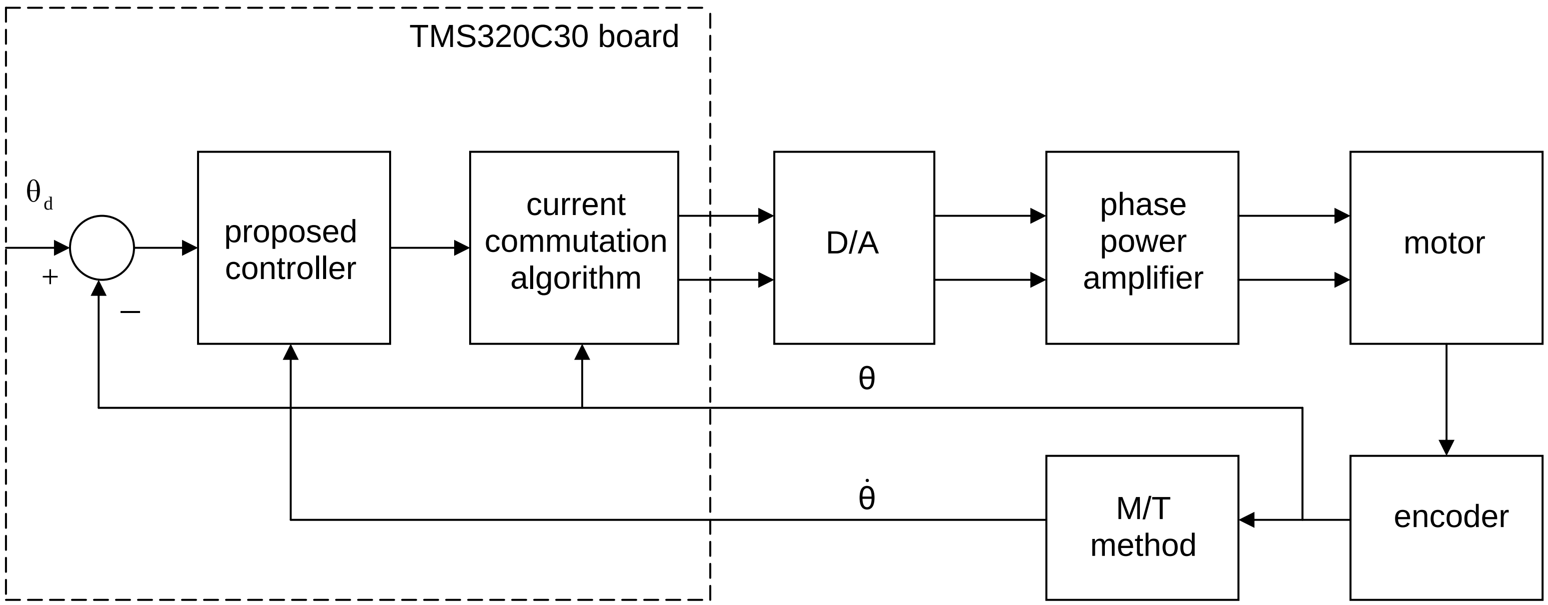

Fig. 3.4 Block diagram representation of the experimental setup

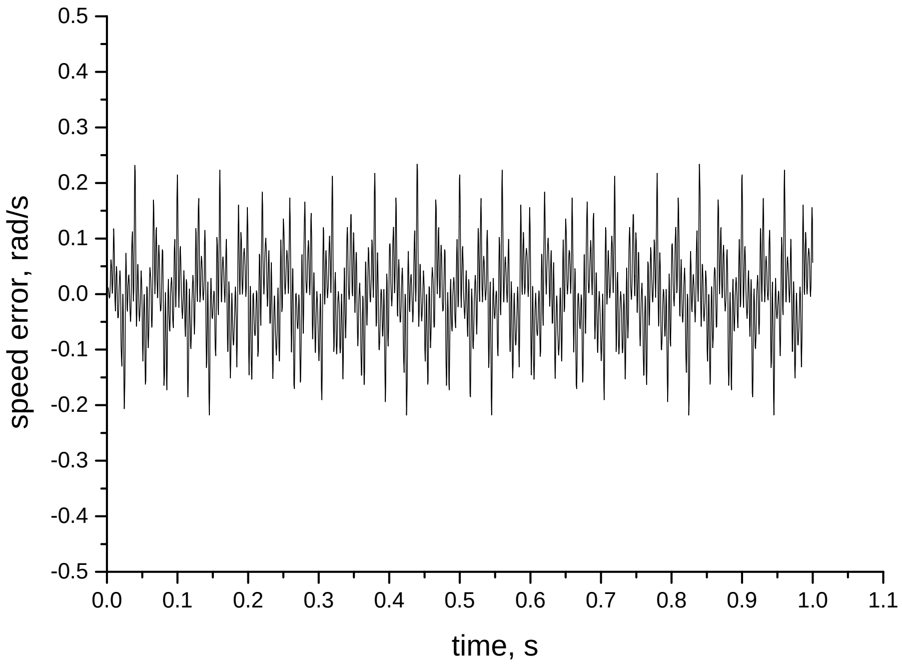

a

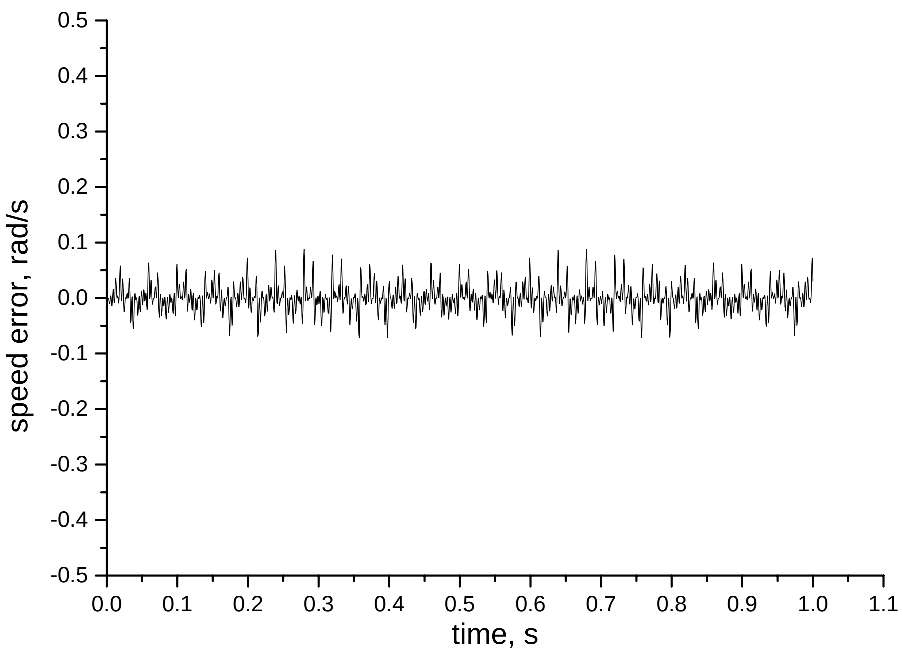

b

Fig. 3.5 Speed errors of sinusoidal current control and proposed control scheme
(a) Sinusoidal current control
(b) Feedback linearizing control

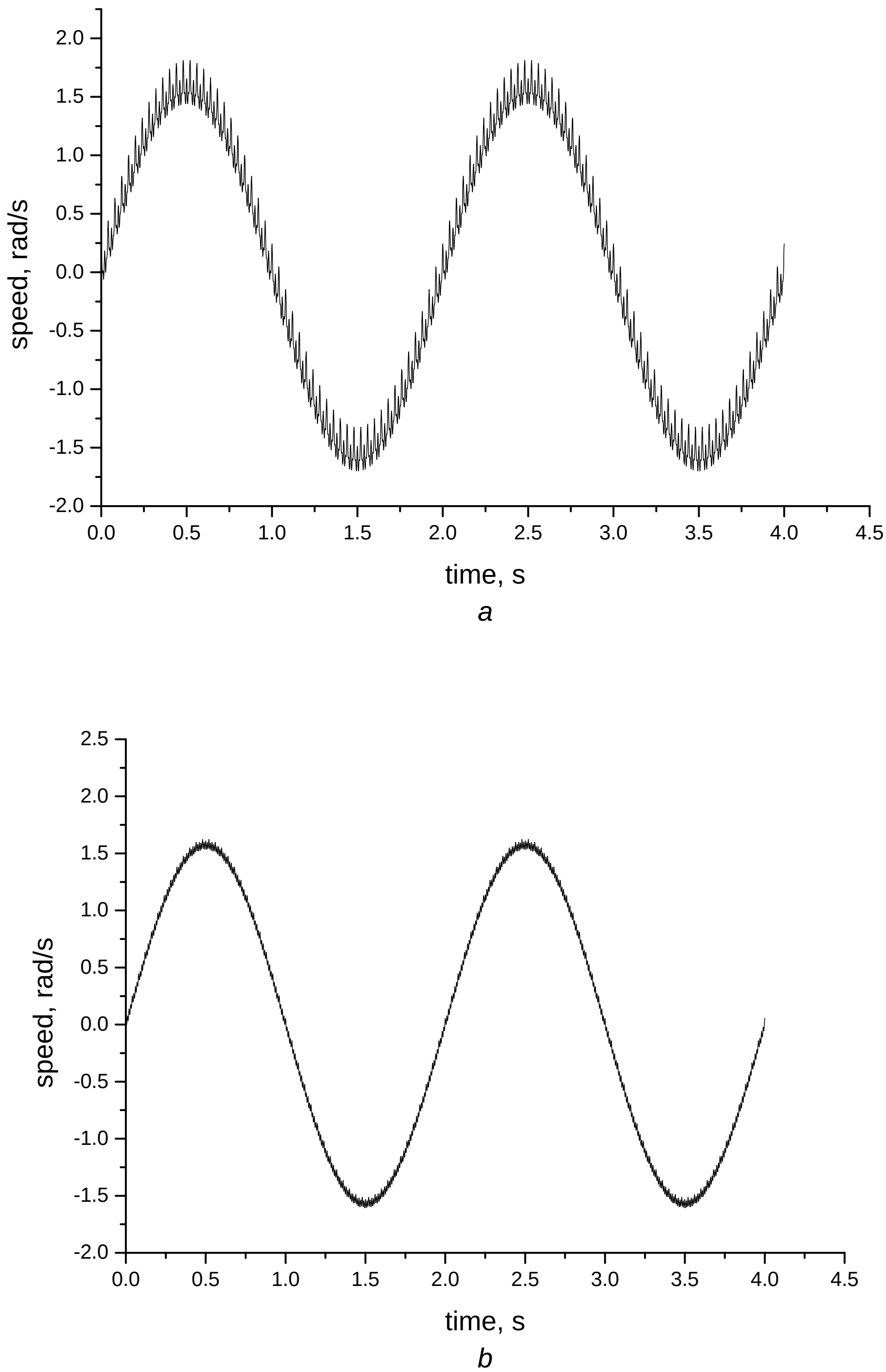

Fig. 3.6 Steady-state behavior of sinusoidal profile tracking
(a) Sinusoidal current control
(b) Feedback linearizing control

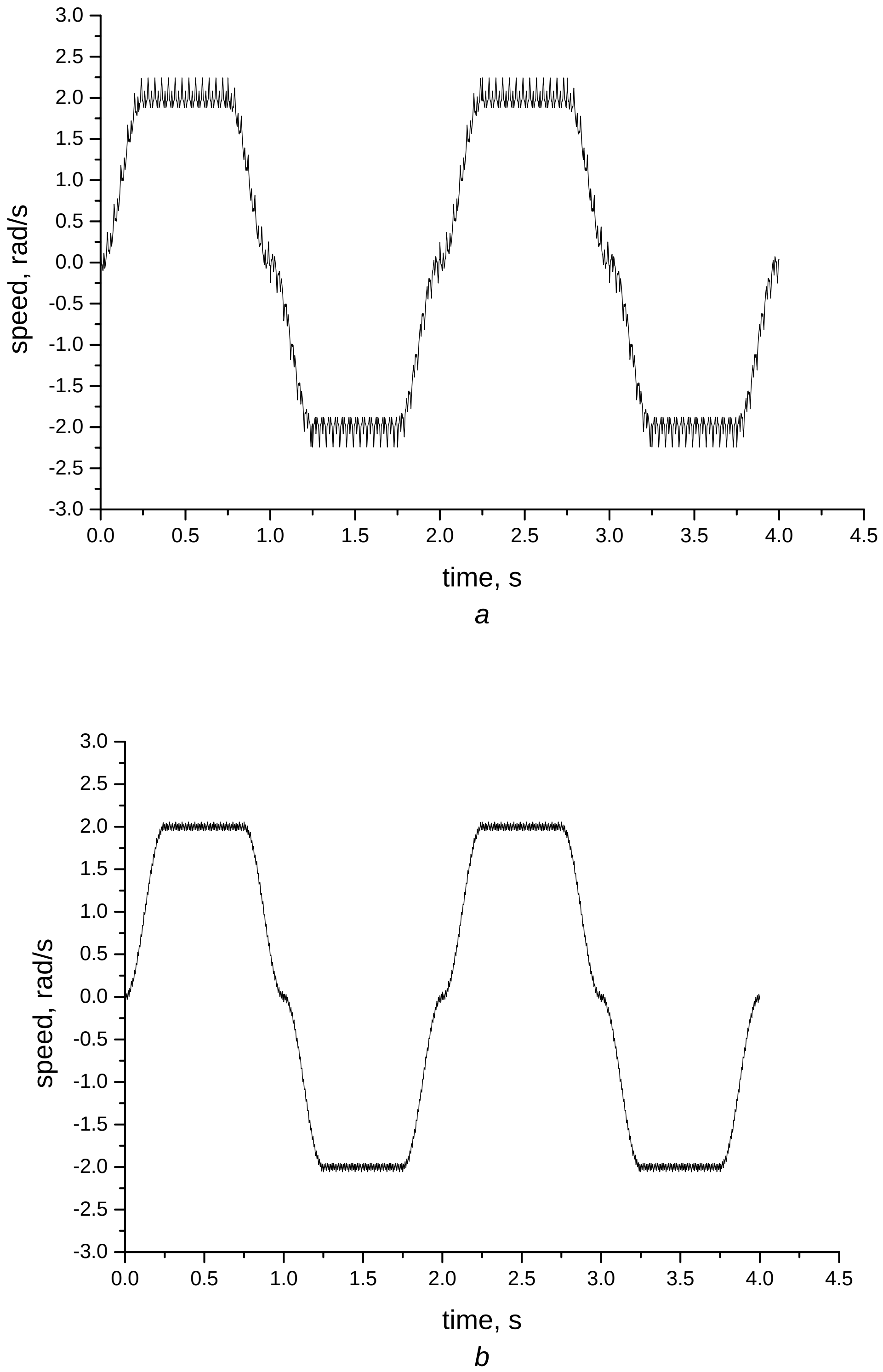

Fig. 3.7 Steady-state behavior of trapezoidal profile tracking
(a) Sinusoidal current control
(b) Feedback linearizing control

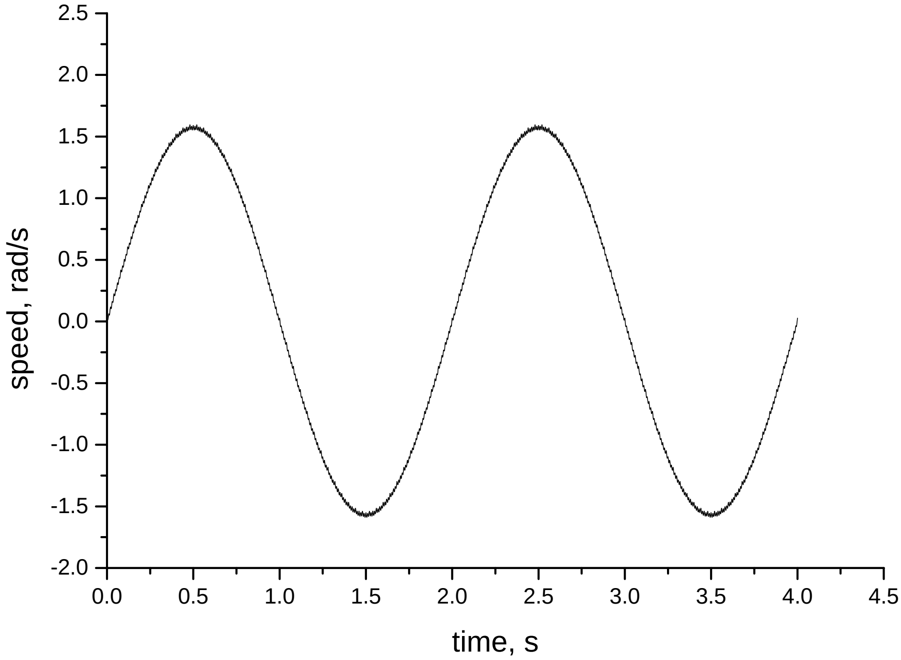

a

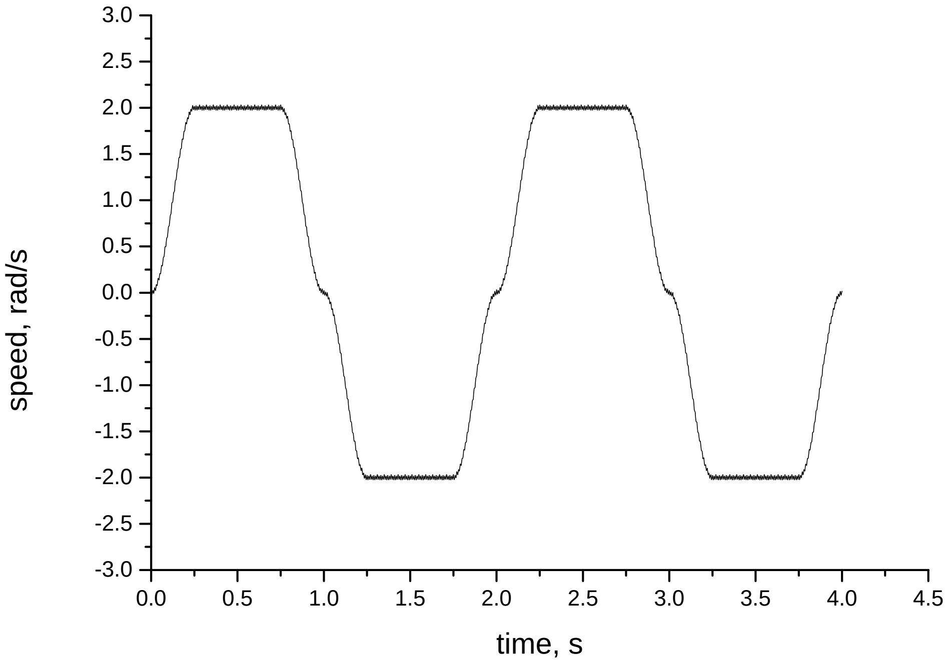

b

Fig. 3.8 Profile tracking performance of robust adaptive control
(a) Sinusoidal profile tracking
(b) Trapezoidal profile tracking

performance quantitatively. The SRF in the proposed scheme is greatly reduced, to about 30% of that in the conventional scheme. In addition, from Fig. 3.6 and Fig. 3.7, we can see that the good speed control performance shown previously has clearly indicated the ability of the feedback linearizing control to improve the profile tracking performance.

To further illustrate the performance enhancement from the use of the proposed robust adaptive controller, control results, as shown in Fig. 3.8, considering similar profiling tracking tasks were evaluated. The effect of the adaptive feedforward component introduced into this control scheme is clearly manifested in the tracking error signals. A comparison between Fig. 3.6b and Fig. 3.8a as well as Fig 3.7b and Fig. 3.8b shows that the use of the robust adaptive controller is not only more effective in reducing the tracking error, but also more useful in eliminating or reducing the inherent torque ripple. The quantification of the performance comparison has indicated that the SRF in this control scheme is reduced to about half of that in the feedback linearizing approach. A radical reason to induce such a performance difference lies in that the former directly incorporated the adaptive ripple compensation (feedforward) into feedback control part for both the stability analysis and the guaranteed control specification, while the latter separated the feedforward design from the feedback one with the special constraint of ripple compensating terms. As a result, the robust adaptive control scheme provides the advantage of suppressing the torque ripple components over a broader ripple frequency band. It is, however, worth noting that the tracking boundary parameter (such as ε_0) included in the control design should be carefully determined to prevent possible control chattering. In conclusion, the experimental results seem to support the theoretical results presented in Section 3.3 and Section 3.4, and demonstrated the practical use of the proposed control algorithms.

3.6 Summary

The low-speed tracking problems associated with hybrid stepping motor drives where the effect of torque ripple is dominant, have been addressed by the use of the model-based control approaches that employ dynamic or nonlinear feedback control together with feedforward compensation. The DQ transformation has been used to provide a framework for identifying the ripple dynamics and for designing the corresponding control strategies. This has been shown to be useful in the facilitation of the desired sinusoidal commutation scheme for fast control implementation. The interaction between the feedforward and feedback control approaches has been explored and they have been shown to be complementary to each other.

In the feedback linearizing control scheme, the new model identification procedure that operates on the measurable position signal and phase current offers attractive features that promise to avoid any significant injection of quantization errors and also to reject other possible noise sources without strict limitations on the operating mode of the motor. The feedback controller that incorporates knowledge of both the ripple dynamics and the motion itself has successfully linearised the system as long as an appropriate choice of control gains is made with sufficient emphasis on integral control. The analysis, simulations and experiments have shown that the derived feedback control permits the motion tracking error system to respond quickly, and reject part of the ripple components. However, the feedback controller alone is not able to create the best speed tracking performance because of the forced excitation caused by the detent torque. This problem has been resolved by the introduction of feedforward compensation. The addition of the feedforward controller significantly improves global tracking results with the speed ripple being suppressed to a reasonably low level.

To further improve the tracking control performance, a robust adaptive control scheme is presented to tackle the torque ripple problem using an integrated control design. The structured uncertainty arising from the dominant detention effect can be separated and expressed as the product of known harmonic functions of the rotor position and a set of unknown constants. This uncertainty is estimated with adaptation and compensated for. The robust adaptive concept is applied to deal with other structured uncertainty resulting from the nonsinusoidal flux distribution, by estimating its bounding constants. The $\mu-$modification scheme is applied to cause parameter adaptation to cease in accordance with the robust adaptive control law. This control scheme can guarantee the uniform boundedness of the motor drive system and assures that the tracking error enters an arbitrarily designated zone in a finite time. A performance comparison between both model-based control schemes gives an impressive result. Finally, given their simple form the potential application of the proposed control algorithms may be easily realized.

CHAPTER 4

REPETITIVE LEARNING CONTROL SCHEMES

4.1 Introduction

In this chapter, a class of model-less-dependent learning approaches is developed for the high-precision motion control of a hybrid stepping motor. The control will minimize torque ripple in the motor with specific emphasis on low-speed conditions. The torque ripple is periodic and nonlinear in the system states. The learning control employs a modified standard repetitive update rule and has a very simple structure consisting of two time-domain components in additive form: a feedback control mechanism using either a pure linear form or some nonlinear form, and a learning mechanism using a saturation function that simply adds up a past tracking error sequence. To ensure that the stability analysis accommodates the use of the saturation function in the standard repetitive update rule, a Lyapunov-based approach, as introduced in Section 4.2, is first utilized. This will illustrate the generality of the learning-based update law and its ability to force a general error system with a nonlinear disturbance to achieve global asymptotic tracking within a defined period.

Impelled by such a design philosophy, two concrete learning control schemes are then considered in Section 4.3 and Section 4.4 respectively. Under the boundedness and Lipschitz continuity conditions of the system dynamics, both the Lyapunov-based technique and other performance analysis techniques are used to design the learning-based controller. The controller will compensate for nonlinear ripple dynamics and assure global motion tracking. A rigorous analysis of the convergence of the proposed update scheme is presented. It is revealed that all the error signals in the learning control system are bounded and the motion trajectory converges to the desired value asymptotically. The proposed control scheme, as opposed to a multiple step process, is updated continuously with time during the transient response (versus during the steady-state), and hence, an improved transient response is facilitated. Experiments are performed with a typical hybrid stepping motor to test its profile tracking performance, which is evaluated in Section 4.5. Results demonstrate that low-speed high-precision tracking control of the hybrid stepping motor is attainable.

4.2 General Problem

To illustrate the generality of the proposed learning control scheme, we consider the following error dynamics:

$$\dot{e} = f(t,e) + B(t,e)[w(t) - \hat{w}(t)] \tag{4.2.1}$$

where $e(t) \in \Re^n$ is an error vector, $w(t) \in \Re^m$ is an unknown nonlinear function, $\hat{w}(t) \in \Re^m$ is a subsequently designed learning-based estimate of $w(t)$, and the auxiliary functions $f(t,e) \in \Re^n$ and $B(t,e) \in \Re^{n \times m}$ are bounded provided $e(t)$ is bounded. We further assume that (4.2.1) satisfies the following assumptions.

Assumption 1: The origin of the error system $e(t) = 0$ is uniformly asymptotically stable for

$$\dot{e} = f(t,e). \tag{4.2.2}$$

Furthermore, there exists a first-order differentiable, positive-definite function $V_1(e,t) \in \Re$, a positive-definite, symmetric matrix $Q(t) \in \Re^{n \times n}$, and a known matrix $R(t) \in \Re^{n \times m}$ such that

$$\dot{V}_1 \leq -e^T Qe + e^T R[w - \hat{w}]. \tag{4.2.3}$$

Assumption 2: The unknown nonlinear function $w(t)$ is periodic with a known period *T*; hence,

$$w(t-T) = w(t). \tag{4.2.4}$$

Furthermore, we assume that the unknown function $w(t)$ is bounded as follows:

$$|w_i(t)| \leq \beta_i, \quad \text{for } i = 1, 2, ..., m \tag{4.2.5}$$

where $\beta = [\beta_1 \ \ \beta_2 \ \ \cdots \ \ \beta_m] \in \Re^m$ is a vector of known, positive bounding constants.

4.2.1 Control Objective

The control objective for the general problem given in (4.2.1) is to design a learning-based estimate $\hat{w}(t)$ such that

$$\lim_{t \to \infty} e(t) = 0 \tag{4.2.6}$$

for any bounded initial condition denoted by $e(0)$. To quantify the mismatch between the learning-based estimate and $w(t)$, we define an estimation error term, denoted by $\tilde{w}(t) \in \Re^m$, as follows:

$$\tilde{w}(t) = w(t) - \hat{w}(t). \tag{4.2.7}$$

4.2.2 Learning-Based Estimate Formulation

Based on the error system given in (4.2.1) and the subsequent stability analysis, we design the learning-based estimate $\hat{w}(t)$ as follows:

$$\hat{w}(t) = \text{sat}_\beta(\hat{w}(t-T)) + k_e R^T e \tag{4.2.8}$$

where $k_e \in \Re$ is a positive constant control gain, and $\text{sat}_\beta(\cdot) \in \Re^{\text{m}}$ is a vector function whose elements are defined as follows:

$$\text{sat}_{\beta_i}(\xi_i) = \begin{cases} \xi_i, & \text{for } |\xi_i| \le \beta_i \\ \beta_i \,\text{sgn}(\xi_i), & \text{for } |\xi_i| \ge \beta_i \end{cases} \qquad \forall\ \xi_i \in \Re, \quad i = 1, 2, \ldots, m \tag{4.2.9}$$

where β_i represent the elements of β defined in (4.2.5), and $\text{sgn}(\cdot)$ denotes the standard signum function. From the definition of $\text{sat}_\beta(\cdot)$ given in (4.2.9), we can prove that (see Appendix B)

$$(\xi_{1i} - \xi_{2i})^2 \ge (\text{sat}_{\beta_i}(\xi_{1i}) - \text{sat}_{\beta_i}(\xi_{2i}))^2 \qquad \forall\ |\xi_{1i}| \le \beta_i, \quad \xi_{2i} \in \Re, \quad i = 1, 2, \ldots, m. \tag{4.2.10}$$

To facilitate the subsequent stability analysis, we substitute (4.2.8) into (4.2.7) for $\hat{w}(t)$, to rewrite the expression for $\tilde{w}(t)$ as follows:

$$\tilde{w}(t) = \text{sat}_\beta(w(t-T)) - \text{sat}_\beta(\hat{w}(t-T)) - k_e R^T e \tag{4.2.11}$$

where we utilized (4.2.4), (4.2.5), and the fact that

$$w(t) = \text{sat}_\beta(w(t)) = \text{sat}_\beta(w(t-T)). \tag{4.2.12}$$

4.2.3 Stability Analysis

Theorem 1: The learning-based estimate defined in (4.2.8) ensures that

$$\lim_{t\to\infty} e(t) = 0 \tag{4.2.13}$$

for any bounded initial condition denoted by $e(0)$.

Proof: To prove Theorem 1, we define a nonnegative function $V_2(t, e, \tilde{w}) \in \Re$ as follows:

$$V_2 = V_1 + \frac{1}{2k_e}\int_{t-T}^{t} [\text{sat}_\beta(w(\tau)) - \text{sat}_\beta(\hat{w}(\tau))]^T \cdot [\text{sat}_\beta(w(\tau)) - \text{sat}_\beta(\hat{w}(\tau))] d\tau \tag{4.2.14}$$

where $V_1(e, t)$ was described in Assumption 4.1. After taking the time derivative of (4.2.14), we obtain the following expression:

$$\dot{V}_2 \le -e^T Qe + e^T R\tilde{w}(t) + \frac{1}{2k_e}[\mathrm{sat}_\beta(w(t)) - \mathrm{sat}_\beta(\hat{w}(t))]^T \cdot [\mathrm{sat}_\beta(w(t)) - \mathrm{sat}_\beta(\hat{w}(t))]$$

$$-\frac{1}{2k_e}[\mathrm{sat}_\beta(w(t-T)) - \mathrm{sat}_\beta(\hat{w}(t-T))]^T \cdot [\mathrm{sat}_\beta(w(t-T)) - \mathrm{sat}_\beta(\hat{w}(t-T))]$$

(4.2.15)

where (4.2.3) was utilized. After utilizing (4.2.11), we can rewrite the above as follows:

$$\dot{V}_2 \le -e^T Qe + e^T R\tilde{w}(t) - \frac{1}{2k_e}[\tilde{w}(t) + k_e R^T e]^T \cdot [\tilde{w}(t) + k_e R^T e]$$

$$+\frac{1}{2k_e}[\mathrm{sat}_\beta(w(t)) - \mathrm{sat}_\beta(\hat{w}(t))]^T \cdot [\mathrm{sat}_\beta(w(t)) - \mathrm{sat}_\beta(\hat{w}(t))]. \qquad (4.2.16)$$

After performing some simple algebraic operations, we can further simplify (4.2.16) as follows:

$$\dot{V}_2 \le -e^T \left(Q + \frac{k_e}{2} RR^T \right) e - \frac{1}{2k_e}[\tilde{w}(t)^T \tilde{w}(t)$$

$$-[\mathrm{sat}_\beta(w(t)) - \mathrm{sat}_\beta(\hat{w}(t))]^T \cdot [\mathrm{sat}_\beta(w(t)) - \mathrm{sat}_\beta(\hat{w}(t))]]. \qquad (4.2.17)$$

Finally, we can utilize (4.2.5), (4.2.7), and (4.2.10) to simplify (4.2.17) to

$$\dot{V}_2 \le -e^T Qe. \qquad (4.2.18)$$

Based on (4.2.14), (4.2.18) along with the fact that Q is a positive-definite symmetric matrix, it is clear that $e(t) \in L_2 \cap L_\infty$. Based on the fact that $e(t) \in L_\infty$, it is clear from (4.2.1), (4.2.8), (4.2.9), and (4.2.11) that $\hat{w}(t)$, $\tilde{w}(t)$, $f(t,e)$, $B(t,e) \in L_\infty$. Given that $\hat{w}(t)$, $\tilde{w}(t)$, $f(t,e)$, $B(t,e) \in L_\infty$, it is clear from (4.2.1) that $\dot{e}(t) \in L_\infty$, and hence, $e(t)$ is uniformly continuous. Since $e(t) \in L_2 \cap L_\infty$ and uniformly continuous, we can utilize Barbalat's Lemma (Lewis *et al*. 1993) to prove (4.2.13).

Remark 1: From the previous stability analysis, it is clear that we exploit the fact that the learning-based feedforward term given in (4.2.8) is composed of a saturation function. That is, it is easy to see from the structure of (4.2.8), that if $e(t) \in L_\infty$ then $\hat{w}(t) \in L_\infty$.

4.3 Control Design (I)

In the previous section, we exploited the fact that the unknown nonlinear dynamics, denoted by $w(t)$, were periodic with a known period *T*. Unfortunately, a practical tracking system using the hybrid stepping motor may not adhere to the ideal assumption that all of the unknown nonlinear dynamics are entirely periodic with respect to time for various control tasks. Since the learning-based feedforward term, developed in the previous section, is generated from a straightforward Lyapunov-like stability analysis, by defining the control task over a finite time duration, we can utilize other Lyapunov-based control design techniques to develop hybrid control schemes that utilize learning-based feedforward terms to compensate for periodic ripple dynamics and feedback terms to reject the effect of random and nondeterministic disturbances. To illustrate this point, we now develop a hybrid control scheme for a hybrid stepping motor, in the following subsections.

4.3.1 Modified Representation of Dynamic Model

To facilitate the analysis that follows, the dynamic model of the motor given in (3.2.2) can be expressed in the following form:

$$M(\theta)\ddot{\theta} + D(\dot{\theta}, \theta) = i_q \tag{4.3.1}$$

where

$$M(\theta) = \frac{J}{K_m + \sum_{l=1}^{\infty}[K_{qsl}\sin(lN_r\theta) + K_{qcl}\cos(lN_r\theta)]} \tag{4.3.2}$$

$$D(\dot{\theta},\theta)=\frac{\sum_{l=1}^{\infty}[K_{dsl}\sin(lN_r\theta)+K_{dcl}\cos(lN_r\theta)]+B\dot{\theta}}{K_m+\sum_{l=1}^{\infty}[K_{qsl}\sin(lN_r\theta)+K_{qcl}\cos(lN_r\theta)]}\ . \tag{4.3.3}$$

The function M and D are considered to be unknown due to parametric uncertainty in their expressions, but it is clear that they are periodic with respect to θ in the sense of $2\pi/N_r$, i.e.,

$$M(\theta+2\pi/N_r)=M(\theta)\,,\qquad \forall\theta\in\Re \tag{4.3.4}$$

$$D(\dot{\theta},\theta+2\pi/N_r)=D(\dot{\theta},\theta)\,,\qquad \forall(\dot{\theta},\theta)\in\Re\times\Re\ . \tag{4.3.5}$$

With regard to dynamics given by (4.3.1), it is easy to see that all of the terms are bounded if $\theta,\dot{\theta},$ and $\ddot{\theta}$ are bounded. Furthermore, the following properties hold good for the function M and D that will be used in the controller development and analysis.

Property 1: The function M and D satisfy the Lipschitz condition, i.e., there exist constants μ_m, μ_{d2}, $\mu_{d2}>0$ such that

$$\left|M(\theta_1)-M(\theta_2)\right|\le\mu_m\left|\theta_1-\theta_2\right|,\qquad \forall\ \theta_1,\theta_2\in\Re \tag{4.3.6a}$$

$$\left|D(\dot{\theta}_1,\theta_1)-D(\dot{\theta}_2,\theta_2)\right|\le\mu_{d1}\left|\dot{\theta}_1-\dot{\theta}_2\right|+\mu_{d2}\left|\theta_1-\theta_2\right|,\qquad \forall\dot{\theta}_1,\dot{\theta}_2,\theta_1,\theta_2\in\Re. \tag{4.3.6b}$$

Property 2: The function M is continuously differentiable and there exist positive constants $M_{\min}$, and $M_{\max}$ that satisfy

$$M_{\min}\le\left|M(\theta)\right|\le M_{\max},\qquad \forall\theta\in\Re. \tag{4.3.7}$$

Furthermore, the periodicity in (4.3.4) along with (4.3.7) implies that there exists a constant $k_m>0$ such that

$$\left|M'(\theta)\right|\le k_m,\qquad \forall\theta\in\Re. \tag{4.3.8}$$

4.3.2 Control Objective

The control objective is to design a global position tracking controller despite parametric uncertainty in the dynamic model given in (4.3.1). To quantify this objective, we define the position tracking error $e(t)$ as follows:

$$e = \theta_d - \theta \tag{4.3.9}$$

where we assume that the desired trajectory $\theta_d(t)$ and its first and second-order time derivatives are assumed to be bounded periodic functions of time with a known period T such that

$$\theta_d(t) = \theta_d(t-T) \qquad \dot{\theta}_d(t) = \dot{\theta}_d(t-T) \qquad \ddot{\theta}_d(t) = \ddot{\theta}_d(t-T)\,. \tag{4.3.10}$$

4.3.3 Control Formulation

To facilitate the subsequent control development and stability analysis, we examine the error dynamic expression corresponding to (4.3.1) by defining a filtered tracking error-like variable $z(t)$ as follows:

$$z = \dot{e} + \alpha e \tag{4.3.11}$$

where α is a positive constant control gain. After taking the time derivative of (4.3.11), pre-multiplying the resulting expression by $M(\theta)$, utilizing (4.3.1) and (4.3.9), and then performing some algebraic manipulations, we obtain the following expression:

$$M\,\dot{z} = w_d + \chi - i_q \tag{4.3.12}$$

where the auxiliary expressions $w_d(t)$, $\chi(t)$ are defined as follows:

$$w_d = M(\theta_d)\ddot{\theta}_d + D(\dot{\theta}_d, \theta_d) \tag{4.3.13}$$

$$\chi = M(\theta)(\ddot{\theta}_d + \alpha\dot{e}) + D(\dot{\theta}, \theta) - w_d\,. \tag{4.3.14}$$

By Properties 1 and 2 given in (4.3.6) and (4.3.7), and then (4.3.9) and (4.3.11), there exist some constants $\mu_{x1}, \mu_{x2} > 0$ such that

$$\chi = \ddot{\theta}_d[M(\theta) - M(\theta_d)] + D(\dot{\theta}, \theta) - D(\dot{\theta}_d, \theta_d) + \alpha M(\theta)\dot{e}$$

$$\leq \mu_{x1}|e| + \mu_{x2}|z|. \tag{4.3.15}$$

Note that

$$\max[|z|^2, |e|^2] \leq |z|^2 + |e|^2, \qquad |z|\,|e| \leq \tfrac{1}{2}(|z|^2 + |e|^2). \tag{4.3.16}$$

By (4.3.16) and (4.3.15), there exists some constant $\rho > 0$ such that

$$z\chi \leq \rho\|\boldsymbol{x}\|^2 \tag{4.3.17}$$

where the auxiliary signal $x(t) \in \Re^2$ is defined as

$$\boldsymbol{x}(t) = [z, e]^T. \tag{4.3.18}$$

Furthermore, based on the expression given in (4.3.13) and the boundedness assumptions with regard to the motor dynamics and the desired trajectory, it is clear that

$$w_d(t) = w_d(t - T), \qquad |w_d(t)| \leq \beta_d \qquad \forall\ t \in \Re_+ \tag{4.3.19}$$

where β_d is a known positive bounding constant.

Given the open-loop error system in (4.3.12), we design the following control input:

$$i_q = k\,z + \tfrac{1}{2}k_m|\dot{\theta}|z + e + \hat{w}_d \tag{4.3.20}$$

where k is a positive constant control gain, k_m was defined in (4.3.8) and $\hat{w}_d(t)$ is generated on-line according to the following learning-based algorithm:

$$\hat{w}_d(t) = \mathrm{sat}_{\beta_d}(\hat{w}_d(t - T)) + k_L z \tag{4.3.21}$$

with k_L being a positive constant learning gain, and $\mathrm{sat}_{\beta_d}(\cdot)$ is defined in the same manner as in (4.2.9).

To develop the closed-loop error system for $z(t)$, we substitute (4.3.20) into (4.3.12) to obtain the following expression:

$$M\,\dot{z} = -k\,z - e + \tilde{w}_d + \chi - \tfrac{1}{2}k_m\left|\dot{\theta}\right|z \qquad (4.3.22)$$

where $\tilde{w}_d(t)$ is a learning estimation error signal defined as follows:

$$\tilde{w}_d = w_d - \hat{w}_d\,. \qquad (4.3.23)$$

After substituting (4.3.21) into (4.3.23) for $\hat{w}_d(t)$, utilizing the fact that $w_d(t)$ is periodic, and then utilizing (4.3.19) to construct the following equality:

$$w_d(t) = \mathrm{sat}_{\beta_d}(w_d(t)) = \mathrm{sat}_{\beta_d}(w_d(t-T))\,, \qquad (4.3.24)$$

we can rewrite (4.3.23) in the following form:

$$\tilde{w}_d = \mathrm{sat}_{\beta_d}(w_d(t-T)) - \mathrm{sat}_{\beta_d}(\hat{w}_d(t-T)) - k_L z\,. \qquad (4.3.25)$$

4.3.4 Stability Analysis

Theorem 2: Given the motor dynamics of (4.3.1), the proposed hybrid learning controller given in (4.3.20)–(4.3.21), ensures global asymptotic position tracking in the sense that

$$\lim_{t\to\infty} e(t) = 0 \qquad (4.3.26)$$

where the control gains $\alpha, k,$ and k_L introduced in (4.3.11), (4.3.20), and (4.3.21) must be selected to satisfy the following sufficient condition:

$$\min\left(\alpha,\ k + \frac{k_L}{2}\right) > \rho \qquad (4.3.27)$$

where ρ was defined in (4.3.17).

Proof: To prove Theorem 2, we define a nonnegative function $V_3(t) \in \Re$ as follows:

$$V_3 = \frac{1}{2}e^2 + \frac{1}{2}Mz^2 + \frac{1}{2k_L}\int_{t-T}^{t}[\mathrm{sat}_{\beta_d}(w_d(\tau)) - \mathrm{sat}_{\beta_d}(\hat{w}_d(\tau))]^2 d\tau . \tag{4.3.28}$$

After taking the time derivative of (4.3.28), we obtain the following expression:

$$\begin{aligned}\dot{V}_3 = {} & e(z-\alpha e) + z(-kz - e - \frac{1}{2}k_m z|\dot{\theta}|) + z(\tilde{w}_d + \chi) + \frac{1}{2}z^2 M'\dot{\theta} \\ & + \frac{1}{2k_L}[\mathrm{sat}_{\beta_d}(w_d(t)) - \mathrm{sat}_{\beta_d}(\hat{w}_d(t))]^2 \\ & - \frac{1}{2k_L}[\mathrm{sat}_{\beta_d}(w_d(t-T)) - \mathrm{sat}_{\beta_d}(\hat{w}_d(t-T))]^2\end{aligned} \tag{4.3.29}$$

where (4.3.11) and (4.3.22) were utilized. After utilizing (4.3.8), (4.3.17), (4.3.19), (4.3.25), and then simplifying the resulting expression, we can rewrite (4.3.29) as follows:

$$\begin{aligned}\dot{V}_3 \le {} & -\alpha e^2 - kz^2 + \rho\|\boldsymbol{x}\|^2 + z\tilde{w}_d - \frac{1}{2k_L}(\tilde{w}_d + k_L z)^2 \\ & + \frac{1}{2k_L}[\mathrm{sat}_{\beta_d}(w_d(t)) - \mathrm{sat}_{\beta_d}(\hat{w}_d(t))]^2 .\end{aligned} \tag{4.3.30}$$

After expanding the first line of (4.3.30) and then canceling common terms, we obtain the following expression:

$$\begin{aligned}\dot{V}_3 \le {} & -\alpha e^2 - (k + \frac{k_L}{2})z^2 + \rho\|\boldsymbol{x}\|^2 \\ & - \frac{1}{2k_L}\left[\tilde{w}_d{}^2 - [\mathrm{sat}_{\beta_d}(w_d(t)) - \mathrm{sat}_{\beta_d}(\hat{w}_d(t))]^2\right].\end{aligned} \tag{4.3.31}$$

By exploiting the property given in (4.2.10), and then utilizing the definition of $\boldsymbol{x}(t)$ given in (4.3.18), we can simplify the expression given in (4.3.31) to obtain

$$\dot{V}_3 \leq -\left(\min\left(\alpha,\ k + \frac{k_L}{2}\right) - \rho\right)\|\boldsymbol{x}\|^2. \tag{4.3.32}$$

Based on (4.3.18), (4.3.27), (4.3.28), and (4.3.32), it is clear that $e(t), z(t) \in L_2 \cap L_\infty$. Based on the fact that $z(t) \in L_\infty$, it is clear from (4.3.11), (4.3.21), (4.3.25) that $\hat{w}_d(t)$, $\tilde{w}_d(t),\ \dot{e}(t) \in L_\infty$, and hence, $e(t)$ is uniformly continuous. Since $e(t) \in L_2 \cap L_\infty$ and uniformly continuous, we can utilize Barbalat's Lemma (Lewis *et al*. 1993) to prove (4.3.26).

Remark 2: From the previous stability analysis, it is again clear that we exploit the fact that the learning-based feedforward term given in (4.3.21) is composed of a saturation function. That is, it is easy to see from the structure of (4.3.21), that if $z(t) \in L_\infty$ then $\hat{w}_d(t) \in L_\infty$.

Remark 3: One of the advantages of the novel saturated learning-based feedforward term is that it is developed through Lyapunov-based techniques. By utilizing Lyapunov-based design and analysis techniques, the boundedness of the feedforward term can be proven in a straightforward manner, and the ability to utilize additional Lyapunov-based techniques to augment the control design (as in the case of the hybrid learning controller) is facilitated. However, it is worth pointing out that the incorporation of additional control elements considered here depends on the use of a nonlinear feedback mechanism (as in (4.3.20)), which will increase the complexity in the practical implementation. To simplify the controller structure, we attempt, in the following section, to develop another learning-based control scheme coupled with a pure linear feedback mechanism. To gain a deeper understanding of the control scheme we are interested in, its profound physical implications are also emphasized.

4.4 Control Design (II)

4.4.1 Control Formulation

To facilitate the subsequent analysis, the dynamic model of the motor given in (3.2.2) can be represented in the typical form as follows:

$$J\ddot{\theta} + F(\dot{\theta}, \theta) = G(\theta)i_q \tag{4.4.1}$$

where

$$F(\dot{\theta}, \theta) = B\dot{\theta} + \sum_{l=1}^{\infty} K_{dsl} \sin(lN_r\theta) + K_{dcl} \cos(lN_r\theta) \tag{4.4.2}$$

$$G(\theta) = K_m + \sum_{l=1}^{\infty} K_{qsl} \sin(lN_r\theta) + K_{qcl} \cos(lN_r\theta)\,. \tag{4.4.3}$$

The function F and G are considered to be unknown due to parametric uncertainty in their expressions, but it is clear that they are periodic with respect to θ in the sense of $2\pi/N_r$, i.e.,

$$F(\dot{\theta}, \theta + 2\pi / N_r) = F(\dot{\theta}, \theta)\,, \qquad \forall(\dot{\theta}, \theta) \in \Re \times \Re \tag{4.4.4}$$

$$G(\theta + 2\pi / N_r) = G(\theta)\,, \qquad \forall\, \theta \in \Re\,. \tag{4.4.5}$$

With regard to dynamics given by (4.4.1), it is easy to see that all of the terms are bounded if $\theta, \dot{\theta},$ and $\ddot{\theta}$ are bounded.

Furthermore, the following properties hold good for the function F and G that will be used in the controller development and analysis:

Property 3: The function F and G satisfy the Lipschitz condition, i.e., there exist constants $\mu_{f1}, \mu_{f2}, \mu_g > 0$ such that

$$\left|F(\dot{\theta}_1, \theta_1) - F(\dot{\theta}_2, \theta_2)\right| \le \mu_{f1}\left|\dot{\theta}_1 - \dot{\theta}_2\right| + \mu_{f2}\left|\theta_1 - \theta_2\right|, \qquad \forall\, \dot{\theta}_1, \dot{\theta}_2, \theta_1, \theta_2 \in \Re \tag{4.4.6a}$$

$$\left|G(\theta_1) - G(\theta_2)\right| \le \mu_g\left|\theta_1 - \theta_2\right|, \qquad \forall\ \theta_1, \theta_2 \in \Re. \tag{4.4.6b}$$

Property 4: The function G is continuously differentiable and there exist positive constants G_m, and G_M that satisfy

$$0 < G_m \le G(\theta) \le G_M, \qquad \forall \theta \in \Re.. \tag{4.4.7}$$

Property 4 follows from the fact that the main torque constant dominates the overall torque constant variation as specified by (3.2.4).

The control objective is to design a learning controller such that through repeated learning trials the motion trajectory $\{\dot{\theta}, \theta\}$ of the motor can track a pre-specified $\{\dot{\theta}_d, \theta_d\}$ defined over $[0, T]$, especially in the sense of asymptotic tracking, despite parametric uncertainty in the dynamic model given in (4.4.1). To quantify this objective, we also define the position tracking error $e(t)$ as follows:

$$e = \theta_d - \theta \tag{4.4.8}$$

where θ_d and its first and second-order time derivatives are assumed to be bounded.

To facilitate the subsequent control development and stability analysis, we also examine the error dynamic expression corresponding to (4.4.1) by defining a filtered tracking error-like variable $z(t)$ as follows:

$$z = \dot{e} + \alpha e \tag{4.4.9}$$

where α is a positive constant control gain which will be used soon. After taking the time derivative of (4.4.9), pre-multiplying the resulting expression by J, utilizing (4.4.1) and (4.4.8), and then performing some algebraic manipulations, we obtain the following expression:

$$J\dot{z} = J\alpha(z - \alpha e) + \Delta F + G(\theta_d) w_d - G(\theta) i_q \tag{4.4.10}$$

where the auxiliary expressions w_d, ΔF are defined as follows:

$$w_d = (J\ddot{\theta}_d + F(\dot{\theta}_d, \theta_d))\big/G(\theta_d) \tag{4.4.11}$$

$$\Delta F = F(\dot{\theta}, \theta) - F(\dot{\theta}_d, \theta_d). \tag{4.4.12}$$

It follows from (4.4.10) and (4.4.11) that w_d can be regarded as the *desired input* that achieves perfect tracking, i.e., $\theta(t) \equiv \theta_d(t)$ if $\theta(0) = \theta_d(0)$, $\dot{\theta}(0) = \dot{\theta}_d(0)$ and $i_q(t) = w_d(t)$ in (4.4.1). Furthermore, based on the boundedness and periodicity conditions concerning the motor dynamics and the desired trajectory, it is clear that

$$w_d(t) = w_d(t-T), \qquad |w_d(t)| \le \beta_d \qquad \forall\, t \in \Re_+ \tag{4.4.13}$$

where β_d is a known positive bounding constant which can be decided from the real excitation limitation of the driving system. Also note that the desired input w_d contains unknown ripple dynamics and other disturbances that need to be tackled.

Given the open-loop error system in (4.4.10), we design the following control input:

$$i_q = k_P z + \hat{w}_d \tag{4.4.14}$$

where k_P is a positive constant control gain, and $\hat{w}_d(t)$ is generated according to (4.3.21). The difference between (4.4.14) and (4.3.20) lies in the fact that the learning-based algorithm is now incorporated with a pure linear feedback control term, which makes the control input easier for implementation.

To develop the closed-loop error system for $z(t)$, we substitute (4.4.14) into (4.4.10) to obtain the following expression

$$J\dot{z} = (J\alpha - k_P G(\theta))z - J\alpha^2 e + \Delta F + G(\theta_d)w_d - G(\theta)\hat{w}_d. \tag{4.4.15}$$

By introducing the new functions f, g, f_d, g_d, Δf, and Δg as defined by

$$\begin{aligned} f &= f(z, e, t) = F(\dot{\theta}_d(t) - z + \alpha e,\ \theta_d(t) - e) \\ g &= g(e, t) = G(\theta_d(t) - e) \end{aligned} \tag{4.4.16a}$$

$$\begin{aligned} f_d &= f(0, 0, t) = F(\dot{\theta}_d(t), \theta_d(t)) \\ g_d &= g(0, t) = G(\theta_d(t)) \end{aligned} \tag{4.4.16b}$$

$$\Delta f = f - f_d\,, \quad \Delta g = g - g_d\,, \tag{4.4.16c}$$

the entire closed-loop error system for $z(t)$ and $e(t)$ can be expressed in the following form:

$$\dot{\boldsymbol{x}} = \boldsymbol{f}_s(\boldsymbol{x}, t) + \boldsymbol{g}_s(\boldsymbol{x}, t)\tilde{w}_d(t) \tag{4.4.17}$$

where

$$\begin{aligned} \boldsymbol{x}(t) &= [z, e]^T \\ \boldsymbol{f}_s(\boldsymbol{x}, t) &= \begin{bmatrix} (\alpha - k_P\, g/J)z - \alpha^2 e + (\Delta f - \Delta g w_d)/J \\ z - \alpha e \end{bmatrix} \\ \boldsymbol{g}_s(\boldsymbol{x}, t) &= \begin{bmatrix} g/J \\ 0 \end{bmatrix}, \end{aligned}$$

and $\tilde{w}_d(t)$ is a learning estimation error signal defined as follows:

$$\tilde{w}_d = w_d - \hat{w}_d\ . \tag{4.4.18}$$

Hereafter, (4.4.17) will be frequently referred to as *learning system*.

Finally, the tracking control problem addressed here can also be stated as follows: How is it possible to validate the learning controller (4.4.14) associated with the learning rule (4.3.21) to generate the unknown desired input w_d that exponentially stabilizes the learning system in (4.4.17), subject to Properties 3-4 and the requirements on the controller gains α, k_P and k_L?

4.4.2 Performance Analysis

To facilitate the performance analysis of the proposed scheme, here we give a *Lemma* which reveals the boundedness relationship among the quantities z, $\dot{z}$, e, $\dot{e}$ and $\hat{w}_d$.

Lemma: For the learning system (4.4.17) satisfying Properties 3-4, the learning control laws (4.4.14) and (4.3.21) ensure that $z, \dot{z}, e, \dot{e}, \hat{w}_d \in L_\infty$.

Proof: Define a Lyapunov function $V(t) \in \Re^1$ as follows:

$$V = \frac{J}{2}(z^2 + \alpha^2 e^2)\,. \tag{4.4.19}$$

Differentiating V with respect to t using (4.4.17) and (4.4.18) along with (4.4.14), we obtain

$$\dot{V} = -\boldsymbol{x}^{\boldsymbol{T}}\boldsymbol{Q}\boldsymbol{x} + \{\Delta f - \Delta g w_d + g\,[w_d - \mathrm{sat}(\hat{w}_d(t-T))]\}\,z \tag{4.4.20}$$

where

$$\boldsymbol{Q} = \begin{bmatrix} (k_P + k_L)g - J\alpha & 0 \\ 0 & J\alpha^3 \end{bmatrix}. \tag{4.4.21}$$

Note that

$$\max[|z|^2, |e|^2] \le |z|^2 + |e|^2 = \|\boldsymbol{x}\|^2, \qquad |z|\,|e| \le \tfrac{1}{2}\|\boldsymbol{x}\|^2\,. \tag{4.4.22}$$

By (4.4.22), (4.3.19), (4.2.9), the definitions of g, Δf and Δg in (4.4.16), and Properties 3-4, there exist some constants $\mu_1, \mu_2 > 0$ such that

$$\{\Delta f - \Delta g w_d + g[w_d - \mathrm{sat}(\hat{w}_d(t-T))]\}z \le (\mu_1\alpha + \mu_2)\|\boldsymbol{x}\|^2 + 2\beta_d G_M \|\boldsymbol{x}\|\,. \tag{4.4.23}$$

Substituting the above into (4.4.20) gives

$$\dot{V} \le -\boldsymbol{x}^{\boldsymbol{T}}\boldsymbol{P}\boldsymbol{x} + 2\beta_d G_M \|\boldsymbol{x}\|$$

where

$$\boldsymbol{P} = \begin{bmatrix} (k_P + k_L)g - J\alpha - \mu_1\alpha - \mu_2 & 0 \\ 0 & J\alpha^3 - \mu_1\alpha - \mu_2 \end{bmatrix}.$$

Now, choose controller gains α and k_P large enough to satisfy

$$\alpha > 1, \quad k_P > J\alpha(1+\alpha^2)/G_m - k_L \tag{4.4.24}$$

$$\mu = J\alpha^3 - \mu_1\alpha - \mu_2 > 0. \tag{4.4.25}$$

Then it follows from (4.4.22), (4.4.24), and (4.4.25) that

$$\dot{V} \le -\mu\|\boldsymbol{x}\|^2 + 2\beta_d G_M\|\boldsymbol{x}\| \le -\frac{2\mu}{J\alpha^2}V + 2\beta_d G_M\left(\frac{2}{J}\right)^{1/2} V^{1/2}. \tag{4.4.26}$$

The last inequality of the above follows from the fact that

$$\frac{J}{2}\|\boldsymbol{x}\|^2 \le V \le \frac{J}{2}\alpha^2\|\boldsymbol{x}\|^2, \qquad \forall \boldsymbol{x} \in \Re^2. \tag{4.4.27}$$

By (4.4.19) and (4.4.26), we then have

$$\frac{dV^{1/2}}{dt} \le -\gamma V^{1/2} + \left(\frac{2}{J}\right)^{1/2}\beta_d G_M, \qquad \forall t \in \Re_+ \tag{4.4.28}$$

where $\gamma = \mu/J\alpha^2$. Using the comparison principle to the above, it can finally be obtained from (4.4.27) that

$$\|\boldsymbol{x}(t)\| \le \alpha\|\boldsymbol{x}(0)\|e^{-\gamma t} + \frac{2\alpha^2\beta_d G_M}{\mu}(1-e^{-\gamma t}), \qquad \forall t \in \Re_+. \tag{4.4.29}$$

Hence, it can be concluded that the solution of the learning system (4.4.17) stays inside the set $\{\boldsymbol{x}: \|\boldsymbol{x}(\boldsymbol{t})\| \le \max[\alpha\|\boldsymbol{x}(0)\|,\ 2\mu^{-1}\alpha^2\beta_d G_M], \forall t \in \Re_+\}$, i.e., $\|\boldsymbol{x}(t)\| \in L_\infty$.

Now, $z(t) \in L_\infty$ and $e(t) \in L_\infty$ are the immediate consequences of $\|\boldsymbol{x}(t)\| \in L_\infty$ and (4.4.22), and hence $\dot{e}(t) \in L_\infty$ according to (4.4.9). From (4.3.21), $z(t) \in L_\infty$ leads to $\hat{w}_d(t) \in L_\infty$, and hence $\dot{z}(t) \in L_\infty$ according to (4.4.15) which completes the proof.

After presenting the above *Lemma*, we are now ready to prove the following.

Theorem 3: (Convergence of learning scheme) Consider the learning system (4.4.17) satisfying Properties 3-4 and all the previous assumptions. Under the control law (4.4.14) and the learning law (4.3.21), as the iteration sequence tends to infinity, the error pair $[z(t), e(t)]$ converges to zero, and $\hat{w}_d(t)$ converges to $w_d(t)$ in the sense of the extended L_2 norm over $t \in [0, T]$.

Proof: To evaluate the learning performance, a performance index based on the extended L_2 norm is defined as follows:

$$J_i = \| \hat{w}_d - w_d \|_2^2 = \int_{(i-1)T}^{iT} [\hat{w}_d(\tau) - w_d(\tau)]^2 \, d\tau \geq 0 \tag{4.4.30}$$

where the subscript $i \in \mathrm{Z}_+$ is used to denote the iteration number. From (4.4.13), (4.3.21), and (4.2.10), the difference of J_i between two consecutive trials, $\forall i \in \mathrm{Z}_+ \bigcap (i \geq 2)$ can be found as

$$\begin{aligned}
\Delta J_i &= J_i - J_{i-1} \\
&= \int_{(i-1)T}^{iT} [\hat{w}_d(\tau) - w_d(\tau)]^2 \, d\tau - \int_{(i-2)T}^{(i-1)T} [\hat{w}_d(\tau) - w_d(\tau)]^2 \, d\tau \\
&= \int_{(i-1)T}^{iT} [\hat{w}_d(\tau) - w_d(\tau)]^2 \, d\tau - \int_{(i-1)T}^{iT} [\hat{w}_d(\tau - T) - w_d(\tau)]^2 \, d\tau \\
&\leq \int_{(i-1)T}^{iT} \{ [\hat{w}_d(\tau) - w_d(\tau)]^2 - [\mathrm{sat}(\hat{w}_d(\tau - T)) - w_d(\tau)]^2 \} \, d\tau \\
&= \int_{(i-1)T}^{iT} [\hat{w}_d(\tau) - \mathrm{sat}(\hat{w}_d(\tau - T))][\hat{w}_d(\tau) + \mathrm{sat}(\hat{w}_d(\tau - T)) - 2w_d(\tau)] \, d\tau \\
&= \int_{(i-1)T}^{iT} \{ k_L^2 z^2(\tau) + 2k_L z(\tau)[\mathrm{sat}(\hat{w}_d(\tau - T)) - w_d(\tau)] \} \, d\tau \,.
\end{aligned} \tag{4.4.31}$$

From (4.4.20), the following can be obtained

$$g^{-1}\dot{V} = g^{-1}\boldsymbol{x}^T\boldsymbol{Q}\boldsymbol{x} + g^{-1}(\Delta f - \Delta g w_d)z + [w_d - \mathrm{sat}(\hat{w}_d(\tau - T))]z \tag{4.4.32}$$

which can be rewritten into

$$\begin{aligned} z[\mathrm{sat}(\hat{w}_d(\tau - T)) - w_d] = &-g^{-1}\dot{V} - (k_P + k_L - g^{-1}J\alpha)z^2 \\ &- g^{-1}J\alpha^3 e^2 + g^{-1}[\Delta f - \Delta g w_d]z. \end{aligned} \tag{4.4.33}$$

Substituting the above into (4.4.31) gives

$$\begin{aligned} \Delta J_i \le &-\int_{(i-1)T}^{iT}\{k_L^2 + 2k_L(k_P - g^{-1}J\alpha)]z^2(\tau) + 2k_L g^{-1}J\alpha^3 e^2(\tau)\}d\tau \\ &-\int_{(i-1)T}^{iT} 2k_L g^{-1}\dot{V}(\tau)d\tau + \int_{(i-1)T}^{iT} 2k_L g^{-1}[\Delta f - \Delta g w_d(\tau)]z(\tau)d\tau \\ \le &-2k_L\int_{(i-1)T}^{iT}[(\tfrac{1}{2}k_L + k_P - g^{-1}J\alpha)z^2(\tau) + g^{-1}J\alpha^3 e^2(\tau)]d\tau \\ &-2k_L\int_{V((i-1)T)}^{V(iT)} g^{-1}dV(\tau) + 2k_L\int_{(i-1)T}^{iT} g^{-1}\left|\Delta f - \Delta g w_d(\tau)\right|\cdot\left|z(\tau)\right|d\tau. \end{aligned}$$

Using (4.4.22), (4.4.13), and Properties 3-4, and then selecting appropriately the controller gains α, k_P and k_L that satisfy

$$\alpha > 1, \quad k_P > J\alpha(1+\alpha^2)\big/G_m - \tfrac{1}{2}k_L, \tag{4.4.34}$$

and (4.4.25), we obtain

$$\begin{aligned} \Delta J_i &\le -2k_L\int_{V((i-1)T)}^{V(iT)} g^{-1}dV(\tau) - 2k_L\int_{(i-1)T}^{iT} g^{-1}\mu\|\boldsymbol{x}(\tau)\|^2 d\tau \\ &\le -2k_L\int_{V((i-1)T)}^{V(iT)} g^{-1}dV(\tau) - 2k_L G_M^{-1}\mu\int_{(i-1)T}^{iT}\|\boldsymbol{x}(\tau)\|^2 d\tau. \end{aligned} \tag{4.4.35}$$

Taking the summation of ΔJ_j from $j = 2$ up to i results in

$$J_i - J_1 \le -2k_L\int_{V(T)}^{V(iT)} g^{-1}dV(\tau) - 2k_L G_M^{-1}\mu\sum_{j=2}^{i}\int_{(j-1)T}^{jT}\|\boldsymbol{x}(\tau)\|^2 d\tau \tag{4.4.36}$$

$\forall i \in \mathrm{Z}_+ \cap (j \ge 2)$. Since $J_i \ge 0$, we have from the above that

$$\sum_{j=2}^{i}\int_{(j-1)T}^{jT}\|\boldsymbol{x}(\tau)\|^2 d\tau \le \frac{1}{2k_L G_M^{-1}\mu}J_1 - \frac{1}{G_M^{-1}\mu}\int_{V(T)}^{V(iT)} g^{-1}dV(\tau). \tag{4.4.37}$$

Since $\hat{w}_d(t) \in L_\infty$ according to *Lemma* and $|w_d(t)| \le \beta_d$ according to (4.4.13), J_i is bounded according to (4.4.30), $\forall i \in Z_+$. In addition, $z(t), e(t) \in L_\infty$ leads to the boundedness of $V(t)$ according to (4.4.19). From (4.4.37), the boundedness of J_1, $V(T)$ and $V(iT)$ as well as g^{-1} using Property 4 ensures that

$$\lim_{i\to\infty} \sum_{j=2}^{i} \int_{(j-1)T}^{jT} \|\boldsymbol{x}(\tau)\|^2 d\tau < \infty \tag{4.4.38}$$

It concludes that: $\lim_{i\to\infty} \int_{(i-1)T}^{iT} \|\boldsymbol{x}(\tau)\|^2 d\tau = 0$. Now, it is easy to deduce from (4.4.22) that as $i \to \infty$, $z(t+(i-1)T)$, $e(t+(i-1)T) \to 0$ on the extended L_2 norm, $\forall t \in [0, T]$.

Next, rearranging the first equation in (4.4.17) gives

$$\hat{w}_d - w_d = (g^{-1}J\alpha - k_P)z - g^{-1}J\alpha^2 e - g^{-1}J\,\dot{z} + g^{-1}(\Delta f - \Delta g w_d)\,. \tag{4.4.39}$$

According to (4.4.16), $z, e \to 0$ leads to $f \to f_d$, $g \to g_d$ which brings that $\Delta f \to 0$ and $\Delta g \to 0$. Thus, it can be derived from (4.4.30) and (4.4.39) that

$$\begin{aligned}
\lim_{i\to\infty} J_i &= \lim_{i\to\infty} \int_{(i-1)T}^{iT} [\hat{w}_d(\tau) - w_d(\tau)]^2 d\tau \\
&= \lim_{i\to\infty} \int_0^T [\hat{w}_d(\tau+(i-1)T) - w_d(\tau+(i-1)T)]^2 d\tau \\
&= \lim_{i\to\infty} \int_0^T [(g^{-1}J\alpha - k_P)z(\tau+(i-1)T) - g^{-1}J\alpha^2 e(\tau+(i-1)T) \\
&\qquad - g^{-1}J\,\dot{z}(\tau+(i-1)T) + g^{-1}(\Delta f - \Delta g w_d(\tau))]^2 d\tau.
\end{aligned}$$

Since $g^{-1} \le G_m^{-1}$ from Property 4 and $|w_d(t)| \le \beta_d$ from (4.4.13), we obtain

$$\begin{aligned}
\lim_{i\to\infty} J_i &= \lim_{i\to\infty} \int_0^T g^{-2} J^2 [\dot{z}(\tau+(i-1)T)]^2 \, d\tau \\
&= \lim_{i\to\infty} \int_{z((i-1)T)}^{z(iT)} g^{-2} J^2 \dot{z}(\tau+(i-1)T)\, dz.
\end{aligned} \tag{4.4.40}$$

Note that $\dot{z}(t+(i-1)T) \in L_\infty$, $\forall t \in [0, T]$ according to *Lemma* and $g^{-2} \leq G_m^{-2}$ according to Property 4. Therefore, $\lim_{i\to\infty} z(iT) = \lim_{i\to\infty} z((i-1)T) = 0$ yields that

$$\lim_{i\to\infty} J_i = 0 \tag{4.4.41}$$

and $\hat{w}_d(t)$ converges to $w_d(t)$, $\forall t \in [0, T]$ which ends the proof.

Remark 4: From the previous performance analysis, it is observed that by applying Lyapunov-based techniques the learning-based feedforward input term given in (4.3.21) can be shown to be bounded in a straightforward manner, and then the convergence property of the learning system for perfect tracking follows directly via a simple analysis technique.

Remark 5: One of the advantages of the proposed learning controller is that the requirement that the system must return to exactly the same initial configuration after each learning trial has been removed. It is updated continuously with time during the transient response rather than during the steady state. From the argument given in (4.4.29) it is evident that the proposed scheme can ensure that $|z(t)|$ enters a pre-specified error bound during the first learning trial without incurring undesirable chattering. Hence an improved transient response could be anticipated.

Remark 6: In the light of the controller architecture, the PI feedback term is updated at each sampling instant in real time so as to stabilize the system and tackle the non-periodic or random disturbances. The feedforward term is iteratively updated to produce an input that best approximates the *desired input* and compensates for the deterministic uncertainties such as the parasitic torque ripple. A clear physical interpretation is that the proposed learning controller estimates the total input instead of the disturbance (or ripple) torque only, and the system is linearized when it is compensated with this estimated input. Although within the framework of linear learning schemes, the proposed controller can determine the optimal nonlinear input/output relationship, and hence it has the capability of nonlinear functional identification.

Remark 7: It should be pointed out that (4.4.34) and (4.4.25) only provide a set of sufficient conditions that make the learning system exponentially stable. It is easy to see from (4.4.35) that for a fixed control gain α too small a learning gain k_L slows down the decrease of ΔJ_i and at the same time it needs a large control gain k_P to ensure the convergence, and vice versa. On the other hand, a larger k_L could also require a larger k_P due to a bigger α being used to enhance the exponential stability and in turn the learning convergence evaluated by (4.4.29) and (4.4.30) respectively. More importantly, it is the feedforward compensation term that eventually guarantees the system's excellent tracking performance. Therefore, a moderate k_L should be used for a faster learning convergence rate whilst there remains a large range of selecting PI control gains.

Remark 8: The proposed learning controller does not require the nonlinear damping term, relative to the previous one (as in (4.3.20)), to provide good tracking performance. This undoubtedly decreases the complexity in the control implementation. In fact, the pure linear feedback control module in the control input is enough to stabilize the entire learning system while the addition of other feedback components exactly induces some conservatism. This learning control has been validated during experimental trials.

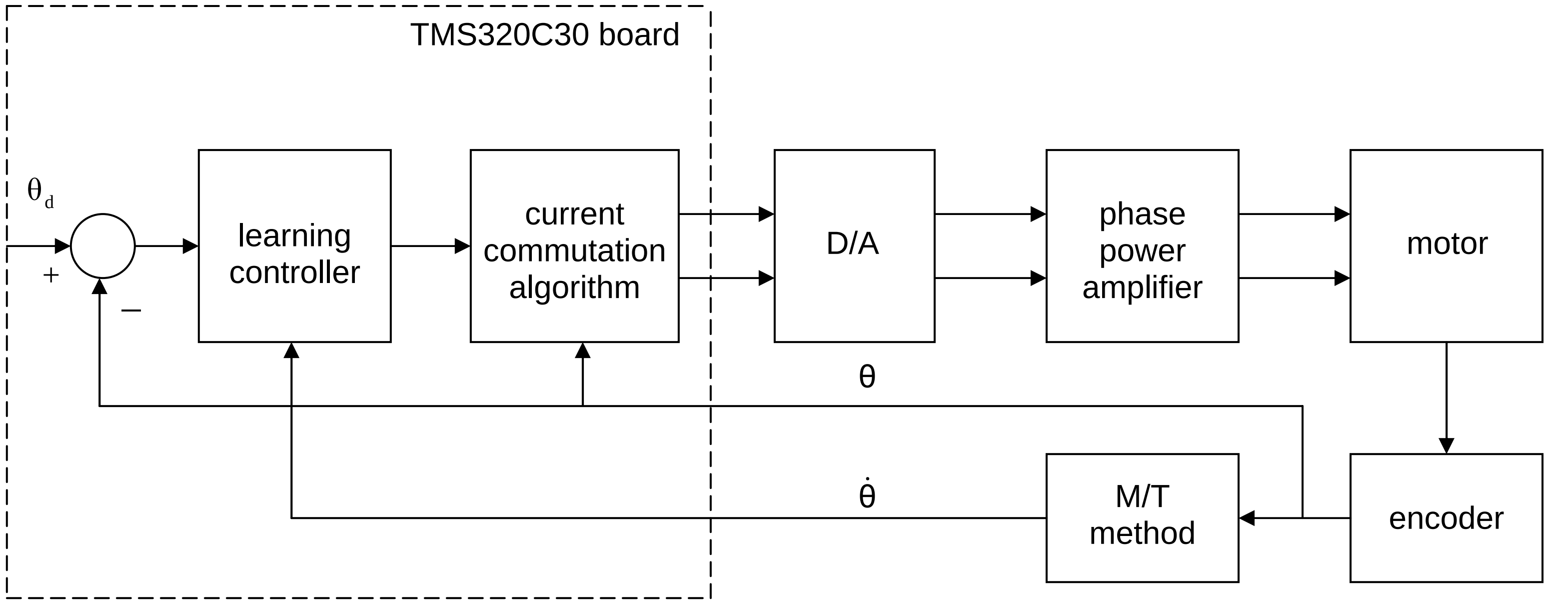

Fig. 4.1 Block diagram representation of the experimental setup

4.5 Experiments and Discussions

To illustrate the effectiveness of the proposed learning-based control approach, the controller presented in the above section was implemented and experimentally verified on a hybrid stepping motor servo for profile tracking at low speed. An experiment has been performed with a typical stepping motor of the brand name VEXTA, model PH264-01B manufactured by Oriental Motor Co. Ltd, Japan, which is a two-phase bifilar-wound hybrid stepping motor with 50 rotor teeth (1.8° per step). The rotor position and speed were obtained by using the well-known MT method along with an optical encoder of 4000 pulses per revolution. The proposed learning control algorithm was implemented on a TMS320C30 DSP chip that can process encoder signals from the motor and supply output control signals to the motor drive in real time. To facilitate the inverse DQ transformation to yield the reference control input (phase currents) from sinusoidal commutation, the required trigonometric functions were stored and updated in a look-up table in RAM for fast control configuration. The reference phase currents were then delivered to the high bandwidth current control circuit. The block diagram for the experimental setup is shown in Fig. 4.1. The desired position trajectory was smoothly generated taking into consideration the physical limits of an actual system, as shown below (see Fig. 4.2)

$$\theta_d(t) = (1-\cos\pi t)(1-e^{-2.5t^2}) \,. \tag{4.5.1}$$

In the experiment, the learning controller in (4.4.14) was implemented, which was ready to be compared with its frequency-domain counterpart. This will be presented in the next chapter. The experiment was performed at a control frequency of 1 kHz. After a tuning process, the following control gains were selected:

$$k_P = 0.4, \qquad \alpha = 15, \qquad k_L = 0.5. \tag{4.5.2}$$

It is worth pointing out that the selection of the control gains should strictly comply with the sufficient conditions given in (4.4.34) and (4.4.25), along with the use of the partial preknowledge about the ripple dynamics of the motor as described by Property 3-4 in the previous section.

To show the effectiveness of the proposed control algorithm, its experimental performance was first compared with that of the conventional sinusoidal current control system. The experimental results of both schemes are summarized in Fig. 4.3-4.5. Initially, the behaviour of the closed-loop system given by (4.4.1) and (4.4.14) was investigated with the feedforward learning input $\hat{w}_d = 0$, that is, only the PI feedback input was used which corresponds to the conventional current control scheme. Fig. 4.3 shows that the responses of $\dot{e}$ and e converge to a steady-state waveform within the

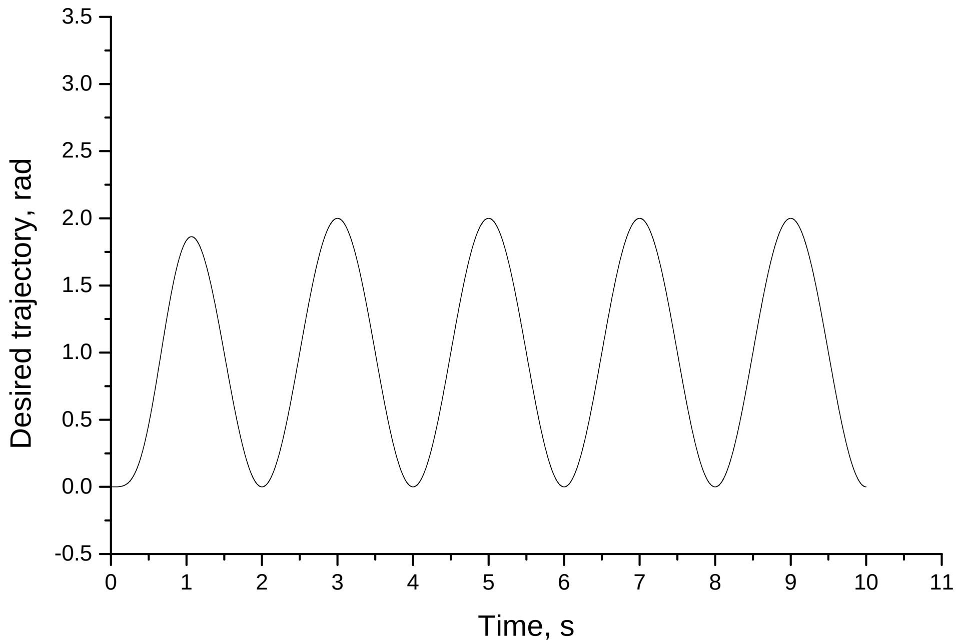

Fig. 4.2 Desired position trajectory

first cycle. The PI control virtually adds significant damping to the motor system that makes the closed-loop system settle quickly into some bound as concluded from the previous analysis. This implies that the controlled system is input-to-state stable if w_d is viewed as an input in (4.4.17). Although the tracking errors show the same periodicity as that of the desired trajectory, they are far from a single-frequency sine waveform and contain higher harmonics. In fact, the remaining tracking errors are exactly the immediate consequences of the ripple dynamics in the motor, which also admits the important fact that the PI controller fails to satisfactorily solve the tracking problem in this application.

By adding the feedforward learning input $\hat{w}_d$ to the PI control, the motor drive is capable of achieving high tracking accuracy. The time histories of $\dot{e}$ and e in Fig.4.4 clearly exhibit the behavior of the learning control scheme used. After a sufficient number of learning trials (about five cycles), the learning algorithm can reduce $\dot{e}$, e to almost zero and at the same time the magnitude of the speed ripple was reduced significantly. In deed, the feedforward compensator acts so as to attenuate the speed ripple, that is closely associated with the torque ripple, for their coordinated reduction. In addition, it is observed from Fig. 4.5 that the updated feedforward input $\hat{w}_d$ corresponding to the estimate for the desired input w_d tends to converge to a specific waveform. This indicates that a good approximation of the desired input has been achieved.

Further comparison of experimental performance between the proposed algorithm and its frequency-domain counterpart will be given in detail in the next chapter. Throughout the experiment, the proposed learning controller shows excellent profile tracking performance, though it is intended here merely as an experimental proof-of-principle. The experimental results validate the theoretical prediction presented in the previous section. The performance of the proposed controller (e.g., transient response, steady-state error) is similar to other repetitive learning-based controllers that update in each period from the initial time instant. However, the proposed controller yields improved transient response when compared to learning-based controllers that are required to wait until the system is in steady-state before the learning-based estimate is applied, as documented in previously mentioned literatures.

4.6 Summary

In this chapter, we illustrate how a learning-based estimate can be used to achieve asymptotic tracking in the presence of undesirable nonlinear dynamics. Based on the fact that the learning-based controller estimate is generated from a Lyapunov-based stability analysis, we demonstrated how the Lyapunov-based design technique can be utilized to construct a learning controller for rejecting components of the ripple dynamics in a hybrid stepping motor. These components are periodic for a class of tracking control tasks defined over a finite duration. By utilizing the Lyapunov-based design and analysis technique, the boundedness of the feedforward term can be proven in a straightforward manner, and the capability of utilizing additional nonlinear feedback components to augment the learning control design (as in the case of the hybrid learning controller) is naturally acquired.

For ease of implementation, we specifically designed a hybrid controller by incorporating a pure linear feedback (PI) control into the repetitive learning mechanism, in which the fixed PI feedback controller takes part in stabilizing the transient response

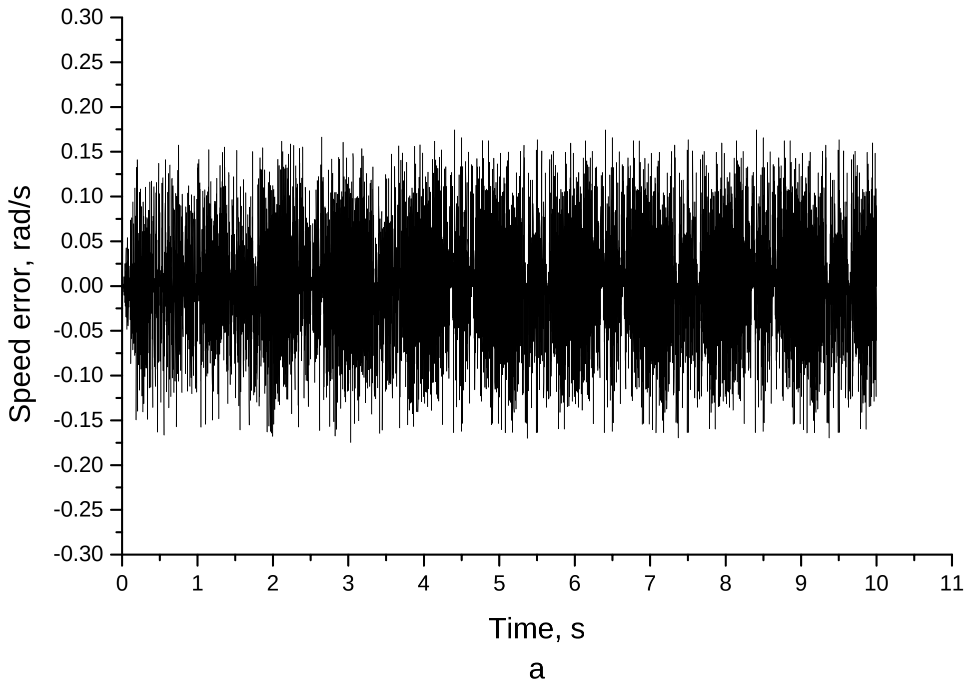

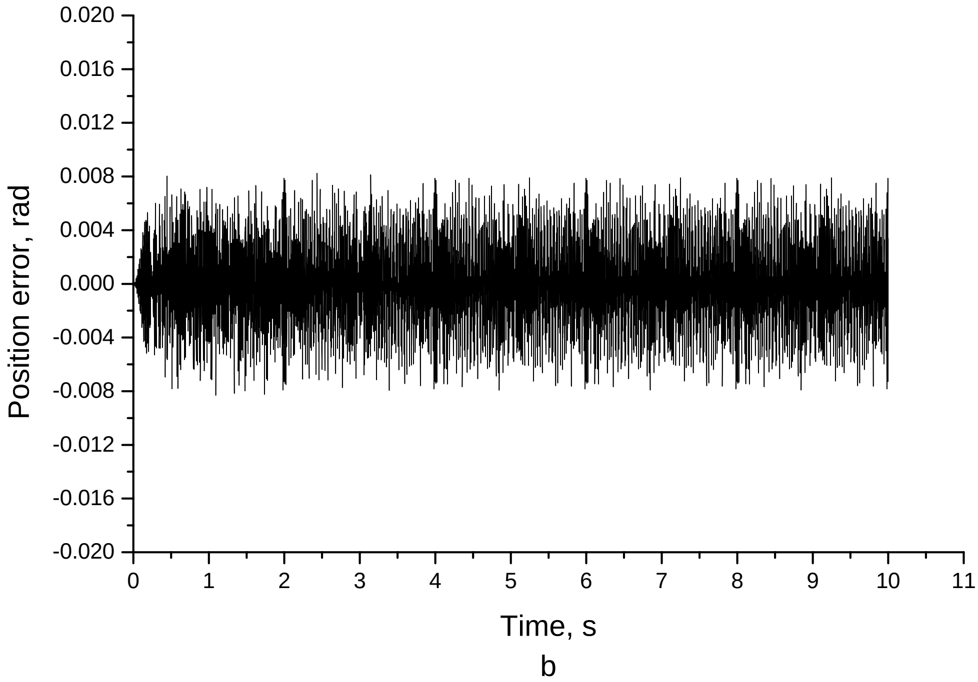

Fig. 4.3 Tracking performance of sinusoidal current control scheme
(a) Speed error
(b) Position error

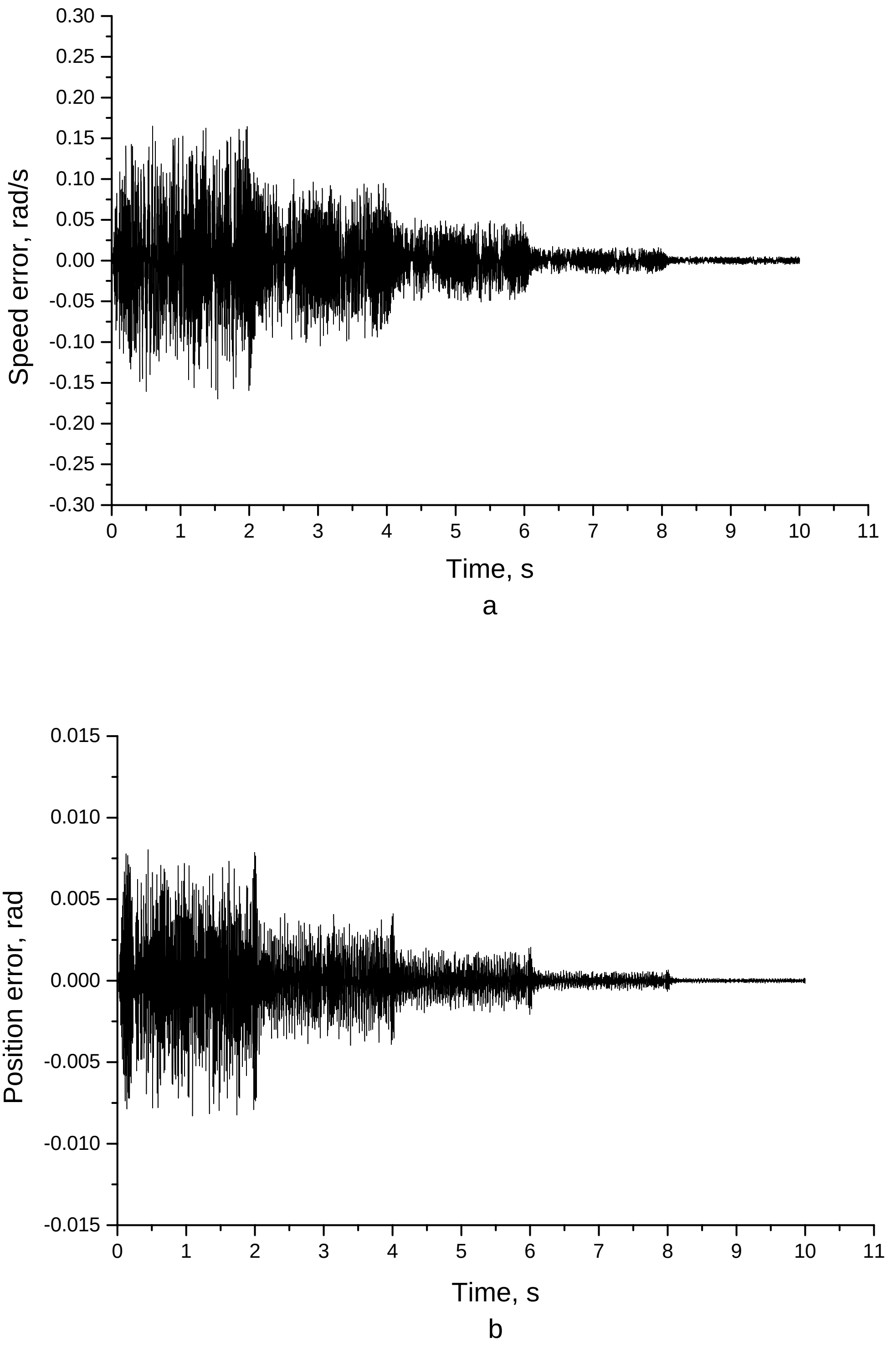

Fig. 4.4 Learning convergence of tracking errors of proposed control scheme
(a) Speed error
(b) Position error

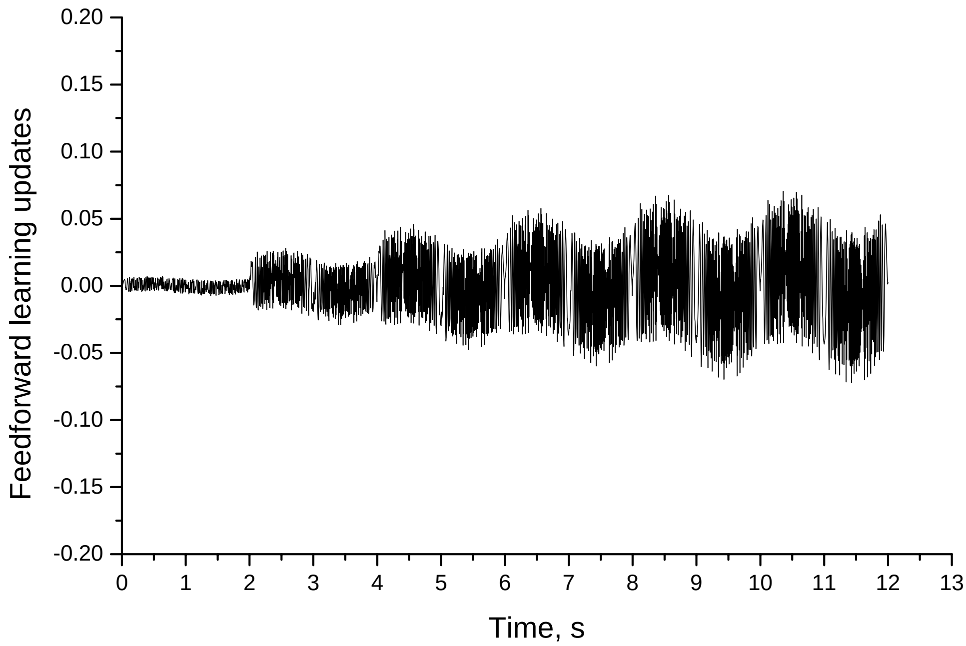

Fig. 4.5 Learning convergence of feedforward input

of the servomotor dynamics and tackling the non-periodic or random disturbances while the feedforward learning controller is responsible for generating a learning control signal to compensate for the effect of the torque ripple. Experimental results illustrated that the tracking performance of a hybrid stepping motor is improved at each period of the desired trajectory due to the mitigating action of the learning estimate.

CHAPTER 5

FREQUENCY-DOMAIN LEARNING CONTROL SCHEME

5.1 Introduction

Recalling the previous time-domain learning control scheme along with important practical consideration, it should be first noted that the repeatability of the learning system implies only countable integer frequencies being involved in the desired input. This ensures the feasibility of constructing component-based learning in the frequency domain. Secondly, nowadays all advanced control approaches (including learning control) have to be implemented using micro-processing technology. According to sampling theory, the learning controller needs only to learn a finite number of frequencies limited to one half of the sampling frequency. Any attempt to learn and manipulate frequencies above that limit will be completely meaningless. Furthermore, most real systems can be characterized as low-pass filters because their bandwidth is much lower than the sampling frequency. It is sufficient for the learning controller to take into account only a small portion of the Fourier series in such cases.

Following from this idea, this chapter presents a decentralized learning control scheme that is implemented in the frequency domain by means of a Fourier series expansion for tracking control of a hybrid stepping motor. The control scheme consists of a time-domain feedback control and a frequency-domain iterative learning control. The former reduces system variability and suppresses the effect of random disturbances and mismatch of initial condition. The later modifies the shape and phase of the control input for suppressing the tracking error caused by the ripple dynamics. Based on the fact that under certain conditions both the desired trajectory and the actual output can be expressed by a Fourier series with constant harmonic magnitudes, a learning controller, as presented in Section 5.2 and Section 5.3, is designed to individually control each harmonic component of the actual output in such a way that each component will converge to that of the desired trajectory within the system bandwidth so that the time-domain tracking error always tends to zero. The suitable conditions for the system stability and convergence of the tracking error are given and discussed in Section 5.4.

Since this decentralized learning controller is designed in Fourier space instead of time domain, the system's time-delay can be easily compensated for. Moreover, this learning controller is based only on local input and output information so that no a priori system modeling is required. Experiments are performed with a typical hybrid stepping motor to test its profile tracking performance, which is examined in Section 5.5. Results demonstrate that this control scheme can significantly improve the tracking control performance by approximating and compensating for deterministic uncertainties caused by the ripple and frictional torque simultaneously.

5.2 Control Formulation

To facilitate the following analysis, the dynamics of the hybrid stepping motor system can be expressed in such a form that the control input current may be simplified as a function of time *t*, which describes the system characteristic corresponding to the rotor position $\theta(t)$ as follows:

$$i_q(t) = f_{i_q}(\ddot{\theta}(t),\ \dot{\theta}(t),\ \theta(t)) \tag{5.2.1}$$

where $f_{i_q}(\cdot)$ represents the relationship between the input and the state of the system. Without loss of generality, the following further assumptions are made for the controlled system.

Assumption 1: The desired trajectory $\theta_d(t)$ of the system lasts for a finite time duration *T*. Also, it complies with the system's driving capacity. In other words, the desired trajectory is physically reachable by the system.

Assumption 2: The system has a finite bandwidth so that it can only respond to input with a certain frequency. Only the system performance within the bandwidth can be ensured, since the signal outside the bandwidth cannot be correctly detected.

The objective of the controller design is to generate a suitable $i_q(t)$ that is as "close" to the desired control $i_q^*(t) = f_{i_q}(\ddot{\theta}_d(t),\ \dot{\theta}_d(t),\ \theta_d(t))$ as possible, so that the tracking error of the system would tend to zero. However, since at low speeds the corresponding input $i_q(t)$ is nonlinear and very complicated, it is not easy to obtain accurately. On the other hand, $i_q(t)$ is the inverse of the system response function which has a finite bandwidth and lasts for a finite time duration so that it can be represented by a Fourier series with finite harmonic terms. If we could find an algorithm, in Fourier space, to acquire all the Fourier coefficients of $i_q(t)$, then its counterpart in the time domain will also be determined. To address this problem, in the next section we will present an effective scheme by designing a decentralized learning controller to estimate these coefficients from the history information of the system so as to achieve the desired control for precise tracking performance.

5.3 Control Design Using Fourier Series

Subject to the above assumptions and based on Fourier analysis, the desired trajectory $\theta_d(t)$ of the system in the given time period of T can be approximated by a Fourier series with finite terms as follows:

$$\theta_d = \frac{\Theta_{dc0}}{2} + \sum_{i=1}^{N} [\Theta_{dci}\cos(i\omega t) + \Theta_{dsi}\sin(i\omega t)], \qquad \forall t \in [0, T] \tag{5.3.1}$$

where

$$\Theta_{dci} = \frac{2}{T}\int_{(k-1)T}^{kT} \theta_d(t)\cos(i\omega t)dt \tag{5.3.2}$$

$$\Theta_{dsi} = \frac{2}{T}\int_{(k-1)T}^{kT} \theta_d(t)\sin(i\omega t)dt \tag{5.3.3}$$

where k is the cycle number (one cycle is the duration time of the desired trajectory), Θ_{dci} and Θ_{dsi} are the magnitudes of the ith sinusoidal and cosine functions of $\theta_d(t)$ in Fourier space respectively, $\omega = 2\pi/T$ is the fundamental frequency of $\theta_d(t)$, and N is a positive integer and depends upon the bandwidth of the system. In this way, the desired trajectory $\theta_d(t)$ is a combination of $(2N+1)$ harmonic sinusoidal and cosine functions with different constant magnitudes. In other words, $\theta_d(t)$ is transformed into Fourier space in terms of $(2N+1)$ nonlinear coordinates or bases

$$\begin{aligned} &1, \cos(\omega t), \cos(2\omega t), \cdots, \cos(N\omega t), \\ &\sin(\omega t), \sin(2\omega t), \cdots, \sin(N\omega t). \end{aligned} \tag{5.3.4}$$

which are orthonormal in the time interval $[0, T]$. Similarly, in the kth cycle, the actual output $\theta_k(t)$ of the system in the same period T can also be expressed as the following Fourier series:

$$\theta_k = \frac{\Theta_{c0k}}{2} + \sum_{i=1}^{N}[\Theta_{cik}\cos(i\omega t) + \Theta_{sik}\sin(i\omega t)], \qquad \forall t \in [0, T] \tag{5.3.5}$$

where

$$\Theta_{cik} = \frac{2}{T}\int_{(k-1)T}^{kT} \theta_k(t)\cos(i\omega t)dt \tag{5.3.6}$$

$$\Theta_{sik} = \frac{2}{T}\int_{(k-1)T}^{kT} \theta_k(t)\sin(i\omega t)dt \tag{5.3.7}$$

where the number N of the harmonic terms in $\theta_k(t)$ is the same as that of the desired trajectory $\theta_d(t)$. In the kth cycle, the position tracking error $e_k(t)$ of the system is defined as

$$e_k = \theta_d - \theta_k. \tag{5.3.8}$$

According to (5.3.1) and (5.3.5), the Fourier format of $e_k(t)$ is given by

$$e_k = \frac{E_{c0k}}{2} + \sum_{i=1}^{N}[E_{cik}\cos(i\omega t) + E_{sik}\sin(i\omega t)], \qquad \forall t \in [0, T] \tag{5.3.9}$$

where

$$E_{cik} = \Theta_{dci} - \Theta_{cik} \tag{5.3.10}$$

$$E_{sik} = \Theta_{dsi} - \Theta_{sik}. \tag{5.3.11}$$

Since the elements of the basis of the Fourier space are orthonormal along with the fact that the harmonic magnitudes of the desired trajectory θ_d are constants and have no relation to the cycle number k, the tracking control problem in the time domain is decentralized into $(2N+1)$ regulation control problems in Fourier space, so that we can design independent controllers to control each element of (5.3.9) individually. If all harmonic magnitudes of e_k in (5.3.9) converge, then the tracking error in the time domain will tend to zero. Therefore, the learning controller in Fourier space should have the same harmonic terms as those of e_k. Besides, in Fourier space, the parameters of the controllers are updated once a cycle. The system would very easily be disturbed by random disturbances within the cycle duration. In order to increase the robustness of the system and to deal with the random disturbances, we introduce a conventional proportional-plus-integral (PI) feedback controller in this learning controller. The PI controller is updated at every time instant. Thus, the learning controller in the *k*th cycle has the following form:

$$i_{qk} = k_P z_k + \hat{i}_{qk} \tag{5.3.12}$$

where $z_k(t) = \dot{e}_k(t) + \alpha e_k(t)$ as similarly defined by (4.3.11), k_P and α are positive constant feedback gains, $\dot{e}_k(t)$ is the speed error in the *k*th cycle, and $\hat{i}_{qk}(t)$ is the estimation of the optimal feedforward input $i_q^*(t)$.

Substituting (5.3.12) into (5.2.1) and applying the Fourier transform on both sides of (5.2.1), we obtain

$$\begin{aligned} &\frac{w_{c0k}}{2} + \sum_{i=1}^{N}[w_{cik}\cos(i\omega t) + w_{sik}\sin(i\omega t)] \\ &= \frac{Z_{c0k}}{2} + \sum_{i=1}^{N}[Z_{cik}\cos(i\omega t) + Z_{sik}\sin(i\omega t)] \\ &+ \frac{\hat{w}_{c0k}}{2} + \sum_{i=1}^{N}[\hat{w}_{cik}\cos(i\omega t) + \hat{w}_{sik}\sin(i\omega t)] \end{aligned} \tag{5.3.13}$$

where the left-hand side of the above represents the dynamic system, and its right-hand side represents the controller output or input phase current; w_{cik} and w_{sik} are the projection of the system function on *i*th harmonic frequency, which are determined by the following:

$$w_{cik} = \frac{2}{T}\int_{(k-1)T}^{kT} f_{i_q}(\cdot)\cos(i\omega t)dt \tag{5.3.14}$$

$$w_{sik} = \frac{2}{T}\int_{(k-1)T}^{kT} f_{i_q}(\cdot)\sin(i\omega t)dt, \tag{5.3.15}$$

Z_{cik} and Z_{sik} are calculated from PI controller output as follows:

$$Z_{cik} = \frac{2}{T}\int_{(k-1)T}^{kT} k_P z_k(t)\cos(i\omega t)dt \tag{5.3.16}$$

$$Z_{sik} = \frac{2}{T}\int_{(k-1)T}^{kT} k_P z_k(t)\sin(i\omega t)dt, \tag{5.3.17}$$

and $\hat{w}_{cik}$ and $\hat{w}_{sik}$ will be generated by the learning controller. Hence, the closed-loop system dynamics in Fourier space can be obtained and expressed as

$$w_{cik} = Z_{cik} + \hat{w}_{cik} \tag{5.3.18}$$

$$w_{sik} = Z_{sik} + \hat{w}_{sik}. \tag{5.3.19}$$

Since the real part and also the imaginary part of Fourier series have similar characteristics, we hereafter use w_{cik}, $\hat{w}_{cik}$, and Z_{cik} to represent the $(2N+1)$ Fourier coefficients of $i_{qk}(t)$, $\hat{i}_{qk}(t)$, and $z_k(t)$ so no confusion is caused. It is obvious from (5.3.18) and (5.3.19) that the controller design task is to develop an algorithm for $\hat{w}_{cik}$ to force $\hat{w}_{cik}$ and w_{cik} to approach the same value, which is the corresponding Fourier coefficient of the optimal feedforward $i_q^*(t)$. Alternatively, in the time domain, $\hat{i}_{qk}(t)$ and $i_{qk}(t)$ will converge to the same function $i_q^*(t)$, and $z_k(t)$ will approach zero simultaneously. The tracking error $e_k(t)$ will then asymptotically converge, since $z_k(t) = 0$ constructs a stable sliding surface. Intuitively, we simply design the recursive update law as

$$\hat{w}_{cik} = \gamma_i \sum_{j=0}^{k-1} Z_{cij} \tag{5.3.20}$$

with the gains $\gamma_i > 0, \quad i = 1, 2, \cdots, N$. Then the closed-loop system dynamic equation in Fourier space may be rewritten as

$$Z_{cik} + \gamma_i \sum_{j=0}^{k-1} Z_{cij} = w_{cik} \tag{5.3.21}$$

To ensure that w_{cik} tends to the constants or Z_{cik} converge to zero as k increases, the gains γ_i should be selected according to the property of the controlled system. The corresponding conditions will be given and discussed in the next section.

Generally repeatable tasks can be classified into two types as follows: iterative learning mode tasks and repetitive mode tasks. Iterative learning mode tasks start with the same initial conditions and usually have time breaks before the next trial. In repetitive mode tasks, the final conditions of a given cycle are the same as the initial conditions of the next cycle and in succession. Considering that the period of a given desired trajectory is known, we may utilize the Discrete Fourier transform (DFT) in our algorithm to distribute the computation work to each sampling period. Therefore, the proposed algorithm can complete tasks of both types. The detailed implementation steps are presented here.

Given Conditions: The sampling period ΔT , and the desired trajectory $\theta_d(t), \ \forall t \in [0, T]$, or $\theta_d[j], \ \ j = 1, 2, \cdots, M$ with $M = T/\Delta T$.

Step 1: Search PI controller gains (k_P, α) to stabilize the controlled system with acceptable tracking performance. Set $\hat{w}_{cik} = 0$ and $\hat{w}_{sik} = 0$ for all i. Set the learning counter $k = 1$.

Step 2: Set sampling counter $j = 1$, $Z_{cik} = 0$, and $Z_{sik} = 0$. Set the learning gain γ_i.

Step 3: Calculate the compensation term

$$comp[j] = \frac{\hat{w}_{c0k}}{2} + \sum_{i=1}^{N} [\hat{w}_{cik} \cos(i(2\pi/M)j) + \hat{w}_{sik} \sin(i(2\pi/M)j)].$$

Apply PI controller to the system and obtain $e_k[j] = \theta_d[j] - \theta_k[j]$, and $z_k[j] = \dot{e}_k[j] + \alpha e_k[j]$, and then output control signal $k_P z_k[j] + comp[j]$.

After each sampling, increase *j* by 1 (i.e., $j \to j+1$) and calculate

$$Z_{cik} \to Z_{cik} + \frac{2}{M} k_P z_k[j] \cos(i(2\pi/M)j)$$

$$Z_{sik} \to Z_{sik} + \frac{2}{M} k_P z_k[j] \sin(i(2\pi/M)j).$$

Step 4: If $j \neq M$, continue step 3.

Step 5: If the tracking error index in the *k*th trial $EI_k < \varepsilon$ (learning process ends), go to step 2.

Step 6: Calculate $\hat{w}_{ci(k+1)} = \hat{w}_{cik} + \gamma_i Z_{cik}$, $\hat{w}_{si(k+1)} = \hat{w}_{sik} + \gamma_i Z_{sik}$.

Increase *k* by 1 (i.e., $k \to k+1$) and go to step 2.

To ensure that the tracking error index decreases as *k* increases, we may repeat the above steps with different PI gains and learning gains. In this case, we reduce the learning gain first, and then modify PI gains as required.

5.4 Stability Analysis

Based on the fact the dynamics of the system is nonlinear, and input and state dependent, when the input changes, the dynamics or the operating point of the system also changes. Suppose that the input to the system described by (5.2.1) only contains a single frequency. The output of the system contains, in general, higher harmonics in addition to the fundamental harmonic component. When the output is fed back to the system, these harmonic components will generate their harmonics. As the system has only a finite bandwidth, harmonics higher than the cutoff frequency are greatly attenuated and were neglected. Therefore, even though the input changes in only one harmonic frequency, it will alter all w_{cik} and w_{sik} in the nonlinear system. The proposed algorithm attempts to eliminate tracking errors in each harmonic individually, no matter by which harmonic component they are generated. Define

$$\Delta w_{cik} = w_{ci(k+1)} - w_{cik} \tag{5.4.1}$$

which gives the system change in the *i*th harmonic frequency due to the input change from the *k*th cycle to the (*k*+1)th cycle. Further define

$$\Delta Z_{cik} = Z_{ci(k+1)} - Z_{cik} \tag{5.4.2}$$

which represents the change of tracking error magnitude in the *i*th harmonic from the *k*th cycle to the (*k*+1)th cycle. After giving the above definition, we are now ready to prove the following.

Theorem 1: Given the motor dynamics of (5.2.1), the learning controller given in (5.3.12) and (5.3.20) ensures the convergence of the tracking error as long as the learning gain γ_i, and the closed-loop system input/output relation in Fourier space satisfy the following sufficient conditions:

$$0 < \gamma_i < 1 \tag{5.4.3a}$$

$$\left| \frac{\Delta w_{ik}}{\Delta Z_{ik}} \right| < 1 - \gamma_i, \qquad \forall i, k \in Z_+ \tag{5.4.3b}$$

where $\Delta w_{ik} \in [\Delta w_{cik},\ \Delta w_{sik}]$, and $\Delta Z_{ik} \in [\Delta Z_{cik},\ \Delta Z_{sik}]$.

Proof: Applying the difference operator defined in (5.4.1) and (5.4.2) to both sides of (5.3.18) and (5.3.19), we obtain

$$\Delta w_{ik} = \Delta Z_{ik} + \Delta \hat{w}_{ik}. \tag{5.4.4}$$

From the update law (5.3.20), we have

$$\Delta \hat{w}_{ik} = \gamma_i Z_{ik} \tag{5.4.5}$$

where $Z_{ik} \in [Z_{cik},\ Z_{sik}]$.

Substituting (5.4.5) into (5.4.4) gives

$$\Delta w_{ik} = \Delta Z_{ik} + \gamma_i Z_{ik} \tag{5.4.6}$$

$$\frac{\Delta w_{ik}}{\Delta Z_{ik}} = 1 + \frac{\gamma_i Z_{ik}}{\Delta Z_{ik}} \tag{5.4.7}$$

$$\frac{\Delta w_{ik}}{\Delta Z_{ik}} - 1 = + \frac{\gamma_i}{\dfrac{Z_{i(k+1)}}{Z_{ik}} - 1} \tag{5.4.8}$$

$$\frac{Z_{i(k+1)}}{Z_{ik}} = \frac{\gamma_i}{\dfrac{\Delta w_{ik}}{\Delta Z_{ik}} - 1} + 1. \tag{5.4.9}$$

If the learning gain is selected to satisfy $0 < \gamma_i < 1$ and the closed-loop system complies with $\left|\Delta w_{ik} / \Delta Z_{ik}\right| < 1 - \gamma_i$, then it is easy to obtain

$$\left|\frac{Z_{i(k+1)}}{Z_{ik}}\right| < \beta < 1. \tag{5.4.10}$$

Thus, a sequence of Fourier coefficients will be produced as the trial number k increases, which has the following property:

$$\left|Z_{ik}\right| < \beta \left|Z_{i(k-1)}\right| < \beta^2 \left|Z_{i(k-2)}\right| < \cdots < \beta^k \left|Z_{i0}\right|. \tag{5.4.11}$$

Since the initial value Z_{i0} is bounded, each Fourier coefficient of the PI controller output $k_P z_k(t)$ will diminish asymptotically as the trial number k increases. This implies that in the time domain, we will finally have

$$z(t) = \dot{e}(t) + \alpha e(t) = 0 . \tag{5.4.12}$$

As α is a positive constant, the above equation constructs a stable sliding surface. $e(t)$ will tend to zero along the sliding surface as time lasts (notice that $t = kT + t'$, $t' \in [0, T]$, as $k \to \infty$, $t \to \infty$), which completes the proof.

Remark 1: In the first trial only the PI controller is used, $\hat{w}_{ci0} = 0$, $\hat{w}_{si0} = 0$, i.e., the feedforward part is zero. From (5.3.18) and (5.3.19), we have $w_{ci0} = Z_{ci0}$, $w_{si0} = Z_{si0}$. So from (5.3.20), in the second trial $\hat{w}_{ci1} = \gamma_i Z_{ci0}$, $\hat{w}_{si1} = \gamma_i Z_{si0}$, that is, the PI controller output in the first trial is used as a feedforward in the second trial. The selection of iterative update-law (5.3.20) does make sense.

Remark 2: Condition $\left|\Delta w_{ik} / \Delta Z_{ik}\right| < 1 - \gamma_i$ is only a sufficient condition for the given controller. Its geometrical meaning is that the first derivative of w_{ik} with respect to Z_{ik} is less than 1, while the trajectory tracking is carried out repeatedly. In linear systems, Δw_{ik} and ΔZ_{ik} vary independently of other harmonic components, and the actual bound of $\left|\Delta w_{ik} / \Delta Z_{ik}\right|$ is smaller. Therefore, the learning gain can be selected as a larger value for fast convergence. In nonlinear systems, both Δw_{ik} and ΔZ_{ik} will be influenced by other harmonic components, the actual bound of $\left|\Delta w_{ik} / \Delta Z_{ik}\right|$ will be larger. We must trade the convergent rate for stability. Whether the above condition can be achieved or not also depends on the system itself. For a given system, if the above condition cannot be satisfied, the controller that we are interested in cannot guarantee the stability.

Remark 3: The main advantage of the Fourier series based learning is the enhancement of learning robustness and the improvement of tracking performance. Note that there is always some system noise or other small non-repeatable factors even in a repeatability dominant control environment. Accumulation of these tiny components contained in the control sequence and the tracking error sequence may degrade the approximation precision of the learning control sequence. The Fourier series based learning mechanism, on the other hand, updates coefficients of the learned frequency components and those coefficients are calculated according to (5.3.16), (5.3.17) and (5.3.20) which take the integration of the tracking error sequence over the entire control interval [0, *T*]. In the sequel, the integration processes play the role of an averaging operation on the two noisy sequences $\hat{w}_{ik}$ and Z_{ik} and are able to remove the majority of those high frequency components.

Remark 4: The controller consists of two parts: PI controller and iterative learning controller. The former is a real time feedback controller that is updated at each sample instant, so that it can stabilize the system, and reduce the effects of random disturbances and the mismatch of initial condition. The latter is a feedforward compensator which is iteratively updated to obtain the optimal feedforward for compensating the deterministic uncertainties resulting from the ripple dynamics. Since it is designed in Fourier space, the parameters $\hat{w}_{cik}$ and $\hat{w}_{sik}$ in (5.3.12) should be updated once in every trial. Although the proposed scheme is a linear learning method in Fourier space when constant learning gains are selected, it can represent the optimal nonlinear input function and the nonlinear input/output relation in the time domain. Hence, it can be applied to nonlinear systems. The system performance mainly depends on the compensation portion and has little to do with PI gains provided that the random disturbances are not serious. So there is a large range for selecting PI gains.

Remark 5: In linear systems, the harmonic components are independent of each other. The compensated harmonic components will not influence the uncompensated parts, so that no spillover-like problems are caused. In nonlinear systems, the harmonic components are cross-related, and spillover-like problems may be caused in uncompensated high-frequency component parts. However, this will not reduce the performance much, since a physical system only has a finite bandwidth and the lower frequency components generally dominate the tracking errors. In addition, the control performance relies on the number N of harmonic terms. The selection of a larger N can ensure more harmonic components of the output error are canceled so that better control performance can be achieved.

Remark 6: Since the controller only contains measurable and local information, there is no requirement for the system modeling. This approach is particularly appropriate to the situation where not all the state variables are measurable.

5.5 Experiments and Discussions

To illustrate the effectiveness of the control scheme presented here, experiments have been conducted on a typical two-phase hybrid stepping motor. A complete control implementation scheme is similar to that adopted in Chapter 4, and is not described here in detail. During the experiments, the motor system was required to track an identical sinusoidal trajectory $\theta_d(t) = 1 - \cos \pi t,\ t \in [0, 2]$ in the sense of position tracking. The desired trajectory lasts for only two seconds. Therefore, tracking the desired trajectory for two seconds is considered as a trial.

The learning and decentralized controller we used in the experiment is of the same form as that of (5.3.12). $\hat{w}_{cik}$ and $\hat{w}_{sik}$ are updated once a cycle according to the recursive algorithms (5.3.20), where *k* denotes the cycle number, and the same learning control gain is utilized for each harmonic component in Fourier space, i.e., $\gamma_0 = \gamma_1 = \gamma_2 = \cdots = \gamma_{2N} = \gamma$. It is easy to see that this controller is exactly a frequency-domain format of (4.4.14).

The experimental results of the position tracking error with certain control parameters are shown in Fig. 5.1, from which we can clearly see the entire convergent procedure. Since the learning gain is less than 1 $(\gamma = 0.5)$, the convergence of the tracking error was achieved after about five cycles. The tracking error was forced inside about 0.0004 rad. Although the tracking error shows a periodicity of 0.5 Hz, which is consistent with that of the desired trajectory, it is far from a single-frequency sine wave. It contains higher harmonics and has a small spike at the moment when the motor changes its rotary direction due to the static frictional force and dead-zone. The number of harmonic terms of the Fourier series in the learning controller is chosen to be $N = 25$, so that the maximum frequency of harmonic components covered in the learning controller is only up to 12 Hz. However, the spikes contain very rich harmonic components and some of their frequencies are higher than 12 Hz. Therefore, the spikes have not been eliminated. Intuitively, if we increase *N*, more harmonic components would be included to achieve better control performance. However, a larger N would require an intensive computing ability for practical implementation. Moreover, there is a limit to the increase of N because the resonant frequency of the controlled system could not be included.

In order to gain more understanding about the proposed controller, a detailed analysis of the experimental results is presented next.

A. Effectiveness of PI Gains

To illustrate the relationship of the PI gains and the performance of the controller, on the basis of Fig. 5.1, we decreased PI gains by half and kept all other parameters unchanged. The experimental results are shown in Fig. 5.2. Comparing Figs. 5.1 and Fig. 5.2, we can see that PI gains did not influence the convergence rate, but they did have a minor influence on the performance. The performance with smaller PI gains is a little worse than that with larger PI gains. This is because random noise and disturbances existed in this system. This means PI control is useful for rejecting random and nondeterministic signals.

B. Effectiveness of Learning Gain

Fig. 5.3 is the experimental result with a larger learning gain $\gamma = 0.75$, while other parameters were the same as those in Fig. 5.1 ($\gamma = 0.5$). Comparing Fig. 5.3 with Fig. 5.1, we can see that only the convergence rate is influenced by the learning gain. In Fig. 5.3, the convergence time is within three cycles. Hence, the larger the value of γ (less than one), the faster will be the convergence rate, as indicated in Remark 2.

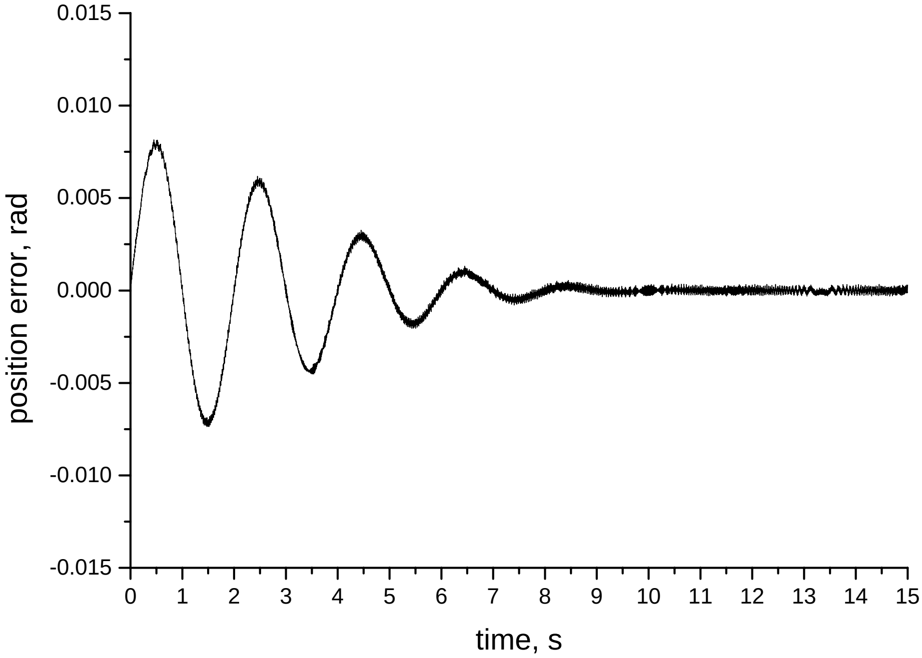

Fig. 5.1 Learning convergence of tracking error of proposed controller with higher PI gains ($k_p = 0.4, \quad \alpha = 15, \quad \gamma = 0.5, \quad N = 25$)

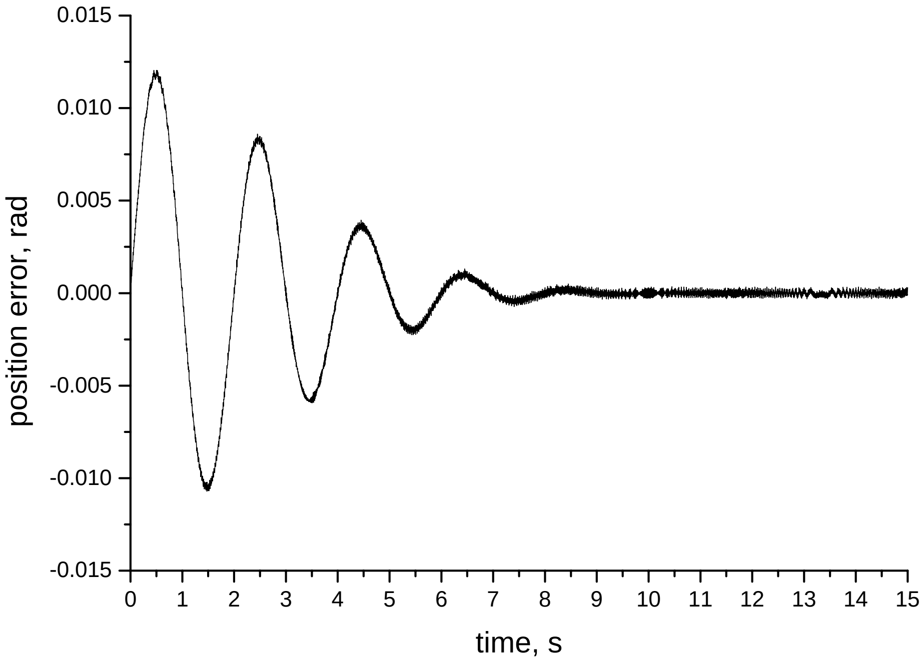

Fig. 5.2 Learning convergence of tracking error of proposed controller with smaller PI gains ($k_p = 0.2, \quad \alpha = 15, \quad \gamma = 0.5, \quad N = 25$)

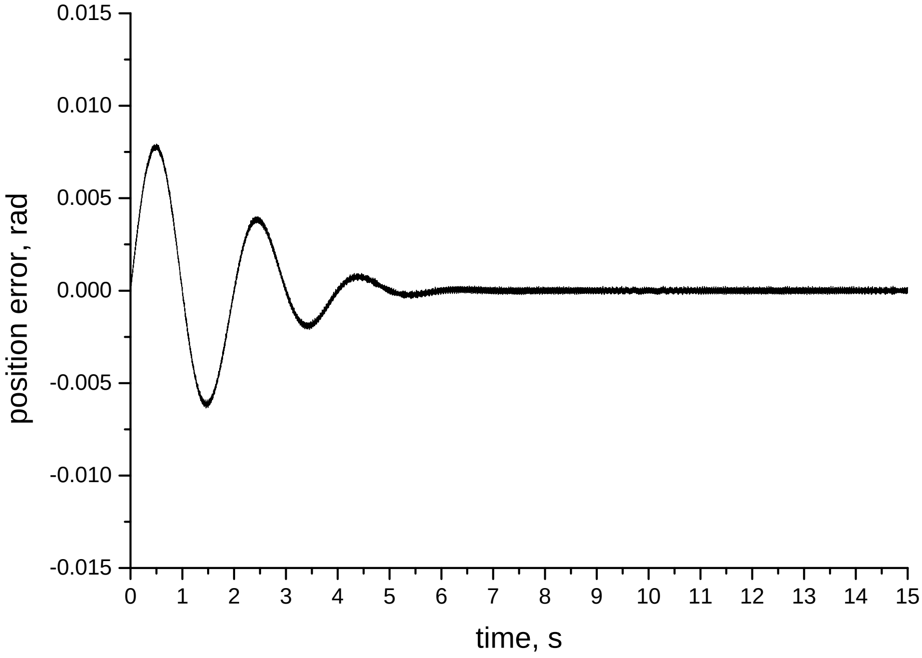

Fig. 5.3 Learning convergence of tracking error of proposed controller with higher PI gains ($k_p = 0.4, \quad \alpha = 15, \quad \gamma = 0.75, \quad N = 25$)

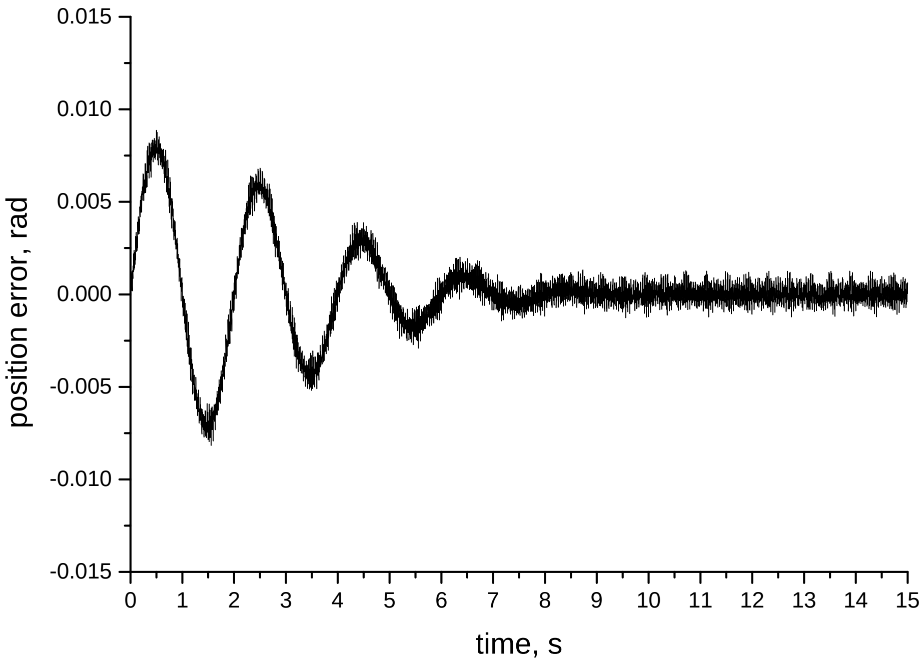

Fig. 5.4 Learning convergence of tracking error of proposed controller with higher PI gains ($k_p = 0.4, \quad \alpha = 15, \quad \gamma = 0.5, \quad N = 9$)

C. Effectiveness of Different Harmonic Terms

In order to show how the harmonic terms N in the Fourier series of the learning controller influence the system's performance, we used a smaller N for the controller design. In this experiment, we kept all the control parameters unchanged as above, except for $N = 9$. The position tracking error is shown in Fig. 5.4. From this figure, we can see that the convergence rate is almost the same as that in Fig. 5.1. But the performance is much worse. The reason is very explicit. In Fig. 5.4, those components with the harmonic frequencies between 4–12 Hz were not included in the learning controller compared with Fig. 5.1. Therefore, they were not compensated for and still remained in the tracking error.

D. Enhanced Performance of Controller over the Time-Domain Counterpart

By comparing Fig. 5.3 with Fig. 4.4(b), it is clear that frequency-domain learning further improves tracking control performance relative to its time-domain counterpart. This is because the integration processes provided by (5.3.16) and (5.3.17) play the role of an averaging operation on the two noisy sequences (both control sequence and tracking error sequence), which are able to nullify the majority of high frequency components caused by quantization error and other non-ideal factors due to limited sampling frequency. Learning in the frequency-domain with (5.3.20) obtains the fastest convergence. Moreover, it is shown in both Fig. 5.3 and Fig. 4.4(b) that the frequency-domain learning experienced a fairly smooth tracking history except that its tracking accuracy is subject to limitation of the encoder's resolution.

5.6 Summary

In this chapter, a new learning and decentralized controller based on a Fourier series is presented for tracking control of the hybrid stepping motor. The stability and convergence conditions of the learning controller were presented. Both the theoretical analysis and the experimental results have shown that the proposed learning controller has some special features relative to others.

(1) The proposed controller has a general and decentralized format. It consists of two parts. One is a PI feedback controller which should be updated at each sample instant. It is used to deal with the random disturbances and the nondeterministic portion of the system. The other is a compensation portion designed in Fourier space which had to be updated once a cycle and is used to cope with the deterministic portion of the system such as the ripple dynamics. Since this controller only includes measurable and local information, there is no requirement for the system modeling. Therefore, it is a decentralized and model-free controller.

(2) The fundamental point of this learning controller is that it is designed in Fourier space with orthonormal bases. The signals, such as desired trajectory and actual output, can be represented by a number of independent harmonic components. As a result, the nonlinear tracking control problem in the time domain is decentralized into a number of independent regulation problems. Thus, in Fourier space, it is very simple to design the regulation controllers.

(3) Since the controller is designed in Fourier space, it can automatically tune the controller not only toward a suitable magnitude but toward a suitable phase. The controller is therefore very effective in coping with the system’s time-delay.

(4) The implementation of this controller is very easy. Only a few control parameters such as k_P, α, γ, and harmonic term N have to be tuned. Since PI gains have little influence on the closed-loop performance after the system converges, they can be selected from a large range. γ could be estimated according to the system nonlinearity or adjusted by "trial and error", and can be selected according to the computation ability, sample interval, and the performance required.

(5) The convergence rate of the frequency-domain learning could be very fast. In our experiment, convergence was achieved in two to three cycles (Fig. 5.3). It is much faster than the corresponding time-domain counterpart. The reason for fast convergence lies in the fact that the proposed controller is designed in Fourier space, and the high frequency noise and resonance frequency of the controlled system could be easily removed by selecting a suitable number of harmonic terms, so that a higher learning gain could be used.

CHAPTER 6

CONCLUSIONS

The development of simple and efficient control algorithms to solve the highly nonlinear torque-current-position characteristics at low speed of closed-loop commuted stepping motors for high-precision tracking has been investigated. The principles of several control schemes have been exploited to minimize the motor's torque ripple that is periodic and nonlinear in the system states with specific emphasis on low-speed conditions. The proposed control algorithms are based on a modular control strategy where the feedback control module is first designed to ensure global stability and achieve bounded tracking accuracy while the feedforward control module is added to further improve the tracking performance. The interactions between the feedforward control module and the feedback control module have been explored and were shown to be complementary to each other. The DQ transformation has been utilized as a platform for control design. This has been shown to be useful in the facilitation of the desired sinusoidal commutation scheme for fast control implementation. The proposed control algorithms are diversified from the model-based design to the model-free design in either the time-domain or the frequency-domain.

In the model-based control schemes, a feedback linearizing control approach has been used to test the profile tracking performance. A novel model identification procedure that operates on the measurable position signal and phase current offers attractive features that promise to avoid any significant injection of quantization errors and also promise to reject other possible noise sources without strict limitations on the operating mode of the motor. The feedback controller that incorporates knowledge of both the ripple dynamics and the motion itself has successfully linearised the system as long as an appropriate choice of control gains is made with sufficient emphasis on integral control. The analysis, simulations and experiments have shown that the derived feedback control permits the motion tracking error system to respond quickly, and reject part of the ripple components. However, due to the forced excitation caused by the detent torque, the feedback controller alone is not sufficient to create the best speed tracking performance. This problem has been resolved by the introduction of feedforward compensation. The addition of the feedforward controller significantly improves global tracking results with the speed ripple being suppressed to a reasonably low level.

A robust adaptive control approach has been considered for the purpose of improving the performance of the above scheme using an integrated control concept. By uncovering the properties of nonlinear uncertainties in the system dynamics and incorporating them into the control design, we have constructed a completely integrated controller to reduce torque ripple and at the same time to enhance tracking performance. The system uncertainties are classified into two categories of structured uncertainties. The structured uncertainty arising from the dominant detention effect can be separated and expressed as the product of known harmonic functions of the rotor position and a set of unknown constants. This uncertainty is estimated with adaptation and compensated for. The robust adaptive method is applied to deal with other structured uncertainty resulting from the nonsinusoidal flux distribution by estimating its bounding constants. The $\mu -$modification scheme is applied in order to stop parameter adaptation in accordance with the robust adaptive control law. This control scheme can guarantee the uniform boundedness of the motor drive system and assures that the filtered tracking error enters an arbitrarily pre-specified zone in a finite time, and in turn the trajectory tracking error asymptotically converges to a pre-specified boundary.

Performance comparison between both model-based control schemes has shown that the robust adaptive control is clearly superior to the feedback linearizing control in generating a precise profile. A radical reason to induce such a performance difference lies in that the former directly incorporates the adaptive ripple compensation (feedforward) into the linear feedback control part together with a robust adaptive component for both the guaranteed global stability and the control specification, while the latter separates the feedforward design from the feedback with the special constraint of the ripple compensating terms and subjects to the requirement on the accurate estimation of torque ripple constants. As a result, the robust adaptive control scheme provides the advantage of suppressing the torque ripple components over a broader ripple frequency band.

In the model-free control schemes, two categories of the learning-based approaches have been considered for our purpose. The first is based on a modified standard repetitive learning control. This has a very simple structure which consists of two time-domain components in additive form: a feedback control mechanism using either a pure linear form or some nonlinear form, and a learning mechanism that simply adds up a past tracking error sequence. We have illustrated how a learning-based estimate can be used to achieve asymptotic tracking in the presence of undesirable nonlinear dynamics. Basing on the fact that the estimate of the learning-based controller is generated from a Lyapunov-based stability analysis, we have demonstrated how the Lyapunov-based design technique could be utilized to construct a learning control for rejecting components of the ripple dynamics in a hybrid stepping motor. For easier implementation, we have specifically designed a hybrid controller by incorporating a pure linear feedback control into the repetitive learning mechanism. The proposed control scheme, as opposed to the use of a multiple step process, is updated continuously with time during the transient response (versus during the steady-state) and hence an improved transient response is facilitated.

The second learning based approach is based on a decentralized learning control that is implemented in the frequency domain by means of a Fourier series expansion for tracking control of a hybrid stepping motor. Basing on the fact that for a class of tracking control tasks defined over a finite duration both the desired trajectory and the actual output can be expressed by a Fourier series with constant harmonic magnitudes, the learning controller has been designed to individually control each harmonic component of the actual output so that it converges to that of the desired trajectory within the system bandwidth. Since this decentralized learning controller is designed in Fourier space instead of in time domain, the system's time-delay can be easily compensated for. Moreover, this learning controller is only based on local input and output information so that no a priori system modeling is required. The control scheme can significantly improve the tracking control performance due to its control design philosophy in Fourier space and the peculiar capability of independent harmonic control.

In comparison to the corresponding time-domain counterpart, frequency-domain learning control can obtain better tracking accuracy and faster convergence. This is because the integration processes inherent in the frequency-domain algorithm have played the role of an averaging operation on the two noisy sequences (both control sequence and tracking error sequence) nullifying majority of the high frequency components caused by quantization errors and other non-ideal factors due to limited sampling frequency. Learning in the frequency-domain experiences a fairly smooth tracking history except that its tracking accuracy is subject to the limitation of the encoder's resolution.

The experiments were conducted on a typical hybrid stepping motor to illustrate the effectiveness of the different control systems in precision profile generation. The experimental results have validated the theoretical predictions presented. Although the performance comparisons between the model-based control schemes as well as the model-free control schemes are given respectively, the model-free schemes exhibit better application potential because they have the inherent capability of nonlinear functional identification to compensate for the ripple dynamics. This offers guidance for the selection of a practical control algorithm in tuning computer-controlled drives. The impressive results obtained in this study pave the way for the stepping motors to be used in many applications previously not suitable for open loop steppers such as in low-speed direct-drive systems.

APPENDIX A

PROOF OF EXISTENCE

From (3.4.16), it can be seen that $\dot{V} < 0$ if

$$k_P z^2 > \tfrac{1}{2}\mu_1 \Theta^T \Theta + \tfrac{1}{2}\mu_2 \phi^2 + \varepsilon\,; \tag{A1}$$

then ε_0' can be easily determined by solving the following equation:

$$\frac{\varepsilon + c}{\varepsilon_0^2} z^2 = \tfrac{1}{2}\mu_1 \Theta^T \Theta + \tfrac{1}{2}\mu_2 \phi^2 + \varepsilon\,. \tag{A2}$$

Substituting μ_1 and μ_2 in terms of (3.4.11) and letting $|z| = \varepsilon_0'$ yields

$$\frac{\varepsilon + c}{\varepsilon_0^2} \varepsilon_0'^2 = \tfrac{1}{2} g_1 (\varepsilon_0 - \varepsilon_0') \Theta^T \Theta + \tfrac{1}{2} g_2 (\varepsilon_0 - \varepsilon_0') \phi^2 + \varepsilon\,. \tag{A3}$$

Denote

$$A = \frac{\varepsilon + c}{\varepsilon_0^2}\,,$$

$$B = \tfrac{1}{2}(g_1 \Theta^T \Theta + g_2 \phi^2)\,,$$

$$C = \tfrac{1}{2} g_1 \varepsilon_0 \Theta^T \Theta + \tfrac{1}{2} g_2 \varepsilon_0 \phi^2 + \varepsilon\,;$$

then (A3) can be transformed to the following:

$$A \varepsilon_0'^2 + B \varepsilon_0' - C = 0\,. \tag{A4}$$

The solutions of the above equation are

$$\varepsilon_0' = \frac{-B \pm (B^2 + 4AC)^{1/2}}{2A}\,. \tag{A5}$$

It is obvious that the solutions $\varepsilon_0' \in \Re$. Note that ε_0' is positive; hence the desired solution is

$$\varepsilon_0' = \frac{-B + (B^2 + 4AC)^{1/2}}{2A} > 0. \tag{A6}$$

APPENDIX B

PROOF OF INEQUALITY

To prove the inequality given in (4.2.10), we divide the proof into three possible cases as follows.

Case 1: $|\xi_{1i}| \le \beta_i, \quad |\xi_{2i}| \le \beta_i$

From the definition of $\mathrm{sat}_{\beta}(\cdot)$ given in (4.2.9), we can see that for this case

$$\mathrm{sat}_{\beta_i}(\xi_{1i}) = \xi_{1i}, \qquad \mathrm{sat}_{\beta_i}(\xi_{2i}) = \xi_{2i}. \tag{B1}$$

After substituting (B1) into (4.2.10), we obtain the following expression:

$$(\xi_{1i} - \xi_{2i})^2 = (\mathrm{sat}_{\beta_i}(\xi_{1i}) - \mathrm{sat}_{\beta_i}(\xi_{2i}))^2 \tag{B2}$$

for $|\xi_{1i}| \le \beta_i, \quad |\xi_{2i}| \le \beta_i$, hence, the inequality given in (4.2.10) is true for Case 1.

Case 2: $|\xi_{1i}| \le \beta_i, \quad \xi_{2i} > \beta_i$

From the definition of $\mathrm{sat}_{\beta}(\cdot)$ given in (4.2.9), it is clear for this case that

$$(\xi_{2i} + \beta_i) \ge 2\xi_{1i}, \text{ for } |\xi_{1i}| \le \beta_i, \quad \xi_{2i} > \beta_i. \tag{B3}$$

After multiplying both sides of (B3) by $\xi_{2i} - \beta_i$ and then simplifying the left-hand side of the inequality, we can rewrite (B3) as follows:

$$(\xi_{2i}^2 - \beta_i^2) \ge 2(\xi_{2i} - \beta_i)\xi_{1i} \tag{B4}$$

where we have utilized the fact that $\xi_{2i} - \beta_i > 0$ for this case. After adding the term ξ_{1i}^2 to both sides of (B4) and then rearranging the resulting expression, we obtain the following expression:

$$\xi_{1i}^2 - 2\xi_{1i}\xi_{2i} + \xi_{2i}^2 \ge \xi_{1i}^2 - 2\beta_i\xi_{1i} + \beta_i^2. \tag{B5}$$

Based on the expression given in (B5), we can utilize the facts that

$$\mathrm{sat}_{\beta_i}(\xi_{1i}) = \xi_{1i}, \qquad \mathrm{sat}_{\beta_i}(\xi_{2i}) = \beta_i \tag{B6}$$

to prove that

$$(\xi_{1i} - \xi_{2i})^2 \geq (\mathrm{sat}_{\beta_i}(\xi_{1i}) - \mathrm{sat}_{\beta_i}(\xi_{2i}))^2 \tag{B7}$$

for $|\xi_{1i}| \leq \beta_i, \quad \xi_{2i} > \beta_i$.

Case 3: $|\xi_{1i}| \leq \beta_i, \quad \xi_{2i} < -\beta_i$

From the definition of $\mathrm{sat}_\beta(\cdot)$ given in (4.2.9), it is clear for this case that

$$(\xi_{2i} - \beta_i) \leq 2\xi_{1i}, \text{ for } |\xi_{1i}| \leq \beta_i, \quad \xi_{2i} < -\beta_i. \tag{B8}$$

After multiplying both sides of (B8) by $(\xi_{2i} + \beta_i)$ and then simplifying the left-hand side of the inequality, we can rewrite (B8) as follows:

$$(\xi_{2i}^2 - \beta_i^2) \geq 2(\xi_{2i} + \beta_i)\xi_{1i} \tag{B9}$$

where we have utilized the fact that $\xi_{2i} + \beta_i < 0$ for this case. After adding the term ξ_{1i}^2 to both sides of (B9) and then rearranging the resulting expression, we obtain the following expression:

$$\xi_{1i}^2 - 2\xi_{1i}\xi_{2i} + \xi_{2i}^2 \geq \xi_{1i}^2 + 2\beta_i\xi_{1i} + \beta_i^2. \tag{B10}$$

Based on the expression given in (B10), we can utilize the facts that

$$\mathrm{sat}_{\beta_i}(\xi_{1i}) = \xi_{1i}, \qquad \mathrm{sat}_{\beta_i}(\xi_{2i}) = -\beta_i \tag{B11}$$

to prove that

$$(\xi_{1i} - \xi_{2i})^2 \geq (\mathrm{sat}_{\beta_i}(\xi_{1i}) - \mathrm{sat}_{\beta_i}(\xi_{2i}))^2 \tag{B12}$$

for $|\xi_{1i}| \leq \beta_i, \quad \xi_{2i} < -\beta_i$; hence, we have proven that (4.2.10) is true for all possible cases.

REFERENCES

Aiello, M., Rekowski, R., Bodson, M., Chiasson, J., and Schuerer, D. “Experimental results of parameter identification and nonlinear control on a PM stepper motor,” *Microprocessors in Robotic and Manufacturing Systems*, Tzafestas, S.G., Ed., pp.353-368, New York: Kluwer, 1991.

Arimoto, S. “Robustness of learning control for robot manipulators,” *Proc. IEEE Int. Conf. Robotics and Automation*, 1990.

Arimoto, S., Kawamura, S., and Miyazaki, F. “Bettering operation of robots by learning,” *J. Robot. Syst.*, vol. 1, no. 2, pp. 123–140, 1984.

Arimoto, S., Kawamura, S., and Miyazaki, F. “Realization of robot motion based on a learning method,” *IEEE Trans. Syst., Man, Cybern.*, vol. 18, no. 1, pp. 126–134, 1988.

Arimoto, S. *Control Theory of Non-Linear Mechanical Systems: A Passivity-Based and Circuit-Theoretic Approach*. Oxford, U.K.: Clarendon, 1996.

Blauch, A., Bodson, M., and Chiasson, J. “High-speed parameter estimation of stepper motors,” *IEEE Trans. Contr. Syst. Technol.*, vol. 1, no. 4, pp. 270-279, 1993.

Bodson, M., Chiasson, J., Novotnak, R., and Rekowski, R. “High-performance nonlinear feedback control of a permanent magnet stepper motor,” *IEEE Trans. Contr. Syst. Technol.*, vol. 1, no. 1, pp. 5-14, 1993.

Brogliato, B., and Trofino Neto, A. “Practical stabilization of a class of nonlinear systems with partially known uncertainties,” *Automatica*, vol. 1**,** pp. 145-150, 1995.

Cai, L., and Tang, X. “A model-free decentralized control for robot manipulator,” *Proc. IEEE Conf. Robot. Automat.*, vol. 4, pp. 3106-3111, 1997.

Cheah C. C., Wang, D., and Soh, Y. C. "Convergence and robustness of a discrete-time learning control scheme for constrained manipulators," *J. Robot. Syst.*, vol. 11, no. 3, pp. 223–238, 1994.

Cheah C. C., Wang, D., and Soh, Y. C. "Learning control of motion and force for constrained robotic manipulators," *Int. J. Robot. Automat.*, vol. 10, no. 3, pp. 79–88, 1995.

Cheah C. C., Wang, D., and Soh, Y. C. "Learning control for a class of nonlinear differential-algebraic systems with application to constrained robots," *J. Robot. Syst.*, vol. 13, no. 3, pp. 141–151, 1996.

Cheah, C. C. and Wang, D. "A Model-reference learning control scheme for a class of nonlinear systems," *Int. J. Contr.*, vol. 66, no. 2, pp. 271–287, 1997.

Chen, D. and Paden, B. "Nonlinear adaptive torque-ripple cancellation for step motor," *29th IEEE Conference on Decision and Control*, pp. 3319-3324, Honolulu, USA, December 1990.

Chew, K. and Tomizuka, M. "Digital control of repetitive errors in disk-driver system," *IEEE Contr. Syst. Mag.*, vol. 10, pp. 16–20, Jan. 1990.

Cho, S.-I. and Ha, I.-J. "A learning approach to tracking in mechanical systems with friction," *IEEE Trans. Automat. Contr.*, vol. 45, pp. 111–116, Jan. 2000.

Chu, S.H., Ha, I.J., Lee, I.J. and Kang, J.H. "Feedback linearizing control of hybrid stepping motors," *Proc. IEEE Conf. Robotics and Automation*, pp 2039-2044, 1994.

Clark, R. and Gibbs, G. "A novel approach to feedforward higher-harmonic control," *J. Acoust. Soc. Am.*, vol. 96, no. 2, pp. 926-936, 1994.

Clarkson, P. J. and Acarnley, P. P. "Closed-loop control of stepping motor systems," *IEEE Trans. Industrial Appl.*, vol. 24, pp. 685-691, 1988.

Clarkson, P. M. *Optimal and Adaptive Signal Processing*. pp. 308-323, Florida: CRC Press, 1993.

Corless, M. J. and Leitmann, G. “Adaptive control for systems containing uncertain functions and uncertain functions with uncertain bounds,” *J. Optim. Theory Applicat.*, vol. 41, pp. 155–168, 1983.

Costic, B., de Queiroz, M. S. and Dawson, D. M. “A new learning control approach to the active magnetic bearing benchmark system,” in *Proc. American Control Conf.*, Chicago, IL, 2000, pp. 2639–2643.

Dawson, C. M., Qu, Z., Dorsey, J. F. and Lewis, F. L. “On the learning control of a robot manipulator,” *J. Intelligent and Robotics Syst.*, vol.4, pp. 43-53, 1991.

Doh, T. Y., Moon, J. H., Jin, K. B. and Chung, M. J. “Robust iterative learning control with current feedback for uncertain linear systems,” *Intern. J. Systems Science*, vol. 30, no.1, pp. 39-47, 1999.

Dote, Y. *Servo Motor and Motion Control Using Digital Signal Processors*. New Jersey: Prentice-Hall, 1990.

Engelmann, R. H. and Middendorf, W. H. *Handbook of electric motor*. New York: M. Dekker, 1995.

Freeman, R. A. and Kokotovic, P. V. *Robust Nonlinear Control Design: State Space and Lyapunov Techniques*. Boston, MA: Birkhaüser, 1996.

Freeman, R. A. and Kokotovic, P. V. “Tracking controllers for systems linear in the unmeasured states,” *Automatica*, vol. 32, pp. 735–746, 1996.

Goodnick, S. and Hannifin, P. “Electronic damping cures step motor resonance,” *Power Conversion & Intelligent Motion*, vol. 11, no. 5, pp. 32-43, 1997.

Gorinevsky, D., Torfs, D. E. and Goldenberg, A. A. “Learning approximation of feedforward control dependence on the task parameters with application to direct-drive manipulator tracking,” *IEEE Trans. Robot. Automat.*, vol. 13, pp. 567–581, Aug. 1997.

Ham, C., Qu, Z. and Johnson, R. “A nonlinear iterative learning control for robot manipulators in the presence of actuator dynamics,” *Int. J. Robot. Automat.*, vol. 15, no. 3, pp. 107–119, June 2000.

Ham, C., Qu, Z. and Kaloust, J. “Nonlinear learning control for a class of nonlinear systems,” *Automatica*, vol. 37, no. 3, pp. 419–428, Mar. 2001.

Han, S. H., Kim, Y. H. and Ha, I. J. “Iterative identification of state dependent disturbance torque for high precision velocity control of servo motors,” *IEEE Trans. Automat. Contr.*, vol. 43, pp. 724–729, May 1998.

Hara, S., Yamamoto, Y., Omata, T. and Nakano, M. “Control systems: A new type servo system for periodic exogenous signals,” *IEEE Trans. Automat. Contr.*, vol. 33, pp. 659–668, July 1988.

Heinzinger, D., Fenwick, B., Paden, B. and Miyazaki, F. “Robot Learning Control,” *Proc. IEEE Conf. Decision and Control*, 1989.

Horowitz, R. “Learning control of robot manipulators,” *ASME J. Dynam. Syst., Meas. Contr.*, vol. 115, pp. 402–411, 1993.

Huang, W., Cai, L. and Tang, X. “Decentralized learning control for robot manipulators,” *Proc. IEEE Int. Conf. on Robotics and Automation*, pp. 843–848, 1999.

Ilic-spong, M., Marino, R., Persada, S. M. and Taylor, D. G. “Feedback linearizing control of switched reluctance motors,” *IEEE Trans. Automat. Contr.*, vol. 32, no. 5, pp. 371-379, 1987.

Ioannou, P. and Kokotovic, P. V. *Adaptive Systems with Reduced Models*. Berlin: Springer-Verlag, 1983.

Ioannou, P. and Sun, J. *Robust Adaptive Control. Englewood Cliffs*. New Jersey: Prentice-Hall, 1996.

Isidori, A. *Nonlinear Control Systems II*. New York: Springer-Verlag, 1999.

Jang, T. J., Choi, C. H. and Ahn, H. S. "Iterative learning control in feedback systems," *Automatica*, vol. 31, pp. 243-248, 1995.

Kavli, T. "Frequency domain synthesis of trajectory learning controllers for robot manipulators," *J. Robot. Syst.*, vol. 9, pp. 663–680, 1992.

Kenjo, T. and Sugawara, A. *Stepping Motors and Their Microprocessor Controls*. Oxford: Clarendon Press, 2nd ed., 1994.

Khalil, H. *Nonlinear Systems*, 2nd ed. Upper Saddle River, NJ: Prentice-Hall, 1996.

Kim, Y. H. and Ha, I. J. "A learning approach to precision speed control of servomotors and its application to a VCR," *IEEE Trans. Automat. Contr.*, vol.43, pp.724–729, 1998.

Kim, Y. H. and Ha, I. J. "Asymptotic state tracking in a class of nonlinear systems via learning-based inversion," *IEEE Trans. Automat. Contr.*, vol. 45, pp. 2011–2027, 2000.

Kokotovic, P. V. *Foundations of Adaptive Control*. Berlin: Springer-Verlag, 1991.

Krstic, M., Kanellakopoulos, I. and Kokotovic, P. V. *Nonlinear and Adaptive Control Design*. New York: Wiley, 1995.

Kuo, T. Y. and Han, W. G. "Adaptive PID learning of periodic robot motion," *Proc. IEEE conf. Decision and Control*, pp. 186-191, Tampa, Florida, Dec. 1998.

Lee, J. W., Lee, H. S. and Bien, Z. "Iterative learning control with feedback using Fourier series with application to robot trajectory tracking," *Robotica*, vol. 11, pp. 291–298, 1993.

Lewis, F., Abdallah, C. and Dawson, D. *Control of Robot Manipulators*. New York: MacMillan, 1993.

Liao, T. L., Fu, L. C. and Hsu, C. F. "Adaptive robust tracking of nonlinear systems and with an application to a robotic manipulator," *Systems and Control Letters*, vol. 15, pp. 339-348, 1990.

Liu, X.Z., Verghese, G.C., Lang, J.H. and Onder, M.K. "Generalizing the Blonded-Park transformation of electrical machines: Necessary and sufficient conditions," *IEEE Trans. Circuit Syst.*, vol. 36, no. 8, pp. 1058-1067, Aug. 1989.

Marino, R. and Tomei, P. "Robust adaptive regulation of linear time varying systems," *IEEE Trans. Automat. Contr.*, vol. 45, pp. 1301–1311, July 2000.

Messner, W., Horowitz, R., Kao, W.-W. and M. Boals. "A new adaptive learning rule," *IEEE Trans. Automat. Contr.*, vol. 36, pp. 188–197, Feb. 1991.

Mita, T. and Kato, E. "Iterative control and its application to motion control of robot arm (a direct approach to servo-problems)," *Proc. IEEE Conf. on Decision and Control*, pp. 1393–1398, Ft. Lauderdale, FL, 1985.

Moore, K. L. "Iterative learning control—An expository overview," *Appl. Comput. Contr., Signal Process., Circuits*, vol. 1, pp. 151–214, 1999.

Moore, K. L. *Iterative Learning Control for Deterministic Systems, Advances in Industrial Control*. London: Springer-Verlag, 1993.

Narendra, K. and Annaswamy, A. M. *Stable Adaptive Systems*. Englewood Cliffs, New Jersey: Prentice-Hall, 1989.

Padiew, F. and Su, R. "An H^{∞} approach to learning control systems," *Int. J. Adaptive Contr. Signal Processing*, vol. 4, pp. 465–474, 1990.

Park, P. H., Kuo, T-Y and Lee, J. S. "Adaptive learning control of uncertain robotic systems," *Int. J. Control*, vol. 65, no. 5, pp. 725-744, 1996.

Peterson, B. B. and Narendra, K. S. "Bounded error adaptive control," *IEEE Trans. Automat. Contr.*, vol. 27, pp. 1161-1168, 1982.

Pomet, J. B. and Praly, L. "Adaptive nonlinear regulation: estimation from Lyapunov equation," *IEEE Trans. Automat. Contr.*, vol. 37, pp. 729-740, 1992.

Qu, Z. "Global stabilization of nonlinear systems with a class of unmatched uncertainties," *Syst. Control Lett.*, vol. 18, pp. 301–307, 1992.

Qu, Z. "Robust control of nonlinear uncertain systems under generalized matching conditions," *Automatica*, vol. 29, pp. 985–998, 1993.

Qu, Z., Dorsey, J., Dawson, D. M. and Johnson, R. W. "Linear learning control of robot motion," *J. of Robot. Syst.*, vol. 10, no. 1, pp. 123-140, 1993.

Qu, Z. H. *Robust Control of Nonlinear Uncertain Systems.* New York: John Wiley & Sons, Interscience Division, 1998.

Qu, Z. "Robust control of nonlinear systems by estimating time variant uncertainties," *Proc. IEEE Conf. Decision Control*, Sydney, Australia, Dec. 2000, pp. 3019–3024.

Qu, Z. H. "Robust and adaptive boundary control of a stretched string on a moving transporter," *IEEE Trans. Automat. Contr.*, vol. 46, no. 3, 2001.

Qu, Z. H. and Xu, J. X. "Asymptotic learning control for a class of cascaded nonlinear uncertain systems," *IEEE Trans. Automat. Contr.*, vol. 47, no. 8, 2002.

Qu, Z. H. "Robust control of nonlinear systems in the presence of unknown exogenous dynamics," *IEEE Trans. Automat. Contr.*, vol. 48, no. 2, 2003.

Qu, Z. H. “Adaptive and robust control of uncertain systems with nonlinear parameterization,” *IEEE Trans. Automat. Contr.*, vol. 48, no. 10, 2003.

Sadegh, N. and Horowitz, R. “Stability and robustness analysis of a class of adaptive controllers for robotic manipulators,” *Int. J. Robot. Res.*, vol. 9, no. 9, pp. 74–92, 1990.

Sadegh, N., Horowitz, R., Kao, W. W. and Tomizuka, M. “A unified approach to the design of adaptive and controllers for robot manipulators,” *ASME J. Dynam. Syst., Meas. Contr*., vol. 112, pp. 618–629, 1990.

Saab, S. S. “On the P-type learning control,” *IEEE Trans. Automat. Contr.*, vol. 39, no. 11, pp. 2298-2302, 1994.

Sastry, S. and Isidori, A. “Adaptive control of linearizable systems,” *IEEE Trans. Automat. Contr.*, vol. 34**,** pp. 1123-1131, 1989.

Schweid, S., Mcinroy, J. and Lofthus, R. “Closed loop low-velocity regulation of hybrid stepping motors amidst torque disturbances,” *IEEE Trans. Ind. Electron.*, vol. 42, no. 3, pp. 316-324, 1995.

Slotine,J.J. and Li, W. *Applied Nonlinear Control.* Englewood, NJ: Prentice-Hall, 1991.

Sun, M. and Wang, D. “Sampled-data iterative learning control for nonlinear systems with arbitrary relative degree,” *Automatica,* vol. 37, pp. 283–289, 2001.

Taylor, D. G., Woollley, M. J. and Ilic-spong, M. “Design and implementation of a linearizing and decoupling feedback transformation for switched reluctance motors,” *17th Annual Symposium on Incremental Motion Control System Devices*, pp. 173-184, June 1988.

Taylor, D., Kokotovic, P. V., Marino, R. and Kanellakopoulos, I. “Adaptive regulation of nonlinear systems with unmodeled dynamics,” *IEEE Trans. Automat. Contr.*, vol. 34, pp. 405-412, 1989.

Toffner-Clausen, S. *System Identification and Robust Control*. New York: Springer, 1996.

Tomizuka, M., Tsao, T. and Chew, K. “Discrete-time domain analysis and synthesis of controllers,” *ASME J. Dynam. Syst., Meas. Contr.*, vol. 111, pp. 353–358, 1989.

Tsai, M., Anwar, G. and Tomizuka, M. “Discrete-time control for robot manipulators,” *Proc. IEEE Int. Conf. Robotics and Automation*, pp. 1341–1347, 1988.

Wang, D. “On D-type and P-type ILC designs and anticipatory approach,” *Int. J. Contr.*, vol. 23, no. 10, pp. 890–901, 2000.

Wang, D., Soh, Y. C. and Cheah, C. C. “Robust motion and force control of constrained manipulators by learning,” *Automatica*, vol. 31, no. 2, pp. 257–262, 1995.

Wang, J. and Qu, Z. H. “Robust adaptive control of strict-feedback nonlinear systems with nonlinear parameterization,” *Proc. American Contr. Conf.*, pp 3026-3031, Denver, Colorado, June, 2003.

Xu, J. X., Lee, T. H. and Jia,Q. W. “An adaptive robust control scheme for a class of nonlinear uncertain systems,” *International Journal of Systems Science*, vol. 28**,** pp. 429-434, 1997.

Xu, J. X. and Qu, Z. “Robust iterative learning control for a class of nonlinear systems,” *Automatica*, vol. 34, no. 8, pp. 983–988, 1998.

Xu, J. X. “An integrated learning variable structure control method,” *Variable Structure Systems: Towards the 21st Century, LNCIS 274,* pp. 33-55, 2002.

Yao, Z., Costescu, N. P., Nagarkatti, S. P. and Dawson, D. M. “Real-time linux target: A MATLAB-based graphical control environment,” *Proc. IEEE Conf. Control Applications*, pp. 173–178, Sept. 2000.

Yung, K. L. and Liu, H. "A study on dynamic performance of closed-loop commuted stepping motor to improve precision motion control," *Precision Engineering*, vol. 16, no. 4, pp. 276-282, 1994.

Yung, K. L., Cheng, K. W. and Song, G. "Analysis of stepping motor torque ripple control for precision profiling," *Intern. J. Power and Energy Systems*, *IASTED*, vol. 17, no. 1, pp. 1-7, 1997.

Yung, K. L., Chen, W. D. and Cheng, K. W. "Torque ripple minimization of hybrid stepping motor servo drives for precision tracking," *Research Progress Report*, Department of Manufacturing Engineering, Hong Kong Polytechnic University, 1996.

Zhang, Y. and Ioannou, P. A. "Adaptive control of time varying linear systems," in *Proc. 35th IEEE Conf. Decision Control*, Kobe, Japan, 1996, pp. 837–842.

Zribi, M. and Chiasson, J. "Position control of a pm stepper motor by exact linearization," *IEEE Trans. Automat. Contr.*, vol.36, no. 5, pp. 620-625, 1991.